

CD4 T cell diversification in the tissue

Inauguraldissertation

zur

Erlangung der Würde eines Doktors der Philosophie

vorgelegt der

Philosophisch-Naturwissenschaftlichen Fakultät

der Universität Basel

von

Nivedya Swarnalekha

von India

2021

*Originaldokument gespeichert auf dem Dokumentenserver der
Universität Basel <https://edoc.unibas.ch>*

Genehmigt von der Philosophisch-Naturwissenschaftlichen Fakultät auf Antrag von

(Prof.Dr.Gennaro de Libero, Prof.C.G.King, Prof.R.Tuschiwand)

Basel, 02/03/2021

Dean of Faculty
Prof. Dr. Marcel Mayor

Table of Contents

Acknowledgements.....	01
Abbreviations.....	02
Summary.....	04
1. Introduction.....	05
1.1 Immunology and Vaccines.....	05
1.2 CD4 T cell memory: friend or foe?	06
1.2.1 CD4 T cell differentiation.....	06
1.2.2 CD4 T cell response.....	06
1.2.3 Signals for Th1/TFH generation, function and memory.....	07
2. Immunological memory in barrier tissues.....	11
2.1 TRM.....	11
2.1.1 Identification.....	11
2.1.2 Circulation ability.....	11
2.1.3 Phenotype.....	12
2.1.4 Factors responsible for TRM generation and maintenance.....	12
2.1.5 TRM function: protective and pathogenic roles.....	13
2.2 Influenza and CD4 TRM.....	15
2.2.1 Influenza virus.....	15
2.2.2 IAV proteins as immune targets.....	15
2.2.3 Open questions and goals of thesis.....	16
3. Aim.....	16
4. Results	17
Abstract.....	17
Introduction.....	17
Results.....	18
Discussion	27
Materials and Methods.....	28
Supplementary Materials.....	34
5. Discussion.....	50
5.1 Heterogeneity and tissue-specific genes.....	50
5.2 HIF-1 α and possible role in TRM regulation.....	51
5.3 Dynamics of long-term T-B interactions in the tissue.....	53
5.4 Caveats and Outlook.....	55
5.4.1 Caveats of TRM study design.....	55
5.4.2 CD8 T cell depletion to study CD4 TRM in influenza models.....	56
5.4.3 Contribution of CD4 TRM to OAS.....	56
5.4.4 Relevance of TRM study in the fight against pandemic.....	56
6. References.....	57
7. Appendix.....	61

Acknowledgements

Days melted into each other and it is hard to believe many years have passed and my PhD journey is coming to an end. This was a marvelous adventure of learning and discovery both scientifically and personally and I am grateful to the many that have helped me reach the 'official' finish line (although there is no real end to learning or discovery).

Words don't suffice to thank my supervisor, Carolyn King who has been my guru (teacher) and my sakhi (friend) throughout. Thank you for the opportunity. Next, I would like to thank my labmates Marco, Tamara, David, Ludivine, Clemens, Sanketh. Thank you for being my anchor and tailwind. I also give thanks to my Committee members: Professors Roxane Tussiwand, Gennaro de Libero, Dietmar Zehn, and the PhD student community.

I would not be where I am today without the wonderful women in my life who have epitomized beauty, grace, courage and resilience and stood true role models. My late grandmother Jagathambal, my mother Swarnalekha, my mother-in-law Premalatha, my sister-in-law Archana, my aunt Karuna and my best friends: Shilpa, Meha, Aishwarya and Lekshmi. Thank you for the nudge, push, shove and slap.

To all my family, teachers and friends in India and the rest of the world who were instrumental in shaping me into the person I am today, my heartfelt thank you. Special thanks to my parents, Swarnalekha and Mariyappan, my brother Hariprasad, sister-in-law Archana and my nieces Nakshatra and Shanaya.

Last but not the least I would like to thank my better half Sajeev who has stuck with me through thick and thin. Thank you for marrying me at the start of my PhD and still being around (തീമഴ,പൂമഴ! = in rains of fire or flowers)

Abbreviations

<i>M.tb</i>	Mycobacterium tuberculosis
HIV-1	Human Immuno Virus -1
CD	Cluster of Differentiation
TFH	T follicular helper
GC	Germinal center
APC	Antigen presenting cell
MHC	Major Histocompatibility Complex
TCR	T cell receptor
Th1	T helper 1
IFN- γ	Interferon gamma
CXCR	C-X-C motif chemokine receptor type
CXCL	C-X-C motif chemokine ligand
SLO	Secondary lymphoid organ
ASC	Antibody secreting cell
ICOS	Inducible co-stimulator
ICOSL	Inducible costimulatory ligand
GC-TFH	Germinal center- T follicular helper
IL	Interleukin
DC	Dendritic cell
Bcl6	B cell lymphoma 6
T-bet	T-box transcription factor
PSGL-1	P selectin glycoligand-1
Ly6c	Lymphocyte antigen 6 complex
T _{cm}	T central memory
PD-1	Programmed cell death protein 1
NAD	Nicotinamide adenine dinucleotide
FR4	Folate receptor 4
LCMV	Lymphocytic choriomeningitis virus
TRM	T resident memory
FRT	Female reproductive tract
LN	Lymph node
T _{em}	T effector memory
Klf2	Krüppel-like factor 2
S1pr1	Sphingosine-1-phosphate receptor 1
P2X7R	P2X purinoceptor 7
Ccr7	C-C chemokine receptor type 7
Tcf7	Transcription factor 7
KO	Knockout

iBALT	Inducible bronchus associated lymphoid tissue
HSV	Herpes Simplex Virus
SARS-CoV	Severe Acute Respiratory Syndrome- Coronavirus
CNS	Central Nervous System
IBD	Inflammatory Bowel Disease
IAV	Influenza A Virus
HA	Hemagglutinin
NA	Neuraminidase
ARDS	Acute Respiratory Distress Syndrome
PR8	Strain A/Puerto Rico/8/34 (H1N1)
X31	Strain A/X-31 (H3N2)
NS-1	Non-structural protein 1
M1, M2	Matrix protein 1, 2
PA	Polymerase acidic protein
Treg	Regulatory T cell
HIF-1 α	Hypoxia Inducible Factor 1A
VHL	Von Hippel-Lindau
μ MT	IgM μ -chain mutant
OAS	Original antigenic sin
COVID	Corona virus disease
RNA	Ribonucleic acid
Fth1	Ferritin heavy chain 1
Tnfsf4	Tumor necrosis factor superfamily 4
Eif1	Eukaryotic Translation Initiation Factor 1
Id3	Inhibitor of DNA binding 3
mTOR	Mammalian/Mechanistic Target of Rapamycin
TRAF	Tumor necrosis factor receptor-associated factor
AREG	Amphiregulin
EGF	Epidermal Growth Factor
LCMV	Lymphocytic Choriomeningitis Virus

Summary

Heterogeneity is the hallmark feature of CD4 T cells with the ability to differentiate into effector cells of various phenotypes and perform distinct function. This diversification that is essential for optimal response has not been described in the tissue. Using influenza as an infection model, we investigated long-lived antigen-specific CD4 T cells in the tissue. We identified a heterogeneous population of T resident memory cells (TRM) in the tissue, specifically, a T follicular helper-like subset we called T resident helper (TRH) that was previously not reported. Further characterization by single cell RNA sequencing analysis revealed that TRH possess a unique tissue-specific transcriptional signature distinct from lymphoid TFH and that they can be generated independently of lymphoid replenishment. Histological analysis showed that TRH cluster closely with B cells in inducible bronchus-associated lymphoid tissue (iBALT) and require continued BCL6 signaling for their localization. Interestingly, at very late time points, signals through cognate antigen presentation were dispensable for TRH maintenance and iBALT integrity. Upon heterologous challenge, TRH cells support local antibody production highlighting a previously unexplored function of TRM.

1. Introduction

1.1 Immunology and Vaccines

Vaccines prime the immune system to elicit a protective response against the invading pathogen. The practice of vaccination began in ancient times with the crust of smallpox virus being introduced into open wounds. This resulted in mild symptoms that soon passed, and the individual was subsequently protected from reinfection with smallpox. Knowledge of the method spread to Europe in the 18th century and the practice of vaccination acquired scientific status after Edward Jenner's first vaccination of a child with cowpox, a milder virus than smallpox. With vaccination, the deadly smallpox was eradicated although the mechanism by which protection was conferred was still unknown. Empirically developed undefined vaccine preparations pose a major safety concern. The need to elicit a predictable immune response necessitated a shift from empirical to rational vaccine design ^{1, 2}

Modern vaccination utilizes whole-killed or live-attenuated pathogens that are killed or weaker versions of the pathogen to elicit an immune response without causing a full disease. Subunit or recombinant vaccines prime the immune system with specific pieces of the pathogen or DNA. Antigen-adjuvant combinations were explored to engage the innate immune system that in turn triggers an adaptive immune response. Although the primary line of defense after pathogen entry is a rapid, non-specific response by the innate immune system, adaptive immune responses shape long-lasting immunity against future infections.

In the modern era, pathogens like *Mycobacterium tuberculosis* (*M.tb*), HIV-1, influenza and malaria still pose a threat to humankind with their ability to mutate or otherwise evade the immune system.¹ A deeper understanding of various pathogens and the variability in infectivity made clear that a one-size-fits-all vaccine is not sufficient.

Current vaccines primarily aim to promote neutralizing antibody production by B cells, but a robust antibody response alone is insufficient to provide long-lasting protection. Increasing knowledge about cells that aid antibody generation or promote secondary B cell responses highlight the possibility of harnessing T cell immunity as a vaccine target. T cells are found at mucosal surfaces which is the entry site of pathogens. T cells generated at one site with a priming immunization can be recruited to another by a challenge dose through the prime-and-pull strategy.¹ T follicular helper cells (TFH) support B cell growth, proliferation, differentiation and support germinal center (GC) reactions required for formation of antibodies.³ TFH cells are used as a readout of successful vaccination^{4,5,6}. However, the reported correlates are from TFH cells in circulation whose phenotypes don't mirror those in germinal centers^{7,8,9}. Moreover, the contribution of TFH to mucosal immunity has not been widely explored.

1.2 CD4 T cell memory: friend or foe?

1.2.1 CD4 T cell differentiation

Naive T cells survey the body through blood and lymphatics. When a micro-organism invades the host, antigen-presenting cells (APC) process foreign antigens and present them as peptides loaded on Major histocompatibility complex (MHC)-II complexes to the T cell receptor (TCR). Signals received through TCR, co-stimulatory receptors and extrinsic cytokines trigger CD4 T cell activation and differentiation into heterogeneous effectors of unique phenotype and function. CD4 T cells undergo rapid proliferation at the peak of infection response. Once the infection is resolved, many of the effector cells die and some CD4 T cells persist as memory cells in circulation, secondary lymphoid organs and tissue. Memory cells possess the capacity to rapidly respond upon re-infection.¹⁰

1.2.2 CD4 T cell response

T helper 1 (Th1) and TFH cells are generated upon viral infections. Th1 cells migrate to tissues and through IFN- γ signals, activate innate cells and CD8 T cells for heightened response and accelerated clearance of infected cells.¹¹ TFH cells express chemokine receptor CXCR5 and respond to CXCL13 chemokine cues to navigate into GCs present in secondary lymphoid organs (SLO). Germinal centers are complex structures formed in SLO in response to T cell dependent antigen. Supported by a network of follicular dendritic cells, the GC is characterized by B cell follicles separated by a T cell rich area¹². Here, TFH cells provide survival signals to some of the B cells that are undergoing somatic hypermutation and class-switching to differentiate into high affinity antibody secreting cells (ASC) with specialized effector function. These antibodies are essential for viral control and protection against future infection.¹³

1.2.3 Signals for Th1/TFH generation, function and memory

The signals through the TCR, co-stimulatory molecules and cytokines determine the differentiation of naïve CD4 T cells to Th1 or TFH fate, function and maintenance at memory phase.

TCR

Several contrasting studies outline the delicate balance of antigen affinity, dose and dwell-time that determine T cell fate decision^{14,15,16}. The effect of TCR on GC-TFH is unique in that the APC-T-cell interaction is further supported by ICOS-ICOSL interactions.¹⁷ The nature of these interactions is one of the factors that influences the longevity of T cells in their niche and their phenotype and function upon re-challenge.

Co-stimulation

ICOS-ICOSL interactions are indispensable for differentiation into TFH cells. Some models outline a B cell independent promotion of TFH fate^{18,19} while others implicate B cells in the

initial priming for TFH fate decision.^{20,21} The Crotty group describe a possible transition of antigen presentation from DC to B cells during TFH formation. During early priming, pre-TFH can be generated without B cell help but later TFH differentiation is impaired by B cell deficiency²², as also demonstrated by the Jenkins group²³. Throughout the TFH differentiation process, ICOS-ICOSL interactions are crucial, first provided by DC, then by B cells. B cells are dispensable, however, for differentiation into Th1.

Cytokines

The timing, amount and ratio of inflammatory cytokines drive specific T cell fates. IL-6 and IL-21 are associated with TFH differentiation while IL-12 supports an eventual Th1 fate.²⁴ Early IL-2 producers were shown to differentiate into TFH while the IL-2 consumers followed a path to Th1 differentiation¹⁹. The existing cytokine milieu might be a key determinant in predicting cell fate outcome.

Transcription factors

T-BET and BCL6 are the key transcription factors implicated in regulating Th1 and TFH cell fates respectively although they are not mutually exclusive. Their relative expression can promote or inhibit genes responsible for cell fate decision. In recent studies, BCL6 was highlighted to be a “repressor of repressors” in TFH including repression of itself, highlighting delicate autoregulation. Functional complexes of T-BET-BCL6 are also described in TFH cells. Key Th1 factors are regulated by T-BET in TFH cells. The permissive state of *Bcl6* and *T-bet* loci point to a state receptive to environmental cues from changing infection settings.²⁵

CD4 T cell memory

Long-lived CD4 memory have been classified into 3 subsets: PSGL-1^{hi} LY6C^{hi} Th1 memory, PSGL-1^{hi} LY6C^{lo} T central memory (T_{cm}) and more recently PSGL-1^{lo} LY6C^{lo} TFH memory each with their distinct phenotype, migration and recall properties.²⁶ CXCR5⁺PD-1⁺ TFH effector cells were earlier thought to be absent among T cells surviving long term after the

effector phase.²³ A recent discovery highlighted that TFH cells are susceptible to NAD-induced cell death during cellular processing²⁶. This phenomenon has long biased the conclusions about the longevity of TFH cells. Additionally, Folate receptor 4 (FR4) was described as a phenotypic marker that better discriminates TFH memory cells from Tcm. TFH memory cells can be detected up to 400 days after viral infection, support long-term maintenance of plasma cells in the spleen and display phenotypic plasticity upon recall.²⁶

CD4 T cell memory has been shown to correlate with protection upon secondary challenge infections.²⁷ But specifically eliciting a CD4 T cell memory response as a vaccination strategy has been an interesting research topic. Work by Penaloza-MacMaster et al. showed that specifically re-activating CD4 memory T cells in a chronic LCMV model resulted in excessive weight loss, cytokine storm and multi-organ failure. Microarray analysis revealed a lack of exhaustion markers and a cytokine signature indicative of a bias toward a Th1 phenotype.²⁸ Similarly, dysregulated TFH cells were implicated in pathogenesis of autoimmune diseases and allergy.^{29,30} In contrast, a study of antigen specific T cells against SARS showed that re-activated memory CD4 T cells producing IFN- γ upon recall correlated with protection. Although the focus of the publication was on the Th1-like subset, other parenchymal CD27^{hi} IFN- γ ^{lo} T cell subsets were not absent in the recall response.³¹ These studies highlight an important role for the heterogeneity of CD4 T cell response in balancing host protection and pathology.

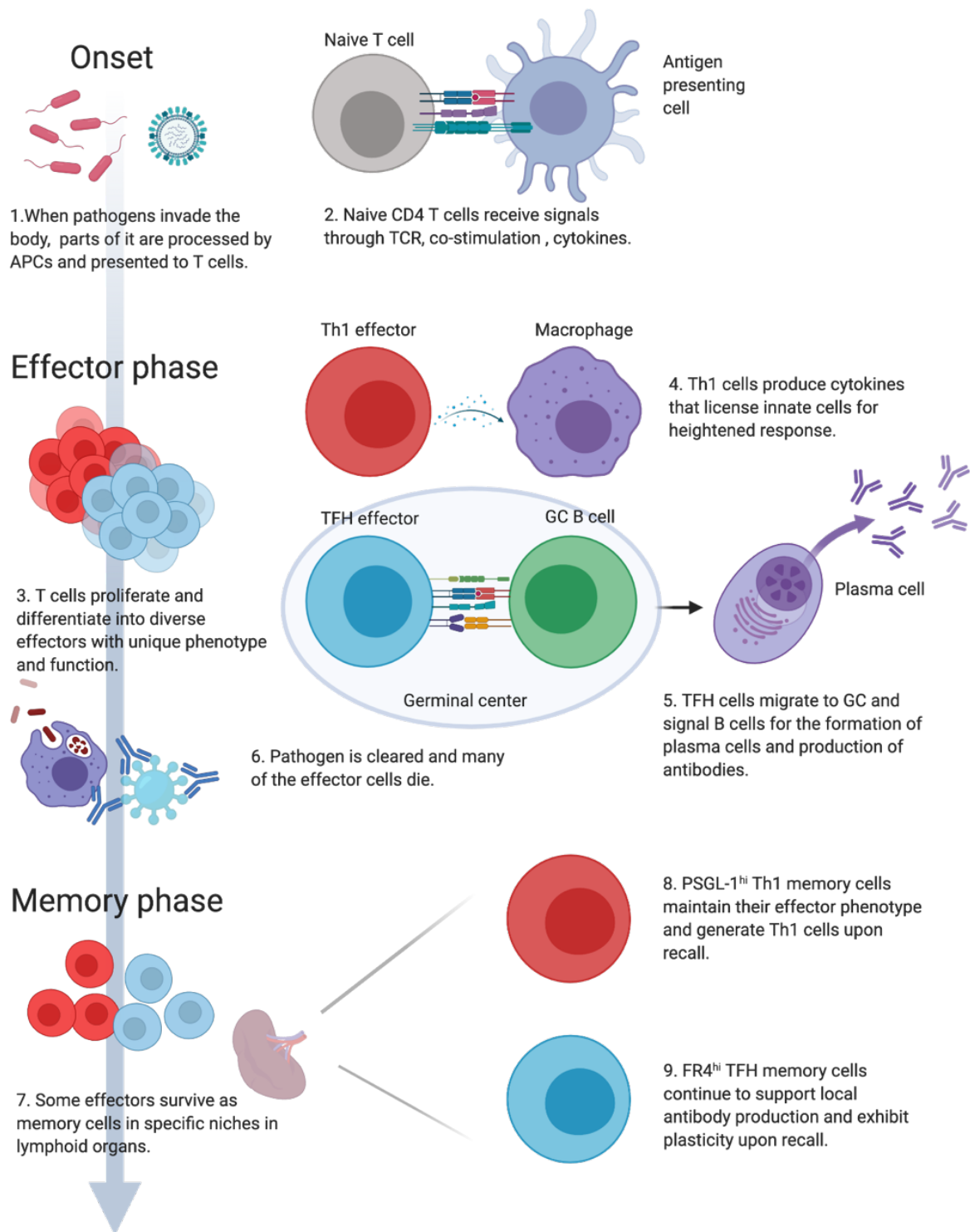


Fig1: CD4 T cell response during infection

2. Immunological memory in barrier tissues

The understanding of immunological memory has changed over time. Earlier thought to be maintained in blood and secondary lymphoid organs, a new wave of studies has shown that memory T cells can be maintained in barrier tissues. These cells called T resident memory (TRM) are phenotypically and transcriptionally distinct from their circulating memory counterparts. Their presence in mucosal niches makes them the first responders to tissue-specific infection. This feature makes TRM a promising potential vaccine target.^{32,33,34}

2.1 TRM

2.1.1 *Identification*

TRM were first identified in tissue isolates after infection that retained their function *ex-vivo*.^{35,36,37} Parabiosis experiments^{38,39,40}, confocal microscopy⁴¹, intravital imaging⁴² and intravascular staining⁴³ confirmed their tissue-resident property. The generation of antigen-specific CD4 and CD8 TRM were identified in an influenza infection model.⁴⁴ These cells were enriched in the mucosal tissue, exhibited tissue tropism on transfer to naive hosts and displayed unique surface marker expression patterns compared to their circulating counterparts³⁸. Over the years, TRM were identified in lung, liver, kidney, FRT, intestine and skin in various infection models with CD4 TRM outnumbering CD8 TRM in barrier tissues⁴⁵. In humans, endogenous TRM were also identified in tissue transplants up to one year in lung⁴⁶ and after longer durations in intestinal grafts.⁴⁷

2.1.2 *Circulation ability*

The circulatory capacity of TRM has long been under scrutiny. Early experiments confirmed that TRM are not re-circulating effector memory cells.^{32,33} Although parabiosis experiments confirmed the non-circulating nature of TRM, time-course studies after influenza showed attrition of CD8 TRM.⁴⁸ Integrated stress responses and amino acid starvation promoted the

apoptosis of CD8 TRM, preventing their long-term retention.⁴⁹ This phenomenon occurred in the lung but not in other barrier tissues. At late time points after influenza infection, retrograde migration of TRM to lung draining LN was also observed. These cells retained a TRM phenotype but were found in the LN-associated lymphatics.⁵⁰

2.1.3 Phenotype

Bulk sequencing analysis of antigen-specific memory CD8 T cells across tissues confirmed that TRM are transcriptionally distinct from T_{em} and T_{cm}.⁵¹ TRM show downregulation of *Klf2* and *S1pr1* genes and upregulation of *Cd69* which are important for cell retention in tissue. TRM express chemokine and integrin molecules essential for homing to and binding tissue surfaces. TRM share a core transcriptional signature that is conserved between mice and humans.⁵² Some TRM markers are also shared between CD4 and CD8 TRM: PD-1, CD69, CXCR6. Genes associated with TCR signaling and cytokine production are also enriched in TRM indicating a state of heightened activation poised for rapid response.⁴⁵ P2X7R is enriched on CD8 TRM and TFH memory cells possibly mirroring the metabolic status of cells “resident” in their respective niches.⁵³

2.1.4 Factors responsible for TRM generation and maintenance

Antigen is required for the generation of T cells in the tissue with ‘classical’ TRM phenotype.³³ Cognate antigen recognition by CD4 T cells at the effector phase is required for TRM formation.⁵⁴ CD8 and CD4 TRM can survive in naïve hosts in an antigen and inflammation-independent manner^{50,38,55} although their long-term maintenance is negatively impacted and accompanied by phenotype changes.⁵⁵

Cytokines IL-2, IL-15 and IL-7 are implicated in TRM generation.^{32,33} IL2 is required for Th1 and Th2 TRM accumulation.^{56,57,58} IL-7 is required for the generation of both CD4 and CD8 TRM^{32,33} although IL-15 is dispensable for CD4 TRM.⁴⁵

Among CD4 TRM, until recently, only Th1 associated cytokine production has been reported.^{59,60}

Many **transcription factors** are described to define tissue residency, but most have been associated with CD8 TRM.⁴⁵ HOBIT and BLIMP1 in CD8 TRM were shown to bind *S1pr1*, *Ccr7* and *Tcf7* genes associated with tissue egress.⁵¹ In CD4 TRM, *Hobit* and *Blimp1* knockout (KO) show decreased TRM accumulation.⁶¹ *Bhlhe40*, which was previously implicated in maintenance of mitochondrial fitness in CD8 TRM,⁶² has been shown to be essential for CD4 TRM sustenance in the tissue.⁶³

Intercellular interactions are crucial for TRM maintenance. Infection with influenza has been shown to generate inducible bronchus associated lymphoid tissue (iBALT). These structures closely resemble germinal centers in secondary lymphoid organs.⁶⁴ iBALT can be formed independently of secondary lymphoid organs and can sustain TRM responses without the need for lymphoid replenishment.⁶⁵ Cytokine and chemokine signals provided by cells within iBALT or cell clusters in the tissue can recruit immune cells and sustain these structures. The presence of iBALT also correlate with reduced pathology in allergy models.⁶⁶ iBALT destruction by DC depletion in the lung is associated with significant decrease in local and systemic antibody production upon re-challenge.⁶⁷ These studies highlight the importance of iBALT in preserving immune homeostasis.

2.1.5 TRM function: protective and pathogenic roles

Upon activation, TRM proliferate locally, produce cytokines, recruit innate cells and dominate the local secondary response.^{68,69,70} Secondary effectors of CD4 TRM display a multi cytokine production profile compared to primary effectors. Here TFH effectors were identified although their tissue residency status was not clearly defined.⁵⁹ CD4 TRM have been associated with protection in infection models like influenza⁷⁰, *M.tb*⁵⁵, Herpes Simplex Virus (HSV)⁷¹, and

Severe Airway Respiratory Syndrome coronavirus (SARS-CoV)³¹, but were shown to be pathogenic in the context of asthma⁷², psoriasis⁷³, CNS autoimmunity⁷⁴ and IBD⁷⁵. When focusing on eliciting TRM response as a vaccine target, the immune context needs to be considered.

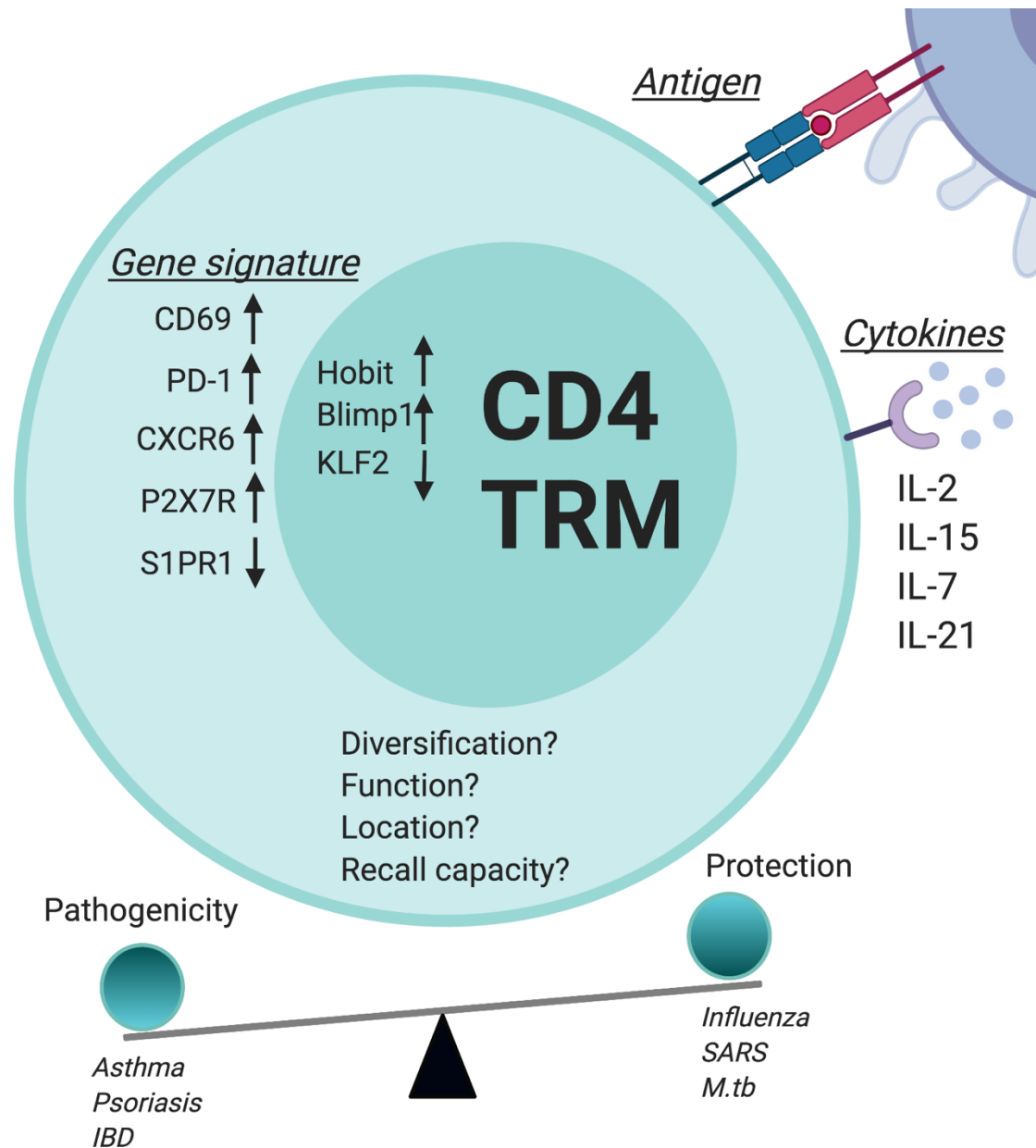


Fig2: CD4 TRM: knowns and unknowns

2.2 Influenza and CD4 TRM

2.2.1 Influenza virus

Influenza is a member of the Orthomyxoviridae family. It contains a segmented, negative sense, single stranded RNA genome. Influenza falls into 4 genera A, B, C, D and can infect a wide spectrum of species. Influenza A virus (IAV) is classified on the molecular structure and genetic characteristics of Hemagglutinin (HA) and Neuraminidase (NA)⁷⁶. IAV infects airway cells causing alveolar epithelial injury and failure of gas exchange. Extreme consequences are acute respiratory distress syndrome (ARDS) and death. IAV is also the causative agent for the pandemic and circulating seasonal epidemic⁷⁷. Annual epidemics result in worldwide deaths ranging between 290,000-650,000.⁷⁸

2.2.2 IAV proteins as immune targets

Nucleoprotein (NP) of the influenza virus is the key component of the ribonucleoprotein (RNP) complex and is required for viral transcription and replication. NP is a conserved CD4 and CD8 T cell epitope. Mouse adapted strains PR8 (H1N1) and H3N2 (X31) are the most commonly used strains administered in succession for the study of heterologous infection models. Here, the NP-epitope overlaps between infections and NP-specific memory cells are re-activated to launch the secondary response^{76,79}. Focus on generating T cell memory against conserved epitopes may be a good strategy for the design of a universal vaccine.

Hemagglutinin is the surface glycoprotein of the flu virus that is important for attachment to host, cell fusion and viral entry. HA contains epitopes that trigger neutralizing antibody production and is the key target for the seasonal influenza vaccine. HA is the dominant determinant that triggers viral mutation and recombination. Mutations in HA lead to rapid viral escape that renders neutralizing antibodies to previous infection ineffective, necessitating new vaccine formulations annually.^{76,79}

Neuraminidase (NA), Non-structural protein 1 (NS1), Matrix proteins 1 and 2 (M1, M2) and Polymerase A (PA) are other epitopes being considered as vaccine candidates. These epitopes cannot independently elicit a strong immune response or generate long-lived memory.^{76,79}

2.2.3 Open questions and goals of thesis

Previous reports of CD4 TRM generated in response to IAV describe a Th1 phenotype.^{38,71,80,59} Previously, eliciting a Th1-biased memory response as a vaccine strategy has been shown to be detrimental to the host.²⁸ In an asthma model, decreased accumulation of CXCR5-negative T cells correlated with less-severe host pathology, highlighting that an inflammatory cytokine-mediated response is not the only form of protection.⁵⁷ Bulk sequencing of T cells in tissues to define a residency signature creates a bias towards cytotoxic or IFN- γ -producing cells due to their predominance during immune response, thus obscuring T cell heterogeneity.⁷⁰ Transgenic mouse models have also been shown to display impaired generation of heterogeneity unlike their polyclonal models, leading to misinterpretation of the immune setting.²⁶ The classical polyclonal CD4 T cell diversification upon infection described earlier has not been reported in the resident compartment.

3. Aim

To examine the hallmark heterogeneity of CD4 T cells in the tissue resident compartment and refine T cell residency signature to account for heterogeneity.

4. Results

ANTIVIRAL IMMUNITY

T resident helper cells promote humoral responses in the lung

Nivedya Swarnalekha^{1*}, David Schreiner^{1*}, Ludivine C. Litzler¹, Saadia Iftikhar², Daniel Kirchmeier¹, Marco Künzli¹, Young Min Son^{3,4}, Jie Sun^{3,4}, Etori Aguiar Moreira⁵, Carolyn G. King^{1†}

Copyright © 2021
The Authors, some
rights reserved;
exclusive licensee
American Association
for the Advancement
of Science. No claim
to original U.S.
Government Works

Influenza is a deadly and costly infectious disease, even during flu seasons when an effective vaccine has been developed. To improve vaccines against respiratory viruses, a better understanding of the immune response at the site of infection is crucial. After influenza infection, clonally expanded T cells take up permanent residence in the lung, poised to rapidly respond to subsequent infection. Here, we characterized the dynamics and transcriptional regulation of lung-resident CD4⁺ T cells during influenza infection and identified a long-lived, *Bcl6*-dependent population that we have termed T resident helper (T_{RH}) cells. T_{RH} cells arise in the lung independently of lymph node T follicular helper cells but are dependent on B cells, with which they tightly colocalize in inducible bronchus-associated lymphoid tissue (iBALT). Deletion of *Bcl6* in CD4⁺ T cells before heterotypic challenge infection resulted in redistribution of CD4⁺ T cells outside of iBALT areas and impaired local antibody production. These results highlight iBALT as a homeostatic niche for T_{RH} cells and advocate for vaccination strategies that induce T_{RH} cells in the lung.

INTRODUCTION

Seasonal influenza epidemics are a major cause of global morbidity and mortality. Although annually administered influenza vaccines are among the most widely used in the world, vaccine-elicited neutralizing antibodies offer poor protection against different influenza strains (1). In contrast, there is evidence that prior influenza infection can accelerate viral clearance after heterotypic infection in both mice and humans (2–6). Emerging data suggest that the targeted generation of CD4⁺ memory T cells recognizing conserved epitopes from internal viral proteins may form the basis of a universal influenza virus vaccine (7, 8). CD4⁺ memory T cells are induced after immunization or infection and can be recalled to generate secondary effectors during a challenge infection. Several subsets of CD4⁺ memory cells have been described, including central memory and effector memory cells, which circulate through secondary lymphoid tissues (LTs) and nonlymphoid tissues (NLTs) (9). More recently, T resident memory (T_{RM}) cells that persist in barrier tissues such as lung and skin have been described (10). Although CD4⁺ T cells actually outnumber CD8⁺ T cells in barrier tissues, most of the studies have focused on the requirements for CD8⁺ T_{RM} cell differentiation. In addition, although CD4⁺ T cells are renowned for their substantial plasticity during immune responses, less is known about diversification within the CD4⁺ T_{RM} cell compartment (11–16).

Influenza infection induces the differentiation of CD4⁺ T_{RM} cells in the lung, where they are maintained in an antigen and inflammation-independent manner (17). After a lethal rechallenge, influenza-specific CD4⁺ T_{RM} cells rapidly produce effector cytokines and promote both viral clearance and host survival (7). Lung CD4⁺ T_{RM} cells can also

be induced by mucosal vaccination and were shown to mediate superior protection after heterologous infection, highlighting their potential as a universal vaccine target (18). Influenza-specific CD4⁺ T_{RM} cells are generally characterized as T helper 1 (T_{H1})-like, with the capacity to produce both interferon- γ (IFN- γ) and interleukin-2 (IL-2) (7, 19). However, IL-2-deficient memory CD4⁺ T cells were recently shown to provide superior protection compared with wild-type memory cells, an outcome that correlated with decreased inflammation and host pathology during rechallenge (20). These data suggest that protection mediated by CD4⁺ T_{RM} cells is not strictly dependent on their ability to produce effector cytokines and that a balanced secondary response is likely to involve the recruitment and coordination of distinct and specialized CD4⁺ T_{RM} cell subsets (21).

Heterogeneity within the non-antigen-specific CD4⁺ T_{RM} cell compartment was recently examined in a study that reported enrichment of genes associated with the tumor necrosis factor (TNF) receptor superfamily and nuclear factor κ B pathways in barrier T cells compared with T cells isolated from their respective draining lymphoid compartments (11). The residency signature derived from this dataset, however, does not take into consideration differences between distinct T cell subsets. Accordingly, this approach tends to overrepresent genes associated with type 1 helper T cells such as *Klrg1*, *Itgae*, *Id2*, and *Cxcr6*, which may incorrectly define residency for other T_H cell subsets. Consistent with this idea, the authors reported the presence of a stronger T_{RM} phenotype in lymphoid T_{H1} memory cells compared with lymphoid T follicular helper (T_{FH}) cells, which they attributed to the relative ability of these cells to adapt to barrier tissues. Similarly, another study addressing the relationship between T_{RM} cells present in secondary lymphoid organs and T_{FH} memory cells reported distinct transcriptional profiles of these subsets (12). However, in this case, the authors analyzed T cell receptor (TCR) transgenic cells that have impaired T_{FH} memory cell generation relative to polyclonal antigen-specific cells (22), likely enhancing a bias in T_{RM} toward genes expressed by cytotoxic and type 1 cytokine-producing cells. On the other hand, it is well appreciated that T_{FH} cells share many surface markers and molecular dependencies

¹Immune Cell Biology Laboratory, Department of Biomedicine, University of Basel, University Hospital Basel, CH-4031 Basel, Switzerland. ²Personalised Health Basel-Oncology Cluster Basel, University of Basel, Basel, Switzerland. ³Department of Medicine, Mayo Clinic, Rochester, MN 55905, USA. ⁴Department of Immunology, Mayo Clinic, Rochester, MN 55905, USA. ⁵Friedrich Miescher Institute for Biomedical Research, Basel, Switzerland.

*These authors contributed equally to this work.

†Corresponding author. Email: carolyn.king@unibas.ch

with T_{RM} cells, including high expression of programmed cell death protein 1 (PD1), P2X7R, CD69, and inducible T-cell costimulator (ICOS), and a requirement for S1PR1 and KLF2 down-regulation to develop (10, 23–26). In support of this idea, T_{FH} memory cells isolated from the spleen after lymphocytic choriomeningitis virus (LCMV) infection display a partially overlapping transcriptional signature with T_{RM} cells, consistent with the noncirculating nature of both subsets (22). However, whether different tissue-resident T_H cell subsets express conserved or distinct residency signatures compared with their lymphoid counterparts remains unresolved.

In this study, we characterized the dynamics and diversification of polyclonal $CD4^+$ T cells present in the lung and draining lymph node (dLN) after influenza, using the resolution provided by single-cell RNA sequencing (scRNA-seq) to decouple residency and functional signatures between these two tissue compartments. Our analyses of influenza-specific $CD4^+$ T cells reveal notable heterogeneity within the lung compartment, composed of two broad subsets that we designate T resident helper (T_{RH}) and T_{RM} 1 cells. T_{RH} cells persist stably and depend on expression of the transcription factor (TF) BCL6 for their differentiation. T_{RH} cells are tightly colocalized with B cells in the lung and require ongoing antigen presentation for their maintenance. $CD4^+$ T cell–intrinsic deletion of *Bcl6* at late time points after primary infection impairs the local humoral response upon reinfection. These data identify a T_{RH} subset that may be a rational target to drive potent and protective immunity in the lung mucosa.

RESULTS

Transcriptional residency signature in $CD4^+$ T cells is biased toward a T_H1 phenotype

To examine influenza-specific $CD4^+$ memory T cell populations, we performed scRNA-seq on memory $CD4^+$ T cells from the lung and lung-draining mediastinal LN of mice 30 days after infection with the PR8 strain of influenza. Virus-specific T cells were detected by tetramer staining for IA^b:NP^{311–325} and were largely protected from intravascular antibody staining for CD45 (Fig. 1A and fig. S1A), a method confirmed to identify tissue-resident cells by parabiosis experiments (27). Treatment of mice with fingolimod (FTY720) to block the egress of memory cells from lymphoid organs did not alter the total number of NP⁺ $CD4^+$ T cells isolated from the lung, indicating that this population can be sustained without input from the circulation at this time point (fig. S1, B and C). After quality control, normalization, and dimensionality reduction, the transcriptomes of lung and LN T cells were clearly distinct, and an expected small population of putative circulating cells identified by elevated expression of *S1pr1*, *Il7r*, and *Bcl2* was also detected in the lung (Fig. 1, B and C, and table S3). Differential expression analysis between lung and LN cells confirmed enrichment of previously reported $CD4^+$ residency genes (e.g., *Crem*, *Vps37b*, *Rora*, *Ramp3*, and *Tnfrsf18*) in the lung (Fig. 1C) (11, 12). To determine whether this residency signature was conserved in another viral infection model, we analyzed GP66-specific memory T cells from the liver and spleen of LCMV-infected mice at 37 days after infection (Fig. 1D). Lung-specific genes from influenza were broadly enriched in liver cells from LCMV and vice versa (fig. S1D). To better define a conserved residency signature, we examined the intersection of genes enriched in LTs and NLTs from both viral infections (Fig. 1E). This tissue-level comparison demonstrated an apparent bias in NLT to-

ward a T_H1 phenotype, with *Ccl5*, *Crip1*, *Vim*, *Nkg7*, *Id2*, and *Cxcr6* among the top shared genes (Fig. 1, E and F). Consistent with transcriptional similarities between the type I cytokine-producing $CD4^+$ and $CD8^+$ cells, lung and liver cells also showed enrichment for a multitissue signature for $CD8^+$ T_{RM} (Fig. 1G). Conversely, T_{FH} signatures including genes such as *Tcf7*, *Izumo1r*, *Dennd2d*, *Shisa5*, *Rgs10*, and *Cxcr5* were enriched in LT, in line with the conception of T_{FH} as a resident population of secondary lymphoid organs (Fig. 1, E and F) (23). The presence of T_H subset-specific genes in both NLT and LT cells reported here and elsewhere calls for a residency signature that separates function from niche (11, 12).

Transcriptional heterogeneity in the lung reveals a tissue signature distinct from T helper function

We next investigated heterogeneity within the NP-specific $CD4^+$ T cell compartment at day 30 in the lung. Unsupervised hierarchical clustering classified the cells into four populations (Fig. 2A). We found clear evidence of a T_{FH} -like phenotype in the lung: cluster 3 showed increased expression of *Sostdc1*, *Sh2d1a*, *Ppp1r14b*, *Rgs10*, *Id3*, and *Tcf7* (Fig. 2B and table S3). Although this T_{FH} -like cluster was lower in many of the genes characterizing residency compared with the other lung clusters, expression was still clearly higher compared with cells in the LN (fig. S2A). Cells in cluster 2 had a T_H1 phenotype including enrichment for *Selplg*, *Nkg7*, *Ccl5*, *Id2*, and *Cxcr6*. The similarity of these clusters to known T helper subsets was further confirmed by scoring each cell according to published T_{FH} and T_H1 memory gene sets (Fig. 2C). Elevated transcription of *S1pr1*, *Il7r*, and *Bcl2* suggested that cluster 4, distinct in principal component 2 and further distinguished by high ribosomal protein content, contained circulating cells recovered during lung processing. While cluster 1 was most similar to the T_{FH} -like cluster, it had a distinct profile characterized by enrichment for *Hif1a*, *Areg*, *Tnfrsf4*, and *Tnfrsf8* and also expressed more *Nr4a3*, suggesting ongoing major histocompatibility complex II (MHC-II) engagement and activation of the calcineurin/nuclear factor of activated T cell pathway (Fig. 2, A to C, and fig. S2B) (28). Cells in cluster 1 were also enriched for *Rora*, which is reportedly induced by extrinsic signals in the microenvironment and plays a role in negatively regulating lung inflammation during infection (29). Further examination of the differences between these two T_{FH} -like clusters was reserved for future investigation.

We next focused our analysis on NP-specific $CD4^+$ T cells from the dLN at day 30, cutting the resulting hierarchical clustering tree to four clusters (Fig. 2D). These clusters were classified similarly to those found in the lung, with a small T_H1 cluster 4 expressing *Nkg7*, *Ccl5*, *Id2*, and *Cxcr6* and tracking with ribosomal protein-rich cluster 1 along principal component 1 (PC 1); strongly T_{FH} cluster 3 with high expression of *Pdcd1*, *Sh2d1a*, and *Sostdc1*; and T_{FH} -like cluster 2 enriched for *Izumo1r*, *Tox*, and *Hif1a* (fig. S2C and table S3). As with the lung data, we scored LN cells using T_{FH} and T_H1 gene sets to further verify this classification (fig. S2D). To generate a more representative signature for lung residency, we performed differential expression analysis on each of the most phenotypically similar cluster pairs between lung and LN, for example, comparing LN T_{FH} with T_{FH} -like lung cells and LN T_H1 with T_H1 -like lung cells. The final conserved residency signature consisted only of genes that were differentially enriched in all of the noncirculating lung clusters compared with their LN counterparts (Fig. 2E). This enrichment was confirmed in our LCMV dataset and other recently published T_{RM} data (fig. S2, E to G). Subsequent removal of these conserved

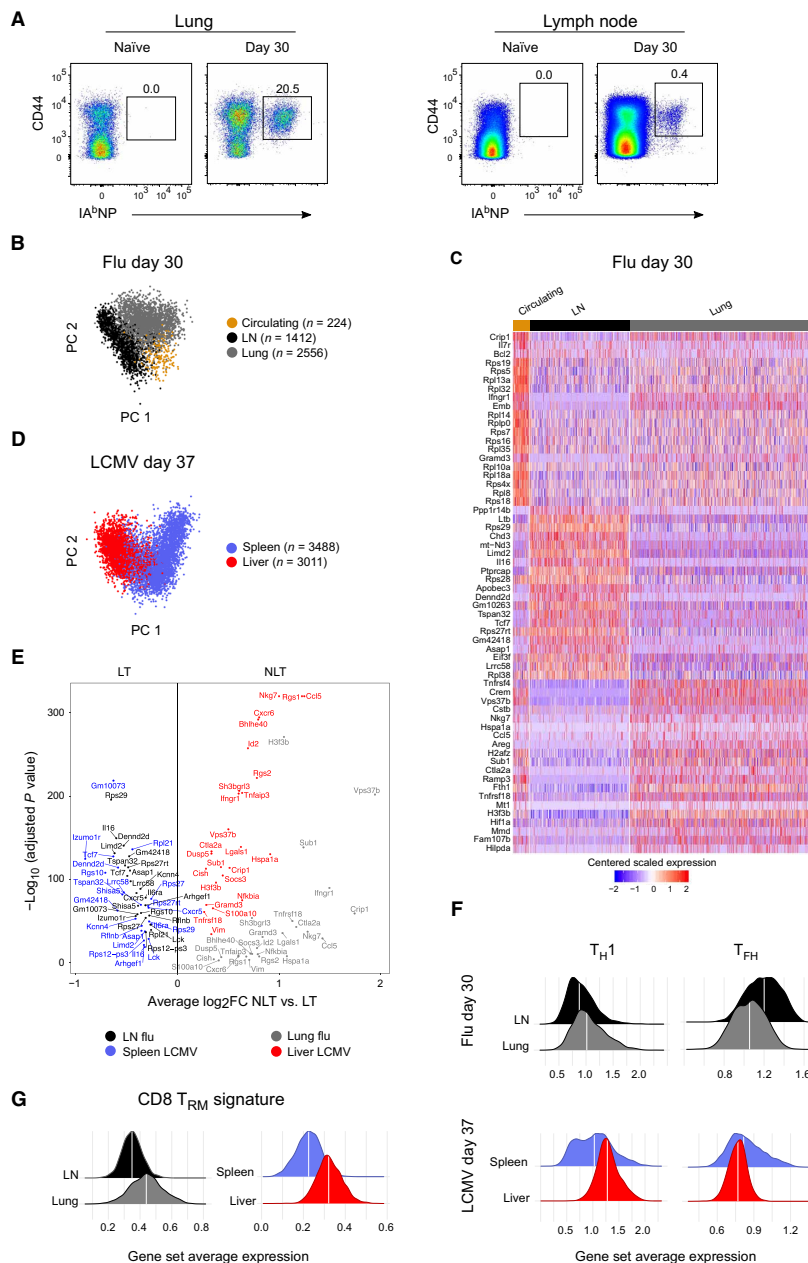


Fig. 1. Inflammatory T cells at site of infection confound a tissue-residency signature. Analysis of scRNA-seq of antigen-specific CD4⁺ T cells >30 days after viral infection. **(A to C)** PR8 influenza-infected mice 30 days after infection. **(A)** Gating strategy for NP-specific CD4⁺ T cells in lung and mLN of naïve and infected mice. **(B)** PCA showing day 30 LN and lung samples, with a putative circulating cluster identified in lung samples. **(C)** Heatmap showing centered scaled single-cell expression of top 20 genes sorted according to cluster average log₂ fold change (FC), adjusted $P < 0.05$. **(D)** PCA showing scRNA-seq of GP66-specific CD4⁺ T cells from spleen and liver of mice 37 days after LCMV infection. **(E)** Differentially expressed genes discriminating lung from LN (flu) or liver from spleen (LCMV). To enable plotting the highest y-axis values, P values of 0 were assigned the lowest nonzero P value. **(F)** Log-normalized average expression of T_{FH} and Th1 memory signatures (22). **(G)** Log-normalized average expression of combined CD8 residency signature from multiple tissues (69, 70). Sequenced cells were pooled from $n = 12$ mice in **(B)** and $n = 2$ in **(D)**.

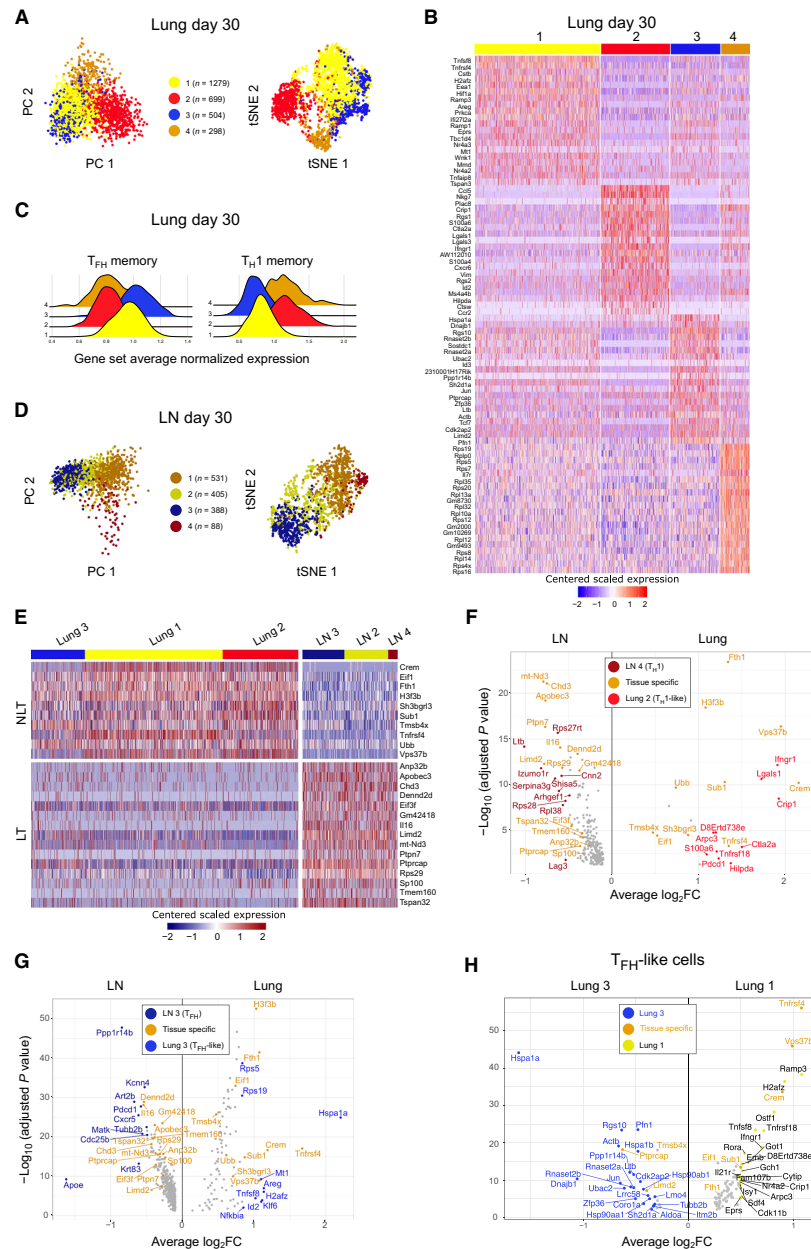
lymphoid signature in cluster 3 and enrichment of the residency signature in cluster 1, suggesting functional diversification of T_{FH}-like cells in the lung (Fig. 2H and table S3).

To gain further insight into the transcriptional regulation of distinct resident CD4⁺ T cell subsets, we next assessed TF activity using single-cell regulatory network inference and clustering (SCENIC) (30). This approach identified active regulatory activity in TFs such as hypoxia inducible factor 1 (HIF-1A), CAMP responsive element modulator (CREM), Fos-related antigen 2 (FOSL2), and known T_H1-related factors PR domain zinc finger protein 1 (PRDM1), Runt-related transcription factor 2 (RUNX2), and Runt-related transcription factor 3 (RUNX3) (fig. S2H). Cluster-specific analysis revealed that the activity of PRDM1, RUNX2, and RUNX3 was limited to T_H1-like clusters, whereas HIF-1 α activity was focused primarily in lung cluster 1, mirroring

residency genes allowed us to identify T_H subset-specific genes differentially expressed between tissue and lymphoid compartments. T_H1-like cells in the lung were enriched over their LN counterparts for genes including *Ctla2a*, *Crip1*, *Lgals1*, *Tnfrsf18*, and *Infrg1*, whereas T_{FF}-like lung cells exhibited higher expression of *Mt1*, *Hspa1a*, *Klf6*, *Tnfsf8*, and *Areg* (Fig. 2, F and G, and table S3). In addition, we compared the two T_{FF}-like clusters in the lung and found a more

gene expression of *Hif1a*. Bcl6 regulatory activity was detected in lung T_{HH}-like cluster 3 and LN T_{HH} cluster 3, along with CCAAT/enhancer-binding protein alpha (CEBPA), which is reported to inhibit both IFN- γ production and TCR-driven proliferation (fig. S2I) (31, 32). FOXP3-associated regulatory activity was enriched in lung over LN although there was only minimal expression of *Foxp3* transcript in the dataset and FOXP3 cells were not detected by fluorescence-activated

Fig. 2. Controlling for T helper function improves tissue residency signature. Analysis of scRNA-seq of NP-specific CD4⁺ T cells at day 30 after influenza infection. (A) Unsupervised hierarchical clustering of lung cells using Ward's method, visualized using PCA and t-distributed stochastic neighbor embedding (tSNE). (B) Heatmap showing centered single-cell expression of top 20 cluster-defining genes sorted according to lung cluster average log₂FC. (C) Log-normalized average expression of T_{FH} and T_H1 memory signatures (22). (D) Unsupervised hierarchical clustering of LN cells using Ward's method; PCA and tSNE. (E) Heatmap of centered scaled single-cell expression from both lung and LN showing conserved genes for NLT and LT. Genes included are differentially expressed in the tissue in all three of the noncirculating cluster pairs. (F) Genes discriminating LN T_H1 cells from lung T_H1-like cells with reference to conserved tissue-specific signature. (G) Genes discriminating LN T_{FH} cells from lung T_{FH}-like cells with reference to conserved tissue-specific signature. (H) Genes discriminating lung T_{FH}-like cluster 3 from lung T_{FH}-like cluster 1 with reference to conserved tissue-specific signature. For (B) and (E) to (H), adjusted *P* < 0.05. Sequenced cells were pooled from *n* = 12 mice.



cell sorting (FACS) in the antigen-specific compartment (fig. S2, J and K). In summary, the scRNA-seq data gathered here constitute a comprehensive picture of CD4⁺ T cell memory to influenza and disentangle residency from helper function to highlight not only conserved differences between NLT and LT but also intratissue heterogeneity and functional diversification of lung-resident T cells.

Resident CD4⁺ T cells include T_H1-like and T_{FH}-like subsets

To determine whether the heterogeneity detected by scRNA-seq was also mirrored at the protein level, we examined the phenotype of NP-specific CD4⁺ T cells using flow cytometry. At day 30 after influenza infection, NP-specific CD4⁺ T cells in the lung could be divided into two major subsets with reciprocal expression of folate receptor 4 (FR4) and P-selectin glycoprotein ligand-1 (PSGL1), markers shown to discriminate virus-specific T_H1 and T_{FH} memory cells. (Fig. 3A) (22). After viral clearance and T cell contraction, the number of cells falling within these two T resident cell subsets remained stable to at least 120 days after infection (Fig. 3B). Treatment with FTY720 at day 30 after infection did not change the number of cells in either subset, indicating that both populations are lung resident (fig. S3A). FR4^{hi}PSGL1^{low}

(hereafter T_{RH}) cells expressed many markers associated with T_{FH} effector cells including PD1, CXCR5, P2X7R, CD73, CXCR4, and ICOS (Fig. 3, C and D). FR4^{lo}PSGL1^{hi} (hereafter T_{RM}1) cells expressed lower levels of T_{FH}-associated markers but higher levels of markers associated with T_H1 cells including CXCR6, T-bet, and CD11a (Fig. 3, E and F). To examine cytokine production by NP-specific

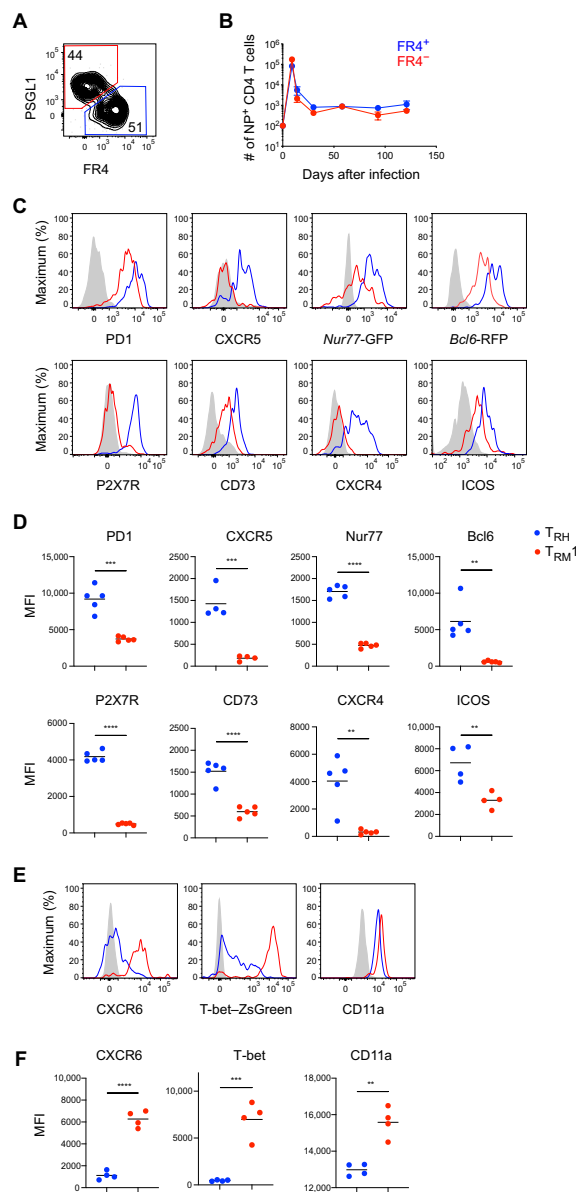


Fig. 3. Protein expression confirms T_H1 and T_{FH} phenotypes in the lung. (A) Representative flow cytometry gating for identification of T_{RM1} (red) and T_{RH} (blue) subsets in NP-specific lung-resident $CD4^+$ T cells. (B) Total numbers of $FR4^+$ and $FR4^-$ NP-specific T cells over time after influenza infection. (C to F) Histograms (C and E) and geometric mean fluorescence intensity (MFI) (D and F) of indicated phenotypic markers in T_{RH} (blue), T_{RM1} (red), and naïve $CD4^+$ T cells (gray). Data are presented as the mean \pm SEM ($n = 5$, representing two experiments) in (B). Thin lines represent mean in (D) and (F) ($n = 4$ to 5, representing two experiments). Significance was determined by unpaired Student's *t* test. *P* values are as follows: ** $P < 0.01$, *** $P < 0.001$, and **** $P < 0.0001$.

T_{RM} , we used IL-21 reporter mice and also performed intracellular cytokine staining for IFN- γ , IL-17, IL-4, and IL-2 (fig. S3, B and C). Consistent with findings in $CD44^+$ T_{RH} at memory time points, NP-specific T_{RH} cells produce significantly more IL-21 than T_{RM1} cells, whereas IFN- γ , IL-17, and IL-4 production was increased in T_{RM1} cells (27). Adoptively transferred OT-II TCR transgenic cells activated by infection with PR8-OVA2 generated mostly T_{RM1} cells (fig. S3, D and E). These data are consistent with earlier reports using TCR transgenic strains that primarily identified T_H1 -like memory $CD4^+$ T cells in the lung after influenza infection. Together, scRNA-seq and flow cytometry confirm the presence of T_{RM1} (T_H1 -like) and T_{RH} (T_{FH} -like) cells in the lung and underscore the importance of studying polyclonal $CD4^+$ T cell responses to understand T cell-dependent immunity.

Resident $CD4^+$ T cell subsets arise asynchronously

To further investigate the kinetics of T_{RM1} and T_{RH} cell differentiation in the lung, we next characterized the phenotype of NP-specific $CD4^+$ T cells at multiple time points after influenza infection. At day 9, most of the $CD4^+$ T cells in the lung had high expression of PSGL1 and bimodal expression of $FR4$ and were negative for T_{FH} markers CXCR5 and PD1 (Fig. 4, A and B). By day 14 after infection, a small proportion of T_{RH} cells emerged in the lung, followed by a clear separation of T_{RM1} and T_{RH} cell subsets by day 30 (Fig. 4A). In contrast to the lung, fully differentiated NP-specific T_{FH} effector cells ($CXCR5^+PD1^+$) were clearly detected in the mediastinal LN at day 9 (Fig. 4B). To understand whether LN T_{FH} effectors give rise to lung T_{RH} cells, we began continuously treating mice with FTY720 between days 9 and 30 to prevent the migration of LN-primed T_{FH} cells into the lung. At day 30 after infection, the number of T_{RH} cells in FTY720-treated mice was equivalent to the number of T_{RH} cells in phosphate-buffered saline (PBS)-treated mice, indicating that full differentiation of lung T_{RH} cells can be independently completed in the lung (Fig. 4C).

To investigate the transcriptional regulation of resident T cell generation, we expanded the scRNA-seq analysis to include NP-specific $CD4^+$ T cells from days 9 and 14 after infection. Cells were clearly discriminated by time point and tissue in reduced dimensions, with day 9 cells appearing more distinct compared with days 14 and 30 (Fig. 3D and fig. S4A). Day 9 lung cells exhibited the lowest per-cell gene counts of any sample, which may reflect their susceptibility to apoptosis under inflammatory conditions. Nevertheless, hierarchical clustering revealed a group of cells (cluster 1) enriched for *Stat4*, *Il7r*, *Icos*, *S1pr1*, and *Selpg*, which may represent recent immigrants from the lymph node (LN) (Fig. 4E). Consistent with the FACS analysis, we observed an enrichment of T_H1 -like characteristics at day 9, whereas T_{RH} cells were more prominent at day 30 (Fig. 4F). To investigate the expression of *Izumo1r* and *Selpg*, encoding the proteins $FR4$ and PSGL1, respectively, we used imputed values, replacing zeros with values estimated from similar cells. In parallel with FACS expression of these markers, day 9 lung cells were *Selpg*^{hi} and *Izumo1r*^{lo}, whereas *Selpg*^{lo} and *Izumo1r*^{hi} T cells emerged at day 14 and were increased by day 30 (fig. S4B). In contrast, most of the cells in the LN were *Izumo1r*^{hi} at all time points. TF activity according to SCENIC analysis tracked the trend from T_H1 -like at day 9 (*Runx2*, *Runx3*, and *Prdm1*) to T_{FH} -like at day 30 (*Lef1* and *Pou2af1*) (Fig. 4G) (33, 34). In addition, a consistent subset of genes associated with lung residency (*Tnfrsf4*, *Vps37b*, *Fth1*, and *Crem*) was detected by differential expression analysis

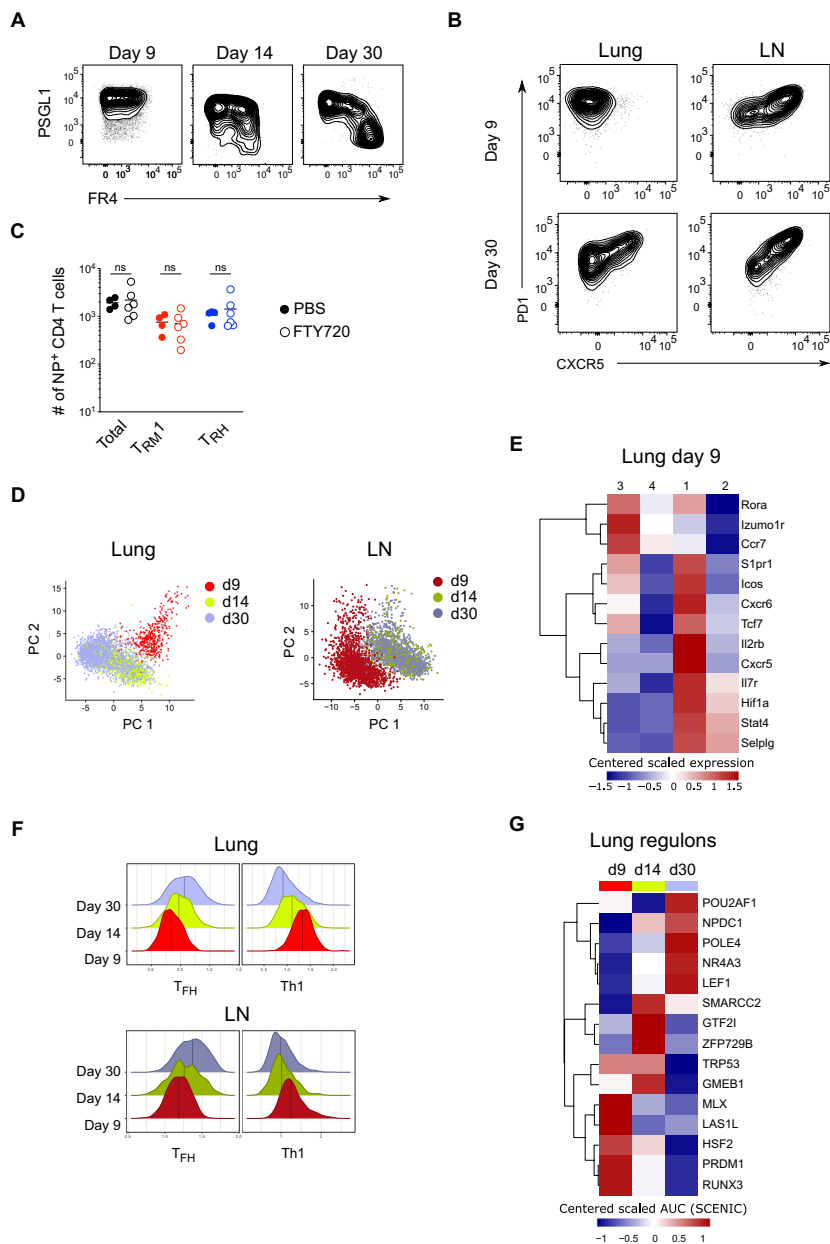


Fig. 4. Progressive differentiation of resident CD4⁺ T cell subsets. (A and B) Representative flow cytometry plots of FR4 and PSGL1 expression on lung NP-specific tissue-resident CD4⁺ T cells (A), and CXCR5 and PD1 expression on NP-specific CD4⁺ T cells in lung and mLN at indicated time points after PR8 infection (B). (C) NP-specific total CD4⁺ T cells, T_{RM1}, and T_{RH} cell numbers in control and FTY720-treated mice. ns, not significant. Data in (C) represent two experiments with $n = 4$ to 6 mice. Statistical significance was determined by unpaired Student's t test. Thin lines represent mean. $P < 0.05$ is considered significant. (D to G) scRNA-seq of pooled cells from $n = 3$ (day 9), $n = 4$ (day 14), and $n = 12$ (day 30) mice. (D) PCA showing time point by tissue. (E) Centered scaled average expression of select genes in lung at day 9. (F) Log-normalized average expression of published T_{FH} and T_{H1} signatures by time point and tissue (22). (G) Centered scaled average area under curve (AUC) calculated with SCENIC showing top five differentially active TFs (regulons) in lung by time point. Adjusted $P < 0.01$.

between lung and LN at each separate time point (fig. S4C). Other genes associated with residency at day 30 (*Gch1*, *Hif1a*, *Selenok*, and *Prkca*) appeared more gradually, potentially reflecting the dynamics of signal access in the tissue microenvironment and the relatively late development of T_{RH} compared with T_{RM1} cells (fig. S4D). A signature for T cell memory was enriched at days 14 and 30, whereas an effector signature dominated at day 9 (fig. S4E). In summary, high expression of PSGL1 by most of the CD4⁺ T cells at day 9 likely reflects their recent migration into the inflammatory lung environment; this time point is dominated by T_{RM1} cells, whereas T_{RH} cells emerge gradually at later time points.

T_{RH} cell generation requires B cells and T cell-intrinsic Bcl6

Given the phenotypic and transcriptional similarities between lung T_{RH} cells and lymphoid homing T_{FH} cells, we hypothesized that T_{RH} cells may depend on B cells and intrinsic Bcl6 expression for their differentiation (24, 35). To test a requirement for B cells, we injected mice with anti-CD20 1 week before influenza infection. Thirty days after influenza infection, both the proportion and number of T_{RH} cells were decreased in the lungs of B cell-depleted mice, correlating with a strong reduction in resident and circulating B cell numbers in the lung (Fig. 5, A to C, and fig. S5A). To assess the contribution of T cell-intrinsic Bcl6 expression, we generated irradiated bone marrow chimeras transplanted with a mixture of congenically marked wild type (CD45.1⁺) and *Bcl6*^{flx/flx} × CD4^{Cre} (*Bcl6*^ΔCD4⁺ and CD45.2⁺) bone marrow. Thirty days after influenza infection, Bcl6-deficient CD4⁺ T cells were incapable of differentiating into lung T_{RH} cells, demonstrating their dependence on intrinsic Bcl6 expression (Fig. 5, D and E). In the absence of Bcl6, the proportions of T_{RM1} cells in the lung and non-T_{FH} cells in the dLN were also significantly reduced compared with wild-type cells, suggesting that Bcl6 also plays a role in the expansion of these cells (Fig. 5E and fig. S5, B and C) (36). Together, these data indicate that similar to lymphoid T_{FH} cells, T_{RH} cells in the lung require B cells and T cell-intrinsic Bcl6 expression for their generation.

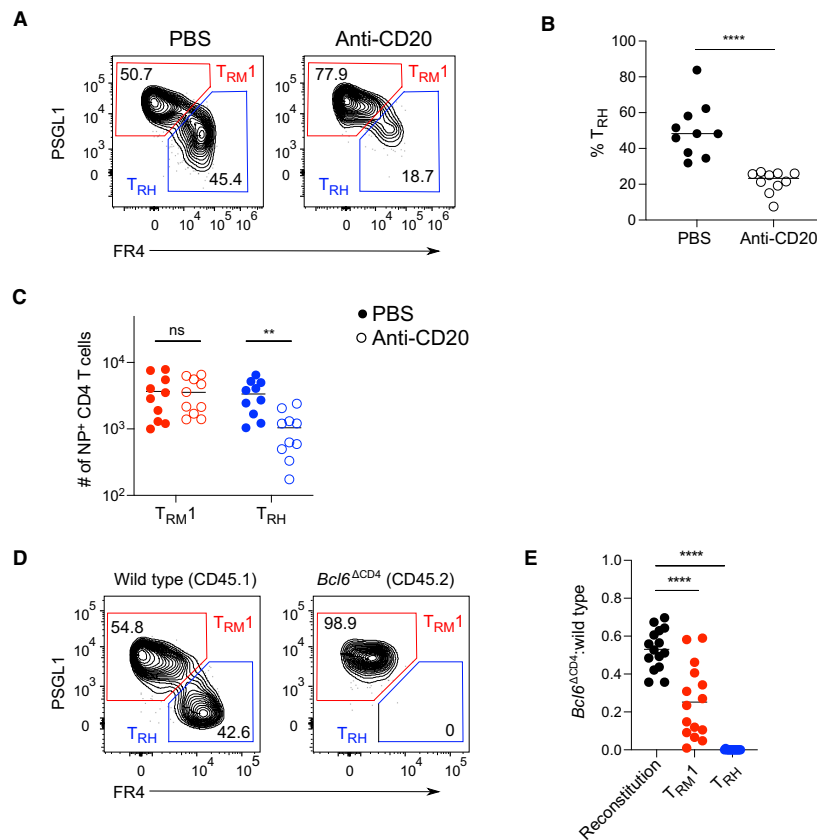


Fig. 5. T_{RH} cell generation requires B cells and T cell-intrinsic *Bcl6*. (A to C) Mice were treated with PBS or anti-CD20 starting 1 week before PR8 infection and euthanized 30 days later. Representative flow cytometry plot of NP-specific T cells (A) frequency of T_{RH} (B) and total number of NP-specific T_{RM1} and T_{RH} cells (C). (D and E) Irradiated mice were reconstituted with *Bcl6* $^{\Delta CD4}$ (CD45.2) and WT (CD45.1) bone marrow cells. Mice were infected with PR8 and euthanized 30 days later. (D) NP-specific T cells in control and *Bcl6*-deficient subsets. (E) *Bcl6* $^{\Delta CD4}$:wild-type ratio in CD4 $^{+}$ T cells after reconstitution from blood (before infection), T_{RM1} , and T_{RH} . Thin lines represent mean in (B) and (C) ($n = 10$, pooled from two experiments) and (E) ($n = 15$, pooled from three experiments). Significance was determined by unpaired Student's *t* test. *P* values are as follows: ** $P < 0.01$ and **** $P < 0.0001$.

CD4 $^{+}$ T_{RH} cells localize with B cells in lymphoid clusters in the lung

Influenza infection leads to the development of ectopic clusters of B cells and T cells in the lung, known as inducible bronchus-associated lymphoid tissue (iBALT), that can persist to at least 100 days after infection (37, 38). The formation of iBALT supports primary T and B cell proliferation and local antibody production and is thought to provide a specialized niche for the reactivation of lung immunity during challenge infection. Given their dependence on B cells, we hypothesized that T_{RH} cells may localize together with B cells in iBALT. To examine this, we assessed the spatial distribution of T_{RM1} and T_{RH} cells in the lungs of influenza-infected *Tbx21* (encoding T-bet) and *Bcl6* reporter mice, respectively. Using flow cytometry, we initially confirmed that infection-induced polyclonal CD4 $^{+}$ T cells in the lung largely phenocopy NP-specific T_{RM1} and T_{RH} cells (fig. S6A). Gating on the minimal markers CD4 and *Tbx21*

or CD4 and *Bcl6*, revealed that more than 85% of these cells fall within the T_{RM1} or T_{RH} compartments, respectively (fig. S6, B and C). We next stained lung sections from *Tbx21* or *Bcl6* reporter mice with CD4 and B220 to identify iBALT regions by spinning disk confocal microscopy (Fig. 6A). T cell localization was quantified using two separate pipelines: one manually guided and one leveraging machine learning (Fig. 6, B to D). The number of Tbet hi or Bcl6 hi CD4 $^{+}$ cell objects inside and outside of the B cell clusters was calculated after normalization by iBALT and tissue slice volumes. Bcl6 hi CD4 $^{+}$ cells were enriched inside of iBALT areas compared with Tbet hi CD4 $^{+}$ cells, whereas Tbet hi CD4 $^{+}$ cells were more prevalent outside of iBALT (Fig. 6, C and D). The preferential colocalization of T_{RH} cells and B cells in the lung indicates that iBALT may provide a homeostatic niche for T_{RH} cell survival.

Maintenance of T_{RH} cells requires antigen presentation

Influenza infection has been shown to induce a depot of viral antigen in the lung, which can be transported to and presented in the dLN to support CD4 $^{+}$ memory T cell accumulation (39). High expression of Nur77 by T_{RH} cells (Fig. 3, C and D) suggested that they might be responding to ongoing antigen presentation in the lung. To determine whether T_{RH} cells are actively proliferating at late time points, we administered bromo-2-deoxyuridine (BrdU) in the drinking water of influenza-infected mice starting at day 50 after influenza infection and analyzed 2 weeks later. Given the low number of NP-specific T cells that can be recovered from the lung after intra-

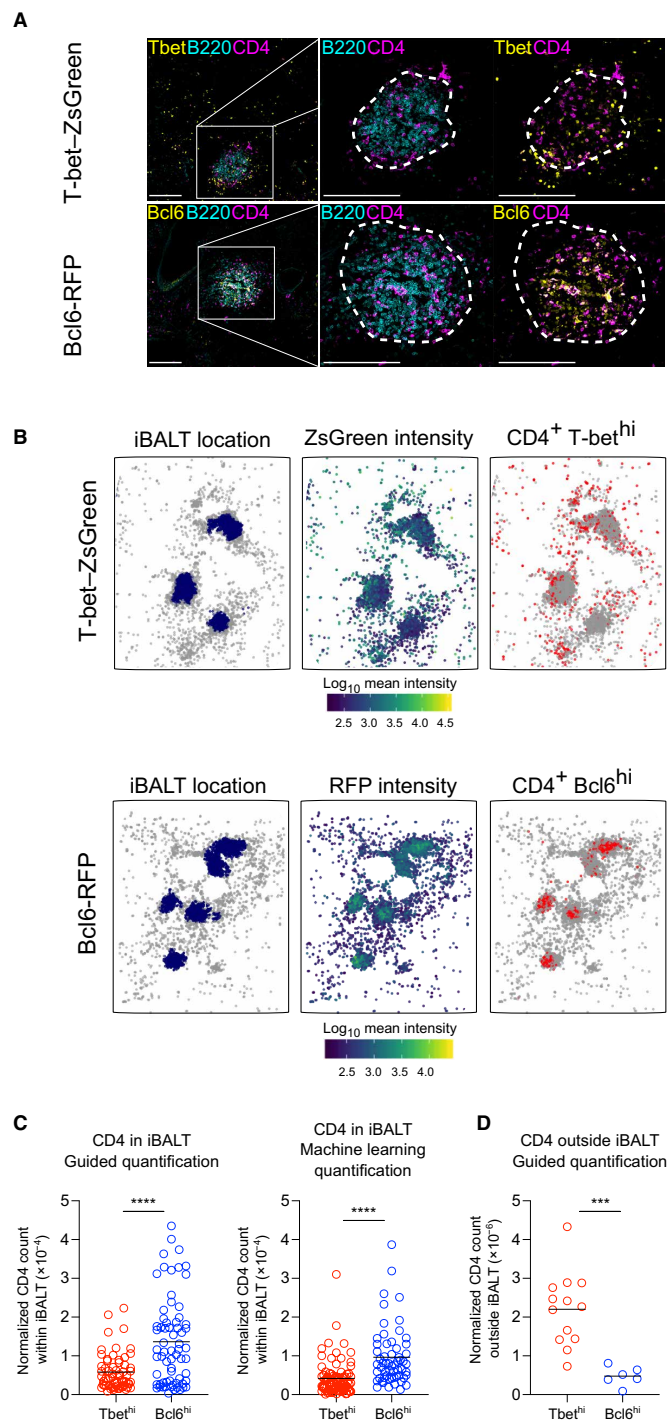
nuclear staining for BrdU, we analyzed both NP $^{+}$ and CD4 $^{+}$ CD44 $^{+}$ T cells that were negative for intravascular staining with CD45. After BrdU treatment, CD4 $^{+}$ T_{RM} cells took up significantly less BrdU compared with “circulating” lung CD4 $^{+}$ T cells that stained positively for intravenous anti-CD45 (Fig. 7, A and B). Comparison of BrdU uptake by T_{RH} and T_{RM1} cells, however, revealed similar levels of proliferation between these two subsets, despite higher expression of Nur77 by lung T_{RH} cells (Fig. 7C). To further determine whether antigen presentation is required to sustain resident CD4 $^{+}$ T cells, we generated MHC-II $^{fllox/fllox}$ x UBC $^{Cre-ERT2}$ mice (MHC-II $^{\Delta UBC-ERT2}$) to induce the widespread deletion of MHC-II at late time points after infection. MHC-II $^{\Delta UBC-ERT2}$ and MHC-II $^{fl/fl}$ control mice were infected with influenza followed by tamoxifen administration beginning at least 40 days after infection (Fig. 7D). Seven days after the last tamoxifen treatment, both resident and circulating B cells isolated from the lungs of MHC-II $^{\Delta UBC-ERT2}$ mice expressed about

Fig. 6. CD4⁺ T_{RH} cells localize in lung B cell clusters. (A) Representative X40 immunofluorescence confocal images from T-bet-ZsGreen and Bcl6-RFP reporter mice, 30 to 60 days after infection, stained with the indicated markers. Scale bars, 200 μ m. (B) Quantified representations of segmented CD4⁺ objects, showing iBALT location, log mean TF intensity per object, and location of Tbet^{hi} (above) or Bcl6^{hi} (below) objects. (C) Count of Tbet^{hi} and Bcl6^{hi} CD4⁺ T cell objects inside B220⁺ iBALT clusters, normalized by iBALT volume, analyzed by Mann-Whitney-Wilcoxon test. Segmentation performed in Imaris (left) or with machine learning algorithm (right). Each dot represents one iBALT. $n = 2$ mice per condition. (D) Count of Tbet^{hi} and Bcl6^{hi} CD4⁺ T cell objects outside B220⁺ iBALT clusters, normalized by tissue volume less iBALT volume, analyzed by Mann-Whitney-Wilcoxon test. Segmentation performed in Imaris. Each dot represents one tissue slice. $n = 2$ mice per condition. P values are as follows: *** $P < 0.001$ and **** $P < 0.0001$.

10-fold lower levels of MHC-II compared with control antigen-presenting cells (fig. S7, A and B). Although the number of B cells in the lung was not affected by MHC-II deletion, the proportion and number of T_{RH} but not T_{RM}1 cells were significantly decreased (Fig. 7, E to G, and fig. S7, C and D). To determine whether dependency on MHC-II decreases at later time points, we repeated these experiments, deleting MHC-II ~100 days after primary infection. We observed that deletion at this very late time point does not have an impact on either T_{RH} or T_{RM}1 cell numbers (Fig. 7H). These data indicate that some of the T_{RH} cells present at earlier time points (up to at least 40 to 50 days after infection) are most likely responding to ongoing antigen presentation, despite their low rate of turnover (Fig. 7C). In contrast, T_{RH} cells no longer depend on MHC-II expression at day 100+ after infection despite their clear presence in iBALT in control mice at this late time point (fig. S7E).

T_{RH} cells are multipotent and support local antibody production during rechallenge

T_{FH} memory cells express high levels of *Tcf7*, a TF associated with self-renewal and stem-like properties, and were recently shown to generate multiple cell fates after recall infection (22). The similarities between T_{RH} cells and T_{FH} cells



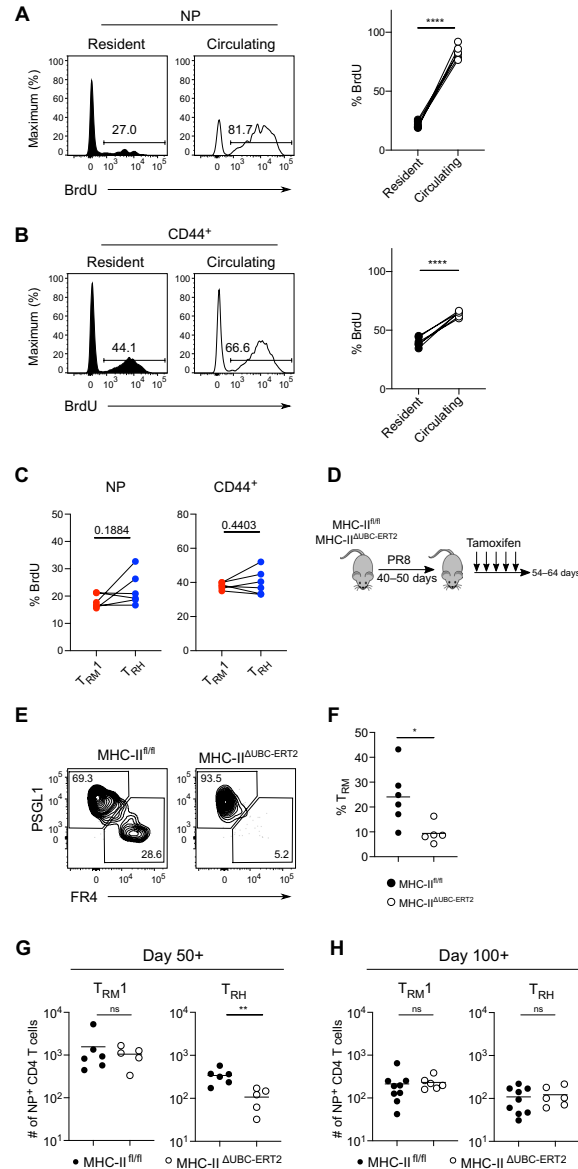


Fig. 7. Maintenance of T_{RH} cells requires antigen presentation. (A and B) Histograms and frequency of BrdU⁺ cells in NP-specific (A) and CD44⁺ (B) lung-resident and circulating cells at day 65 after PR8 infection. (C) Frequency of BrdU⁺ cells in T_{RM}1 and T_{RH}. (D) Infected MHC-II^{fl/fl} and MHC-II^{ΔUBC-ERT2} mice were analyzed 1 week after inducible deletion. (E and F) Flow cytometry plots (E) and T_{RH} frequency (F) in MHC-II^{fl/fl} and MHC-II^{ΔUBC-ERT2} mice. (G and H) Total number of NP-specific T_{RM}1 and T_{RH} from infected MHC-II^{fl/fl} and MHC-II^{ΔUBC-ERT2} mice that were treated with tamoxifen starting at days 40 to 50 (G) or day 100 (H) after infection and analyzed 1 week later. Data in (A) to (C) were analyzed by paired *t* tests (*n* = 5, representing three experiments). Data in (F) to (H) were analyzed by unpaired Student's *t* test (*n* = 3 to 6, representing two experiments). Thin lines represent mean. *P* values are as follows: **P* < 0.05, ***P* < 0.01, and *****P* < 0.0001.

prompted us to investigate our scRNA-seq data for potential developmental trajectories among lung-resident T cells. For this purpose, we chose Potential of Heat-diffusion for Affinity-based Transition Embedding (PHATE) for dimensionality reduction, as it is designed to retain global structure and condense information into two dimensions, and slingshot for trajectory inference and pseudotime calculation through the clusters (40, 41). We chose T_{RH} cluster 3 as the least differentiated starting point for the trajectories because it most closely resembles stem-like, *Tcf7^{hi}Id3^{hi}* T_{FH} cells. We observed a bifurcating trajectory starting with cluster 3, branching at the *Hif1a^{hi}* cluster 1 and terminating in the circulating cluster 4 and the T_{RM}1 cluster 2 (Fig. 8A). Imputed expression of genes emblematic for each terminal cluster could then be followed along developmental pseudotime (Fig. 8B). While we cannot exclude the possibility of circulating cells entering the lung as a starting point for a trajectory, enrichment of *Slpr1* and *Ccr7* in cluster 4 could also mark a “draining” population of cells that are poised to exit to the LN. These data raise the possibility that T_{RH}, like T_{FH}, may be multipotent after recall infection.

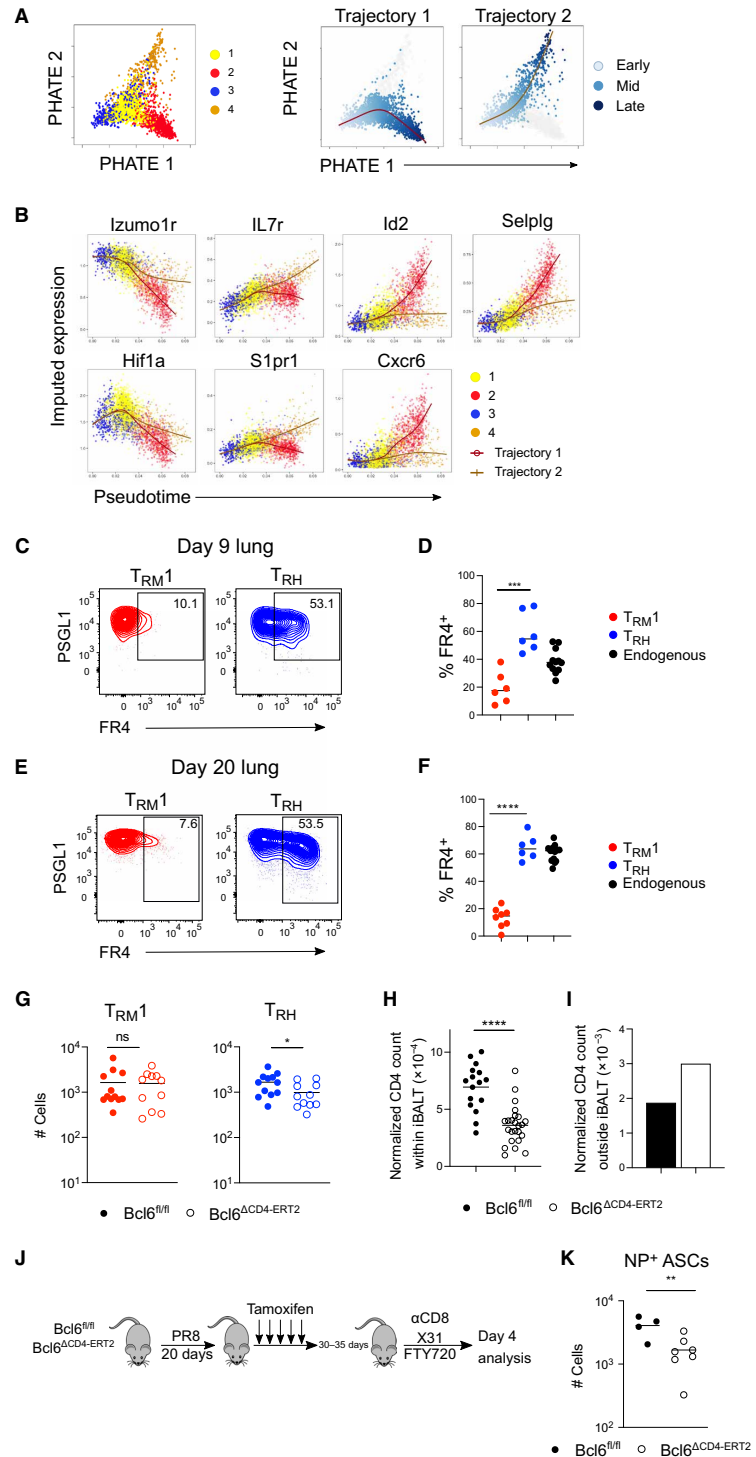
To test this experimentally, we adoptively transferred T_{RH} and T_{RM}1 cells from influenza-infected mice into congenic recipients followed by recall infection with PR8 influenza. Here, we observed a higher proportion of transferred T_{RM}1 cells in the lung compared with T_{RH} cells, whereas T_{RH} cells were more highly represented in the spleen; only a very small proportion of either subset migrated into the LNs (fig. S8A). At days 9 and 20 after challenge infection, both transferred T_{RM}1 and T_{RH} cells maintained high expression of PSGL1, similar to endogenous NP-specific cells at this time point (Fig. 8, C and D). Although most of the transferred T_{RM}1 cells remained negative for FR4 expression, transferred T_{RH} cells gave rise to both FR4^{hi} and FR4^{lo} secondary effectors in the lung as well as both CXCR5⁺PD1⁺ T_{FH} and non-T_{FH} cells in the dLN (sufficient cell numbers in dLN only at day 20) (Fig. 8, C to F, and fig. S8, B and C). These data demonstrate that similar to T_{FH} memory cells (22), T_{RH} cells retain the capacity to generate multiple effector subsets, whereas T_{RM}1 cells appear to be more terminally differentiated at these time points.

T_{FH} memory cells are reported to provide accelerated help to memory B cells during a challenge infection, in a T cell-intrinsic, Bcl6-dependent manner (42, 43). As influenza infection can induce the differentiation of resident memory B cells in the lung, we next assessed the contribution of T_{RH} cells to secondary humoral immunity in the tissue (44). To do this, we generated *Bcl6^{fl/fl} × CD4^{Cre-ERT2}* (*Bcl6^{ΔCD4-ERT2}*) mice that allow for tamoxifen-inducible deletion of Bcl6 in CD4⁺ T cells. *Bcl6^{ΔCD4-ERT2}* and *Bcl6^{fl/fl}* control mice were infected with influenza and treated with tamoxifen starting at 21 days. Before secondary infection, late deletion of Bcl6 in CD4⁺ T cells led to a mild decrease in the number of NP-specific T_{RH} cells, whereas T_{RM}1 cell numbers were not affected (Fig. 8G). To understand whether Bcl6 deletion had an impact on CD4⁺ resident T cell maintenance within iBALT, we examined the lungs of *Bcl6^{ΔCD4-ERT2}* and control mice by histology. While CD4⁺ cells were abundant in dense areas of strong B220 signal in control mice, Bcl6 deletion led to significantly reduced colocalization of these cell types, despite the maintenance of large clusters of B220⁺ cells (Fig. 8H and fig. S8D). In contrast, normalized CD4⁺ cell counts outside of iBALT⁺ areas were higher with Bcl6 deletion (Fig. 8I).

As iBALT can act as a site for the local priming of pulmonary immune responses, we next examined whether Bcl6 deletion in

Fig. 8. T_{RH} cells are plastic and promote local antibody production during re-infection with the X31 influenza strain. (A and B) scRNA-seq analysis from lung day 30. (A) PHATE dimensionality reduction used as input to slingshot trajectory inference. PHATE colored by cluster (left) and pseudotime (right). (B) Imputed expression of selected genes across pseudotime and two trajectories. (C to F) Representative plots of $FR4^+$ cells in rechallenged T_{RM1} and T_{RH} recipients in lung at day 9 (C), frequencies in (D), at day 20 (E), and frequencies in (F). (G) Total numbers of NP-specific T_{RM1} and T_{RH} . (H) Count of $CD4^+$ T cell objects inside B220 $^+$ iBALT clusters, normalized by iBALT volume, and analyzed by Mann-Whitney-Wilcoxon test. Imap segmentation. Each dot represents one iBALT. (I) Count of iBALT-external $CD4^+$ T cell objects across all images, normalized by total tissue volume less iBALT volume. $n = 2$ mice. (J) PR8-infected, tamoxifen-treated $Bcl6^{fllox/flox}$ and $Bcl6^{\Delta CD4-ERT2}$ memory mice were treated with FTY720 and α -CD8 before X31 re-challenge and analyzed 4 days later. (K) Number of NP-specific IgG antibody-secreting cells (ASC) per mouse lung. Data in (D) ($n = 6$, pooled from two experiments), (F) ($n = 6$ to 8, pooled from two experiments), (G) ($n = 11$ to 12, pooled from three experiments), and (K) ($n = 4$ to 7, representing two experiments) were analyzed by unpaired Student's t test. Thin lines represent mean. P values are as follows: * $P < 0.05$, ** $P < 0.01$, *** $P < 0.001$, and **** $P < 0.0001$.

$CD4^+$ T cells would lead to less efficient secondary B cell responses. To test this, we further treated $Bcl6^{\Delta CD4-ERT2}$ and control mice with FTY720 and a CD8 depleting antibody followed by challenge infection with heterotypic X31 influenza (X31) (Fig. 8J). This approach allowed us to examine the impact of $Bcl6$ deletion in lung $CD4^+$ T cells independently from circulating lymphoid T and B cells, as well as memory CD8 T cells, which might otherwise lead to early viral clearance. Antibodies generated after PR8 influenza infection do not neutralize X31 infection, whereas $CD4^+$ T cells responding to the conserved viral epitopes can support the production of nonneutralizing antibodies that contribute to viral clearance upon heterotypic challenge (45–47). Before recall infection, no differences in NP antibody production were observed between $Bcl6^{\Delta CD4-ERT2}$ and control mice (fig. S8E). Four days after recall with X31 influenza, however, $Bcl6^{\Delta CD4-ERT2}$ mice had a fourfold decrease in NP-specific antibody-secreting cells in the lung (Fig. 8K and fig. S8F). While we did not detect a significant difference in viral load between the groups (fig. S8G), our depletion of CD8 T cells may have disrupted the synergy between CD8 memory T cells and non-neutralizing antibodies, previously described to contribute to lowered viremia during heterotypic challenge (47). Together, these data indicate that T_{RH} cells support mucosal antibody production during heterologous challenge.



DISCUSSION

In this study, we used scRNA-seq to characterize the dynamics, heterogeneity, and transcriptional regulation of lung-resident CD4⁺ T cells after influenza infection. In contrast to previous studies that mainly identified T_H1 memory cells with transcriptional resemblance to CD8 T_{RM} cells, our data reveal the presence of long-lived T_{RH} cells with phenotypic and functional similarities to lymphoid T_{FH} cells. In agreement with these earlier studies, many of which tracked monoclonal T cell responses with specificity to a single antigen, we did not observe T_{RH} differentiation by OT-II T cells responding to PR8-OVA, indicating that not all TCR lines recapitulate the heterogeneity of polyclonal T cell populations. Our study identifies phenotypically similar cell clusters in both LN and lung alongside a consistent signature of residency in the lung. The predominance of type 1 responses to viral infection in barrier tissues, the averaging effect of bulk studies, and the paucity of antigen-specific polyclonal models to date likely contributed to previously obscuring a general residency signature.

The T_{RH} population we identified in the lung was itself heterogeneous, with FR4^{hi}PSGL1^{low} cells clustering into two groups transcriptionally. Regulation of these two subsets by Bcl6 and HIF-1 α , respectively, is consistent with a previous study showing that Bcl6 can repress gene programs activated by HIF-1 α in effector CD4⁺ T cells (48). While HIF-1 α has been alternately reported to repress or promote T_{FH} effector cell differentiation (49, 50), our data reveal a gradual up-regulation of HIF-1 α in CD4⁺ T_{RM} cells, coincident with T_{RH} cell differentiation, localization in iBALT, and resolution of the inflammatory/hypoxic phase of infection. HIF-1 α expression might therefore reflect differences in T_{RH} cell localization and the dynamics of access to environmental signals. In addition, expression of *Areg*, encoding the cytokine amphiregulin that promotes epithelial cell proliferation, may also point to a role in tissue homeostasis (51). Amphiregulin produced by regulatory T cells was previously shown to prevent excessive inflammation in the lung at very early time points after primary infection (52). Of interest will be determining whether amphiregulin produced by resident CD4⁺ T cells plays a similar role during recall infection, as a means to balance antipathogen immunity with tissue integrity and niche preservation.

Our data highlight the importance of B cell interactions for the generation of the T_{RH} compartment. B cells have been previously implicated in the differentiation of T_H1 T_{RM} cells after intranasal LCMV infection, where they initially restrained T_H1 cell residency but later promoted their long-term persistence (53). Although these results are consistent with our observation that T_{RM}1 cells differentiate earlier compared with T_{RH} cells, we did not observe any impact on T_{RM}1 cell numbers in B cell-depleted mice. We additionally determined that T_{RH} cells require intrinsic Bcl6 expression. The absence of Bcl6 at the start of infection led to complete ablation of the T_{RH} compartment as well as a significant decrease in T_{RM}1 cells. These data are consistent with a previous study looking at CD4⁺ T cell differentiation in the lung during tuberculosis infection (54). Here, the authors reported that both Bcl6 and ICOS signaling are required for the development of lung-resident T cells with memory-like properties that mediate superior protection compared with more terminally differentiated lung T_H1 cells. Taken together with our observations, these findings suggest that T_{RH} cells maintain the plasticity to differentiate into T_H1 effectors after challenge infection, an idea that is supported by our trajectory analysis and adoptive transfer experi-

ments. A clear limitation of our approach, however, is that we cannot exclude the possibility that transferred T_{RH} cells are further primed in the dLN or spleen before their recruitment to the lung. Nevertheless, the apparent ability of T_{RH} cells to differentiate into multipotent effectors is similar to stem-like T_{FH} memory cells, which were recently reported to generate diverse effectors after secondary infection (22).

Influenza infection results in the development of iBALT, a tertiary lymphoid structure in the lung that can act as an immunological hub, promoting rapid and localized immune responses after secondary infection (55). Compared with T_{RM}1 cells, we detected close localization of T_{RH} cells and B cells within iBALT. The importance of T-B cell interactions in tertiary lymphoid structures has been highlighted in many immune contexts, including tuberculosis infection, where the presence of iBALT correlates with bacterial control, as well as within the tumor microenvironment, where the presence of such structures predicts improved patient outcome (56–60). Our data provide additional insight into these studies, demonstrating T_{RH} cell dependency on Bcl6 expression for their maintenance within iBALT. The decreased number of iBALT-localized CD4⁺ T cells observed after late Bcl6 deletion may be due to lower expression of ICOS, which normally promotes T cell interactions with inducible T-cell costimulator ligand (ICOSL)-expressing B cells (61). Further experiments will help clarify whether Bcl6 is also required for the long-term maintenance of CD4⁺ memory cells or their localization with B cells in other niches such as the tumor microenvironment or in autoimmune diseases such as rheumatoid arthritis, where T_{FH} cells are implicated in health and pathology, respectively.

The traditional requirement that a memory cell must be able to exist independently of antigen has come under increasing scrutiny, in part due to the persistence of antigen depots, for example, by follicular dendritic cells or lymphatic endothelial cells in secondary or tertiary lymphoid structures (62–64). Reduction of T_{RH} but not T_{RM}1 numbers at day 50 after infection after MHC-II deletion suggests a partial dependence on antigen persistence at this time point. However, MHC-II deletion at day 100+ after infection had no effect on T_{RH} numbers, despite the persistence of iBALT in control animals at this late time point. We use the term memory for these cells because of (i) their persistence to very late time points after infection, (ii) their relative quiescence, and (iii) their enrichment for memory T cell transcriptional signatures.

Last, our data demonstrate an important role for resident CD4⁺ T cells in orchestrating local humoral responses during recall infection. This is reciprocal to the relationship between memory T_{FH} cells and memory B cells present in secondary lymphoid organs, where antigen-specific memory B cells induce Bcl6 expression in cognate T_{FH} cells, leading to more efficient T cell help and acceleration of humoral immune responses (42, 43). Our experiments suggest that T_{RH} cells are poised to provide help due to their tight localization with B resident (memory) cells. Thus, the targeted induction of lung T_{RH} cells may serve as the basis for rational design of a universal influenza vaccine. Alternatively, it is possible that by promoting the recall of memory B cells to prior influenza infections, T_{RH} cells may contribute to original antigenic sin and the subsequent impairment of host immunity. In any event, taken together with the observation that T_{RH} cells maintain the capacity to generate T_H1 effectors, these findings have implications for reinvigorating or dampening T cell responses in other contexts where tertiary lymphoid structures are found.

MATERIALS AND METHODS

Study design

The aim of this study was to characterize the underlying attributes and transcriptional features of CD4⁺ lung-resident T cells generated upon influenza infection. We used the murine influenza infection model and MHC-II tetramers, intravascular staining, and FTY720 to identify antigen-specific resident CD4⁺ T cells. Details of the mouse models and individual experiment types are listed below or in figure legends. Infected mice were randomly assigned to treatment versus control groups. Analysis of the experimental data was conducted in an unblinded manner.

Mice

Male and female mice C57BL/6J (CD45.2), B6.SJL-Ptprc^aPepc^b/BoyJ (CD45.1), C57BL/6-Tg(Nr4a1-EGFP/cre)820Khog (Nur77 GFP), Bcl6^{tm1.1Cdon} [Bcl6 red fluorescent protein (RFP)], Tg(*Tbx21*-ZsGreen)E3ZJfz (T-bet-ZsGreen), B6.129X1-H2-Ab1^{tm1Koni}/J B6.Cg-Ndori^{Tg(UBC-Cre/ERT2)1Ejb}/1J (MHCIIA^{UBC-ERT2}) (UBC-ERT2 mice were provided by T. Derfuss, University of Basel), B6.Bcl6^{tm1.1Mito}-Tg(Cd4-cre)1Cwi (Bcl6Δ^{CD4}), B6.Bcl6^{tm1.1Mito} Cd4^{tm1(cre/ERT2)Thb} (Bcl6Δ^{CD4-ERT2}, Bcl6 fl/fl mice were provided by T. Takemori, RIKEN, The Institute of Physical and Chemical Research), B6.Cg-Tg(TcraTcrb)425Cbn/J (OT-II), and IL-21 GFP (IL21^{tm1Nutt}) (provided by S. Nutt, Walter and Eliza Hall Institute of Medical Research) were used. Mice in each experiment were same-sex littermates, 6 to 12 weeks old at the start of experiment, maintained and bred in the specific pathogen-free animal facility at the University of Basel. All animal experiments were performed in accordance with local and Swiss federal guidelines. Nonblinded experimental groups were formed with random assignment of mice and no specific methods were applied to determine sample size.

Infections

Influenza A/PR8/34 OVAII (hereafter PR8) and X31 starter material were provided by P. G. Thomas, St. Jude Children's Research Hospital, and produced at VIRAPUR. PR8 was intranasally administered at 500 to 2000 TCID₅₀ (50% tissue culture infective dose) for all primary infections. Influenza X31 was used at 10⁵ TCID₅₀ for secondary infections. Mice were anesthetized with vaporized isoflurane and infected intranasally with virus diluted in 30- to 40-μl volume of PBS. LCMV infections were carried out as a part of and as detailed in a prior study (22).

Mixed bone marrow chimera

Bone marrow cells from wild-type (CD45.1) and Bcl6^{ACD4} (CD45.2) mice were collected, mixed in 60:40 (CD45.1:CD45.2) ratio to compensate for reconstitution defects of Ly5.1 line, and adoptively transferred into lethally irradiated [2× 500 centigray (cGy)] CD45.1 hosts (65). Reconstitution in blood was checked 6 weeks after irradiation.

Adoptive transfer

Inguinal, brachial, and axillary LNs from naïve OT-II mice were harvested and mashed through a 100-μm nylon cell strainer (Corning). Negative selection for CD8α, CD19, B220, I-A^b, and NK-1.1 using LS columns (Miltenyi Biotec) was performed to enrich CD4⁺ T cells. Cells were enumerated as previously described and 30,000 OT-II cells were transferred into congenic hosts 1 day before infection with PR8-OVA2 (66). For the cell transfer experiment in Fig. 8C, noncirculating CD4⁺ T cells from each subset were sorted and transferred into naïve congenic hosts that were infected with PR8 the following day.

In vivo treatments

Tamoxifen (Sigma-Aldrich) was dissolved in corn oil (25 mg/ml) and stored at 4°C during the duration of treatment. Mice were administered tamoxifen (3.75 mg in 150-μl volume) for 5 to 7 days by oral gavage. Mice were administered BrdU (Roche) in the drinking water (1 mg/ml with 1% glucose) for 13 days and euthanized on the 14th day. ARTC2.2-blocking nanobody s⁺16 [12.5 μg; NAD-induced cell death (NICD) protector] made in-house was intravenously injected into mice at least 15 min before sacrifice. Mice were injected intravenously with 3 μg of fluorochrome-conjugated anti-CD45 AF700 (clone A20; BioLegend, #110724) 3 min before sacrifice to label circulating cells and discriminate them from the noncirculating compartment. B cell depletion was performed by weekly intraperitoneal administrations of 250 μg of murine B cell depletion antibody (anti-mouse CD20, 18B12 obtained from Biogen MA Inc.) starting from 1 week before infection until sacrifice. CD8 depletion was performed by administering InVivoMAb anti-mouse CD8α (clone 2.43, Bio X Cell), 400 μg intraperitoneally and 100 μg intranasally (i.n.) for two consecutive days before secondary infection. The S1P1R agonist FTY720 (AdipoGen Life Sciences) was dissolved in DMSO at a concentration of 20 mg/ml; 1 mg/kg was administered intraperitoneally for three consecutive days before harvest for memory time point experiments (fig. S1), every 2 days starting day 9 for migration experiment (Fig. 4) and every day starting 3 days before secondary infection for recall experiments. For intracellular cytokine experiments, each mouse was administered Influenza NP peptide 311-325 (Eurogentec) 100 μg intravenously (i.v.), 25 μg i.n. and lipopolysaccharide (Sigma-Aldrich, L4391) 66 μg i.v., 33 μg i.n., all dissolved in PBS, 5 hours before sacrifice.

Tissue preparation

Lungs were harvested and diced into gentleMACS C Tubes (Miltenyi Biotec) and washed down with 3 ml of media [RPMI, 10 mM aminoguanidine hydrochloride (Sigma-Aldrich), 10 mM Hepes, penicillin-streptomycin-glutamine (100×, Gibco), 2-mercaptoethanol (50 μM, Gibco)] devoid of fetal calf serum (FCS) and EDTA prewarmed in a 37°C water bath. Digestion mix containing liberase (33.3 μg/ml; Roche, #05401020001) and deoxyribonuclease I (68 μg/ml; Applchem) was added. Lungs were dissociated on a gentleMACS Dissociator (Miltenyi Biotec) and placed in a shaking incubator at 37°C for 30 min. Lungs were dissociated again and mashed through 70-μm MACS SmartStrainers (Miltenyi Biotec). Red blood cells were lysed with 139.5 mM NH₄Cl and 17 mM tris-HCl (Erylysis buffer). For further processing, media containing 2% FCS and 1 mM EDTA were used. Mouse mediastinal LNs were harvested and mashed through a 100-μm Corning nylon cell strainer.

For LCMV-infected liver, perfusion with PBS was done till blood was removed. Organs were harvested and mashed through a 100-μm cell strainer in RPMI 1640 containing 10% FCS. Lymphocytes were purified on a 70%/40% Percoll gradient (Fisher Scientific). Purified lymphocytes were further processed for scRNA-seq as described previously (22).

Tetramer, antibody staining, and flow cytometry

I-A^b NP311-325 (QVYSLIRPNENPAHK) allophycocyanin was obtained from the National Institutes of Health (NIH) tetramer core facility. Single-cell suspensions were tetramer-stained, enriched, and counted as previously described (66). Dasatinib (50 nM) was added to the tetramer mix to reduce peptide-major histocompatibility complex

(pMHC) tetramer binding affinity threshold and activation-induced cell death (67). To analyze B cells, we used the flowthrough collected after tetramer enrichment to enumerate and stain for B cell markers. For all fluorochrome-conjugated antibody dilutions, FACS buffer (PBS, 2% FCS, and 0.1% sodium azide) containing Fc block (InVivoMAb anti-mouse CD16/CD32, Clone 2.4G2, Bio X Cell) was used (table S2). Live-dead stain (Zombie Red Fixable Viability kit; BioLegend, #423109) was added to the antibody mix and stained at 4°C for 30 min. FoxP3 Transcription Factor Staining Buffer Set (eBioscience, #00-5523-00) was used for intracellular staining at room temperature (RT) for 1 hour. For intracellular cytokine experiments, Fixation Buffer (BioLegend, #420801) was used instead of the reagent from the above kit. For BrdU staining, the BD Pharmingen BrdU Flow Kit (#51-2354AK) was used. Flow cytometric analysis was performed on BD LSR Fortessa. Data were analyzed using FlowJo X software (TreeStar).

Gating strategy used in flow cytometric analysis

To gate on resident CD4⁺ T cells, lung cells were gated on Zombie Red⁻ (live), dump⁻ (CD11b, CD11c, B220, and F4/80) lymphocytes, and then on CD4⁺, i.v.⁻ T cells (noncirculating). For antigen-specific T cells, CD44⁺NP⁻ cells were gated on. Non-antigen-specific are considered as CD44⁺NP⁻. The same gating strategy was used for CD4⁺ T cells from dLN.

For B cell staining in the lung, cells were gated on Zombie Red⁻ (live), dump⁻ (CD3e, Gr-1, F4/80, and CD11c) lymphocytes, and then on B220⁺. Further gating on iv⁺ or iv⁻ was done to discriminate between circulating and noncirculating B cells.

Single-cell RNA sequencing

Total NP-specific CD4⁺ T cells (0.5×10^4 to 3×10^4) were sorted from mLN and lung of PR8-OVA2-infected mice at indicated time points and were provided for library preparation using the 10x Chromium platform. Each sample is pooled from 4 to 12 C57BL/6J mice. Sorting was performed using BD FACSAria III and BSortAria III. Single-cell capture and cDNA library preparation were performed with the Single Cell 3' v2 Reagent Kit (10x Genomics) according to the manufacturer's instructions. Sequencing was performed on one flow cell of an Illumina NexSeq 500 at the Genomics Facility Basel of the ETH Zurich. Paired-end reads were obtained, and their quality was assessed with the FastQC tool (version 0.11.5). The length of the first read was 26 nucleotides (nt), composed of individual cell barcodes of 16 nt, and unique molecular identifiers (UMIs) of 10 nt. The length of the second read, composed of the transcript sequence, was 58 nt. The samples in the different wells were identified using sample barcodes of 8 nt.

scRNA-seq analysis

Sequencing data were processed using 10x Genomics Cell Ranger software version 2.1.0, modified to report only one alignment (randomly) for multimapped reads (keep only those mapping up to 10 genomic locations). Raw molecule info from Cell Ranger was initially filtered leniently, discarding cells with fewer than 100 UMI counts, as well as the highest 99.99% to account for likely doublets. The resulting UMI matrix was further filtered to keep only cells with log library size >2.9, log number of features >2.6, percent mitochondrial reads ≤6, and percent ribosomal protein reads ≥20. Genes with average counts <0.007 were removed. Normalization was done using the R package scran's deconvolution method. Technical

noise within gene expression was modeled using scran, and biologically relevant highly variable genes were calculated after separating the technical from biological variance, using false discovery rate <0.05 and biological variance >0.1. Principal components analysis (PCA) was run on the normalized data using the top 500 most variable genes by biological variance, and the PCA was denoised to account for the modeled technical variation. Cells were clustered hierarchically using Ward's method on the distance matrix of the PCA. Default dendrogram cut height using the R package dynamicTreeCut resulted in clusterings that also mapped to the highest average silhouette width. Data subsets, e.g., lung d30 cells only, were subjected to the same pipeline after subsetting. The sex-linked gene *Xist* was removed from the signature residency gene list. Subsequent visualization and analysis were performed using version 3.1.1 of the Seurat R package; dropout imputation was performed using Seurat version 2.3.4. SCENIC was performed using version 0.9.7 and the published workflow on the pySCENIC github repository (30). Pseudotime analysis was performed with slingshot version 1.5.0 and PHATE dimensionality reduction (40, 41). Secondary analysis of published datasets was taken directly from published supplemental material or downloaded from Gene Expression Omnibus (GEO) and analyzed for differential expression between samples by the limma package (68).

Histology

Lungs were inflated with 3% low melting agarose (LMA) (Sigma-Aldrich, #A9414), fixed in 1% formaldehyde (Thermo Fisher Scientific, #28908) for 24 hours at 4°C, washed with PBS, and kept at 4°C in PBS + 0.01%NaN₃. Lung tissues were embedded in 3% LMA, and 100-μm-thick sections were cut at the vibratome (Leica VT 1200S). Sections were placed on microscope slides, circumscribed with ImmEdge pen (Vector), and blocked in TBST (100 ml of tris-HCl, 150 mM NaCl, and 0.05% Tween 20) containing 5% donkey serum (Jackson ImmunoResearch, #017-000-121) for 2 hours at RT. For lung staining from T-bet-ZsGreen mice, sections were incubated with anti-CD4 (1:50 in blocking buffer) overnight at 4°C, then washed (four times for 15 min with TBST) and incubated with anti-rat-AF647 (1:160) for 4 hours at RT, followed by washes and subsequent incubation with anti-B220-BV421 (1:50) overnight at 4°C. For Bcl6-RFP mice, sections were processed similarly by incubating sections with anti-CD4 (1:50) and anti-RFP (1:100) overnight at 4°C, then with anti-rat-AF647 (1:160) and anti-rabbit-AF488 (1:200) for 4 hours at RT, and lastly with anti-B220-BV421 (1:50) overnight at 4°C. For Bcl6^{fl/fl} and Bcl6^{ΔCD4-ERT2} mice, sections were incubated with anti-CD4 (1:50) overnight at 4°C and then washed and incubated with anti-rat-AF647 (1:160) for 4 hours at RT. Then, sections were washed and incubated for 45 min with 5% rat serum in blocking buffer, washed and incubated for 45 min with Fab anti-rat (100 μg/ml), and washed and incubated with anti-B220 (1:50) overnight at 4°C. Sections were then washed and incubated with anti-rat-AF488 (1:300) for 4 hours at RT. After the last wash, sections were mounted using ProLong Glass Antifade Mountant (Invitrogen, P36984).

Microscopy images (16 bits, 1000 × 1000 pixel images) were acquired using ×20 or ×40 magnification objectives at the spinning disc confocal microscope (Nikon CSU-W1) with a photometrics 95B camera.

Image quantification

Confocal images were processed in Bitplane Imaris v9.5. Surfaces were created to segment different features of interest: dense B cell

areas (B220⁺) (automatic threshold; surface detail, 8 μm ; seed point diameter, ≥ 40 ; artifacts removed and final areas unified manually), individual CD4⁺ T cells (automatic threshold; surface detail, 0.8 μm ; seed point diameter, 4 μm), and the total possible volume in which a CD4⁺ T cell could be found (threshold, ~ 150 ; surface detail, 8 μm). Where necessary, surfaces for obvious noncell artifacts were created and used to mask the channels of interest before creating target surfaces. The statistics including shortest distance between surfaces was exported to comma-separated values (CSV) files. To confirm these results, we also processed images using custom computer vision and machine learning algorithms mainly written in python. Two separate image-based classifiers were trained at voxel- and object-level detection and identification for 3D clusters (B220) and 3D single cells (CD4). Features such as intensity, morphology, etc., were then measured per object at cluster and cellular level and colocalized using a parent (cluster) and child (cell) relationship within clusters of B cells. The distances between surfaces were calculated using centroids of cells and clusters. Data from both segmentation pipelines were loaded into R and processed using custom code to quantify and test distributions of CD4⁺ T cells with respect to B cell areas. CD4 objects less than 2.5 μm in radius were discarded as probable artifacts of surface creation. B cell clusters smaller than 20,000 μm^3 were also discarded. Double-positive CD4⁺Tbet⁺ or CD4⁺Bcl6⁺ cells were positively gated as if for FACS on the basis of a log distribution of mean intensity scores per CD4 object—by eye with the manual pipeline and at a threshold of the top 10% of per image data for the machine learning pipeline. Normalization: T cell counts within B cell areas were divided by that B cell area's volume, and counts outside B cell areas were divided by the total available T cell volume minus all B cell areas.

Enzyme-linked immunospot (ELISpot)

Multiscreen IP HTS filter plates (EMD Millipore, #MAIPS4W10) were coated with NP (2 $\mu\text{g}/\text{ml}$; Sino Biological, #11675-V08B) and incubated overnight at 4°C. Plates were blocked with cell culture medium. Cells were plated and incubated at 37°C for 5 hours. Plates were washed in PBS + 0.01% Tween 20 before goat anti-mouse immunoglobulin G (IgG) horseradish peroxidase (Fc γ fragment; Jackson ImmunoResearch, #115-035-008) was added and incubated overnight at 4°C. Plates were washed and developed using AEC Substrate Set (BDBiosciences, #551951). Spots were recorded with AutoImmun Diagnostika GMBH (AID) ELISpot Reader and enumerated manually.

Viral titer assay

Virus titers from lungs were determined on Madin-Darby canine kidney (MDCK) cells (American Type Culture Collection, CCL-34) and expressed as TCID₅₀/ml using the Reed and Muench method. Mice lungs (about 200 mg each) frozen in dry ice after collection were mixed with 800 μl of ice-cold PBS and homogenized using the TissueLyser LT (Qiagen, 50 Hz for 10 min), and the supernatant was collected after centrifugation for 5 min at 1000 rpm. MDCK cells were infected with serial 10-fold dilutions of the supernatant in Dulbecco's modified Eagle's medium, 0.2% bovine serum albumin (BSA), 2 mM L-glutamine, and L-(tosylamido-2-phenyl) ethyl chloromethyl ketone (TPCK)-treated trypsin (1 $\mu\text{g}/\text{ml}$). Infected cells were visualized 72 hours after infection using a primary anti-NP antibody (Thermo Fisher Scientific, PA5-32242) diluted 1:2000 in 1% BSA and a secondary fluorescent antibody (Thermo Fisher Scientific, A-11034) diluted 1:3000 in 1% BSA.

Statistical analyses

Statistical analyses were performed with Prism Graphpad Software (version 8.0). Unpaired or paired *t* tests (two-tailed) or Mann-Whitney-Wilcoxon tests were used according to the type of experiments. *P* < 0.05 was considered significant.

SUPPLEMENTARY MATERIALS

immunology.sciencemag.org/cgi/content/full/6/55/eabb6808/DC1

Fig. S1. Inflammatory T cells at site of infection confound a tissue-residency signature.

Fig. S2. Controlling for T helper function improves tissue-residency signature.

Fig. S3. Protein expression confirms T_H1 and T_{HH} phenotypes in the lung.

Fig. S4. Progressive differentiation of resident CD4⁺ T cell subsets.

Fig. S5. T_{HH} cell generation requires B cells and T cell-intrinsic Bcl6.

Fig. S6. CD4⁺ T_{HH} cells localize in lung B cell clusters.

Fig. S7. Maintenance of T_{HH} cells requires antigen presentation.

Fig. S8. T_{HH} cells are plastic and promote local antibody production during rechallenge.

Table S1. Raw data file.

Table S2. List of antibodies used for flow cytometry and histology.

Table S3. Cluster-defining genes.

Reference (71)

[View/request a protocol for this paper from Bio-protocol.](#)

REFERENCES AND NOTES

1. A. Palache, A. Abelin, R. Hollingsworth, W. Cracknell, C. Jacobs, T. Tsai, P. Barbosa; IFPMA Influenza Vaccine Supply (IFPMA IVS) task force, Survey of distribution of seasonal influenza vaccine doses in 201 countries (2004-2015): The 2003 World Health Assembly resolution on seasonal influenza vaccination coverage and the 2009 influenza pandemic have had very little impact on improving influenza control and pandemic preparedness. *Vaccine* **35**, 4681–4686 (2017).
2. S. Sambhara, A. Kurichh, R. Miranda, T. Tumpey, T. Rowe, M. Renshaw, R. Arpino, A. Tamane, A. Kandil, O. James, B. Underdown, M. Klein, J. Katz, D. Burt, Heterosubtypic immunity against human influenza A viruses, including recently emerged avian H5 and H9 viruses, induced by FLU-ISCOM vaccine in mice requires both cytotoxic T-lymphocyte and macrophage function. *Cell. Immunol.* **211**, 143–153 (2001).
3. T. M. Tumpey, M. Renshaw, J. D. Clements, J. M. Katz, Mucosal delivery of inactivated influenza vaccine induces B-cell-dependent heterosubtypic cross-protection against lethal influenza A H5N1 virus infection. *J. Virol.* **75**, 5141–5150 (2001).
4. J. Rangel-Moreno, D. M. Carragher, R. S. Misra, K. Kusser, L. Hartson, A. Moquin, F. E. Lund, T. D. Randall, B cells promote resistance to heterosubtypic strains of influenza via multiple mechanisms. *J. Immunol.* **180**, 454–463 (2007).
5. K. D. Zens, J. K. Chen, R. S. Guyer, F. L. Wu, F. Cvetkovski, M. Miron, D. L. Farber, Reduced generation of lung tissue-resident memory T cells during infancy. *J. Exp. Med.* **214**, 2915–2932 (2017).
6. K. D. Zens, D. L. Farber, Memory CD4 T cells in influenza. *Curr. Top. Microbiol. Immunol.* **386**, 399–421 (2015).
7. P. Devarajan, B. Bautista, A. M. Vong, K. K. McKinstry, T. M. Strutt, S. L. Swain, New insights into the generation of CD4 memory may shape future vaccine strategies for influenza. *Front. Immunol.* **7**, 136 (2016).
8. S. A. Valkenburg, N. H. L. Leung, M. B. Bull, L. M. Yan, A. P. Y. Li, L. L. M. Poon, B. J. Cowling, The hurdles from bench to bedside in the realization and implementation of a universal influenza vaccine. *Front. Immunol.* **9**, 1479 (2018).
9. F. Sallusto, J. Geginat, A. Lanzavecchia, CentralMemory and EffectorMemory T Cell Subsets: Function, generation, and maintenance. *Annu. Rev. Immunol.* **22**, 745–763 (2004).
10. D. Schreiner, C. G. King, CD4⁺ memory T cells at home in the tissue: Mechanisms for health and disease. *Front. Immunol.* **9**, 2394 (2018).
11. R. J. Miragaia, T. Gomes, A. Chomka, L. Jardine, A. Riedel, A. N. Hegazy, N. Whibley, A. Tucci, X. Chen, I. Lindeman, G. Emerton, T. Krausgruber, J. Shields, M. Haniffa, F. Powrie, S. A. Teichmann, Single-cell transcriptomics of regulatory T cells reveals trajectories of tissue adaptation. *Immunity* **50**, 493–504.e7 (2019).
12. L. K. Beura, N. J. Fares-Frederickson, E. M. Steinert, M. C. Scott, E. A. Thompson, K. A. Fraser, J. M. Schenkel, V. Vezys, D. Masopust, CD4⁺ resident memory T cells dominate immunosurveillance and orchestrate local recall responses. *J. Exp. Med.* **216**, 1214–1229 (2019).
13. M. C. Amezcua Vesely, P. Pallis, P. Bielecki, J. S. Low, J. Zhao, C. C. D. Harman, L. Kroehling, R. Jackson, W. Bailis, P. Licona-Limon, H. Xu, N. Iijima, P. S. Pillai, D. H. Kaplan, C. T. Weaver, Y. Kluger, M. S. Kowalczyk, A. Iwasaki, J. P. Pereira, E. Esplugues, N. Gagliani, R. A. Flavell, Effector TH17 cells give rise to long-lived TRM cells that are essential for an immediate response against bacterial infection. *Cell* **178**, 1176–1188.e15 (2019).

14. B. V. Kumar, W. Ma, M. Miron, T. Granot, R. S. Guyer, D. J. Carpenter, T. Senda, X. Sun, S. H. Ho, H. Lerner, A. L. Friedman, Y. Shen, D. L. Farber, Human tissue-resident memory T cells are defined by core transcriptional and functional signatures in lymphoid and mucosal sites. *Cell Rep.* **20**, 2921–2934 (2017).
15. A. E. Oja, B. Piet, D. van der Zwan, H. Blaauwgeers, M. Mensink, S. de Kivit, J. Borst, M. A. Nolte, R. A. W. van Lier, R. Stark, P. Hombrink, Functional heterogeneity of CD4(+) tumor-infiltrating lymphocytes with a resident memory phenotype in NSCLC. *Front. Immunol.* **9**, 2654 (2018).
16. A. E. Oja, B. Piet, C. Helbig, R. Stark, D. van der Zwan, H. Blaauwgeers, E. B. M. Remmerswaal, D. Amsen, R. E. Jonkers, P. D. Moerland, M. A. Nolte, R. A. W. van Lier, P. Hombrink, Trigger-happy resident memory CD4(+) T cells inhabit the human lungs. *Mucosal Immunol.* **11**, 654–667 (2018).
17. J. R. Teijaro, D. Turner, Q. Pham, E. J. Wherry, L. Lefrancois, D. L. Farber, Cutting edge: Tissue-retentive lung memory CD4 T cells mediate optimal protection to respiratory virus infection. *J. Immunol.* **187**, 5510–5514 (2011).
18. K. D. Zens, J. K. Chen, D. L. Farber, Vaccine-generated lung tissue-resident memory T cells provide heterosubtypic protection to influenza infection. *JCI Insight* **1**, e85832 (2016).
19. N. Deng, J. M. Weaver, T. R. Mosmann, Cytokine diversity in the Th1-dominated human anti-influenza response caused by variable cytokine expression by Th1 cells, and a minor population of uncommitted IL-2+IFN γ -Thpp cells. *PLOS ONE* **9**, e95986 (2014).
20. K. K. McKinstry, F. Alam, V. Flores-Malavet, M. Z. Nagy, S. Sell, A. M. Cooper, S. L. Swain, T. M. Strutt, Memory CD4 T cell-derived IL-2 synergizes with viral infection to exacerbate lung inflammation. *PLOS Pathog.* **15**, e1007989 (2019).
21. T. M. Strutt, K. K. McKinstry, Y. Kuang, L. M. Bradley, S. L. Swain, Memory CD4+ T-cell-mediated protection depends on secondary effectors that are distinct from and superior to primary effectors. *Proc. Natl. Acad. Sci. U.S.A.* **109**, E2551–E2560 (2012).
22. M. Künzli, D. Schreiner, T. C. Pereboom, N. Swarnalekha, L. C. Litzler, J. Lötscher, Y. I. Ertuna, J. Roux, F. Geier, R. P. Jakob, T. Maier, C. Hess, J. J. Taylor, C. G. King, Long-lived T follicular helper cells retain plasticity and help sustain humoral immunity. *Sci. Immunol.* **5**, eaay5552 (2020).
23. A. Asrir, M. Aloulou, M. Gador, C. Peral, N. Fazilleau, Interconnected subsets of memory follicular helper T cells have different effector functions. *Nat. Commun.* **8**, 847 (2017).
24. M. Pepper, A. J. Pagan, B. Z. Igarty, J. J. Taylor, M. K. Jenkins, Opposing signals from the Bcl6 transcription factor and the interleukin-2 receptor generate T helper 1 central and effector memory cells. *Immunity* **35**, 583–595 (2011).
25. C. N. Skon, J. Y. Lee, K. G. Anderson, D. Masopust, K. A. Hogquist, S. C. Jameson, Transcriptional downregulation of S1pr1 is required for the establishment of resident memory CD8+ T cells. *Nat. Immunol.* **14**, 1285–1293 (2013).
26. J. Y. Lee, C. N. Skon, Y. J. Lee, S. Oh, J. J. Taylor, D. Malhotra, M. K. Jenkins, M. G. Rosenfeld, K. A. Hogquist, S. C. Jameson, The transcription factor KLF2 restrains CD4(+) T follicular helper cell differentiation. *Immunity* **42**, 252–264 (2015).
27. Y. M. Son, I. S. Cheon, Y. Wu, C. Li, Z. Wang, Y. Chen, Y. Takahashi, A. L. Dent, M. H. Kaplan, Y.-X. Fu, J. J. Taylor, W. Cui, J. Sun, Tissue-resident CD4+ T helper cells assist protective respiratory mucosal B and CD8+ T cell memory responses. *bioRxiv*, (2020).
28. E. Jennings, T. A. E. Elliot, N. Thawait, S. Kanabar, J. C. Yam-Puc, M. Ono, K.-M. Toellner, D. C. Wraith, G. Anderson, D. Bending, Differential Nr4a1 and Nr4a3 expression discriminates tonic from activated TCR signalling events in vivo. *bioRxiv*, 767566 (2020).
29. W. J. Vilimovsky LH, Henriksson J, Miao Z, Natan E, Kar G, Clare S, Barlow JL, Charidemou E, Mamanova L, Chen X, Proserpio V, Pramanik J, Woodhouse S, Protasio AV, Efremova M, Berriman M, Dougan G, Fisher J, Marioni J, McKenzie ANJ, Teichmann SA, Rora regulates activated T helper cells during inflammation. *bioRxiv*, (2019).
30. S. Aibar, C. B. Gonzalez-Blas, T. Moerman, V. A. Huynh-Thu, H. Imrichova, G. Hulselmans, F. Rambow, J. C. Marine, P. Geurts, J. Aerts, J. van den Oord, Z. K. Atak, J. Wouters, S. Aerts, SCENIC: Single-cell regulatory network inference and clustering. *Nat. Methods* **14**, 1083–1086 (2017).
31. S. Tanaka, K. Tanaka, F. Magnusson, Y. Chung, G. J. Martinez, Y. H. Wang, R. I. Nurieva, T. Kurosaki, C. Dong, CCAAT/enhancer-binding protein α negatively regulates IFN- γ expression in T cells. *J. Immunol.* **193**, 6152–6160 (2014).
32. K. Shimatani, Y. Nakashima, M. Hattori, Y. Hamazaki, N. Minato, PD-1+ memory phenotype CD4+ T cells expressing C/EBP α underlie T cell immunodepression in senescence and leukemia. *Proc. Natl. Acad. Sci. U.S.A.* **106**, 15807–15812 (2009).
33. Y. S. Choi, J. A. Gullicksrud, S. Xing, Z. Zeng, Q. Shan, F. Li, P. E. Love, W. Peng, H. H. Xue, S. Crotty, LEF-1 and TCF-1 orchestrate T(FH) differentiation by regulating differentiation circuits upstream of the transcriptional repressor Bcl6. *Nat. Immunol.* **16**, 980–990 (2015).
34. D. Stauss, C. Brunner, F. Berberich-Siebelt, U. E. Hopken, M. Lipp, G. Muller, The transcriptional coactivator Bob1 promotes the development of follicular T helper cells via Bcl6. *EMBO J.* **35**, 881–898 (2016).
35. R. J. Johnston, A. C. Poholek, D. DiToro, I. Yusuf, D. Eto, B. Barnett, A. L. Dent, J. Craft, S. Crotty, Bcl6 and Blimp-1 are reciprocal and antagonistic regulators of T follicular helper cell differentiation. *Science* **325**, 1006–1010 (2009).
36. S. Keck, M. Schmalzer, S. Ganter, L. Wyss, S. Oberle, E. S. Huseby, D. Zehn, C. G. King, Antigen affinity and antigen dose exert distinct influences on CD4 T-cell differentiation. *Proc. Natl. Acad. Sci. U.S.A.* **111**, 14852–14857 (2014).
37. J. E. Moyron-Quiroz, J. Rangel-Moreno, L. Hartson, K. Kusser, M. P. Tighe, K. D. Klonowski, L. Lefrancois, L. S. Cauley, A. G. Harmsen, F. E. Lund, T. D. Randall, Persistence and responsiveness of immunologic memory in the absence of secondary lymphoid organs. *Immunity* **25**, 643–654 (2006).
38. H. X. Tan, R. Esterbauer, H. A. Vandervlen, J. A. Juno, S. J. Kent, A. K. Wheatley, Inducible bronchus-associated lymphoid tissues (iBALT) serve as sites of B cell selection and maturation following influenza infection in mice. *Front. Immunol.* **10**, 611 (2019).
39. T. S. Kim, M. M. Hufford, J. Sun, Y. X. Fu, T. J. Braciale, Antigen persistence and the control of local T cell memory by migrant respiratory dendritic cells after acute virus infection. *J. Exp. Med.* **207**, 1161–1172 (2010).
40. K. R. Moon, D. van Dijk, Z. Wang, S. Gigante, D. B. Burkhardt, W. S. Chen, K. Yim, A. V. D. Elzen, M. J. Hirn, R. R. Coifman, N. B. Ivanova, G. Wolf, S. Krishnaswamy, Visualizing structure and transitions in high-dimensional biological data. *Nat. Biotechnol.* **37**, 1482–1492 (2019).
41. K. Street, D. Risso, R. B. Fletcher, D. Das, J. Ngai, N. Yosef, E. Purdom, S. Dudoit, Slingshot: Cell lineage and pseudotime inference for single-cell transcriptomics. *BMC Genomics* **19**, 477 (2018).
42. W. Ise, T. Inoue, J. B. McLachlan, K. Kometani, M. Kubo, T. Okada, T. Kurosaki, Memory B cells contribute to rapid Bcl6 expression by memory follicular helper T cells. *Proc. Natl. Acad. Sci. U.S.A.* **111**, 11792–11797 (2014).
43. M. K. MacLeod, A. David, A. S. McKee, F. Crawford, J. W. Kappler, P. Marrack, Memory CD4 T cells that express CXCR5 provide accelerated help to B cells. *J. Immunol.* **186**, 2889–2896 (2011).
44. S. R. Allie, J. E. Bradley, U. Mudunuru, M. D. Schultz, B. A. Graf, F. E. Lund, T. D. Randall, The establishment of resident memory B cells in the lung requires local antigen encounter. *Nat. Immunol.* **20**, 97–108 (2019).
45. D. M. Carragher, D. A. Kaminski, A. Moquin, L. Hartson, T. D. Randall, A novel role for non-neutralizing antibodies against nucleoprotein in facilitating resistance to influenza virus. *J. Immunol.* **181**, 4168–4176 (2008).
46. M. W. LaMere, H. T. Lam, A. Moquin, L. Haynes, F. E. Lund, T. D. Randall, D. A. Kaminski, Contributions of antinucleoprotein IgG to heterosubtypic immunity against influenza virus. *J. Immunol.* **186**, 4331–4339 (2011).
47. B. J. Laidlaw, V. Decman, M. A. A. Ali, M. C. Abt, A. I. Wolf, L. A. Monticelli, K. Mozdzanowska, J. M. Angelosanto, D. Artis, J. Erikson, E. J. Wherry, Cooperativity between CD8+ T cells, non-neutralizing antibodies, and alveolar macrophages is important for heterosubtypic influenza virus immunity. *PLOS Pathog.* **9**, e1003207 (2013).
48. K. J. Oestreich, K. A. Read, S. E. Gilbertson, K. P. Hough, P. W. McDonald, V. Krishnamoorthy, A. S. Weinmann, Bcl-6 directly represses the gene program of the glycolysis pathway. *Nat. Immunol.* **15**, 957–964 (2014).
49. S. H. Cho, A. L. Raybuck, J. Blagih, E. Kemboi, V. H. Haase, R. G. Jones, M. R. Boothby, Hypoxia-inducible factors in CD4(+) T cells promote metabolism, switch cytokine secretion, and T cell help in humoral immunity. *Proc. Natl. Acad. Sci. U.S.A.* **116**, 8975–8984 (2019).
50. Y. Zhu, Y. Zhao, L. Zou, D. Zhang, D. Aki, Y. C. Liu, The E3 ligase VHL promotes follicular helper T cell differentiation via glycolytic-epigenetic control. *J. Exp. Med.* **216**, 1664–1681 (2019).
51. D. M. W. Zaiss, W. C. Gause, L. C. Osborne, D. Artis, Emerging functions of amphiregulin in orchestrating immunity, inflammation, and tissue repair. *Immunity* **42**, 216–226 (2015).
52. N. Arpaia, J. A. Green, B. Molledo, A. Arvey, S. Hemmers, S. Yuan, P. M. Treuting, A. Y. Rudensky, A distinct function of regulatory T cells in tissue protection. *Cell* **162**, 1078–1089 (2015).
53. B. D. Hondowicz, K. S. Kim, M. J. Ruterbusch, G. J. Keitany, M. Pepper, IL-2 is required for the generation of viral-specific CD4(+) Th1 tissue-resident memory cells and B cells are essential for maintenance in the lung. *Eur. J. Immunol.* **48**, 80–86 (2018).
54. A. O. Moguche, S. Shafiani, C. Clemons, R. P. Larson, C. Dinh, L. E. Higdon, C. J. Cambier, J. R. Sissons, A. M. Gallegos, P. J. Fink, K. B. Urdahl, ICOS and Bcl6-dependent pathways maintain a CD4 T cell population with memory-like properties during tuberculosis. *J. Exp. Med.* **212**, 715–728 (2015).
55. A. Silva-Sanchez, T. D. Randall, Role of iBALT in respiratory immunity. *Curr. Top. Microbiol. Immunol.* **426**, 21–43 (2020).
56. S. A. Khader, J. Rangel-Moreno, J. J. Fountain, C. A. Martino, W. W. Reiley, J. E. Pearl, G. M. Winslow, D. L. Woodland, T. D. Randall, A. M. Cooper, In a murine tuberculosis model, the absence of homeostatic chemokines delays granuloma formation and protective immunity. *J. Immunol.* **183**, 8004–8014 (2009).
57. A. Kahnert, U. E. Hopken, M. Stein, S. Bandermann, M. Lipp, S. H. Kaufmann, *Mycobacterium tuberculosis* triggers formation of lymphoid structure in murine lungs. *J. Infect. Dis.* **195**, 46–54 (2007).

58. R. Cabrita, M. Lauss, A. Sanna, M. Donia, M. Skaarup Larsen, S. Mitra, I. Johansson, B. Phung, K. Harbst, J. Vallon-Christersson, A. van Schoiack, K. Lovgren, S. Warren, K. Jirstrom, H. Olsson, K. Pietras, C. Ingvar, K. Isaksson, D. Schadendorf, H. Schmidt, L. Bastholt, A. Carneiro, J. A. Wargo, I. M. Svane, G. Jonsson, Tertiary lymphoid structures improve immunotherapy and survival in melanoma. *Nature* **577**, 561–565 (2020).
59. F. Petitprez, A. de Reynies, E. Z. Keung, T. W. Chen, C. M. Sun, J. Calderaro, Y. M. Jeng, L. P. Hsiao, L. Lacroix, A. Bougouin, M. Moreira, G. Lacroix, I. Nataro, J. Adam, C. Lucchesi, Y. H. Laizet, M. Toulmonde, M. A. Burgess, V. Bolejack, D. Reinke, K. M. Wani, W. L. Wang, A. J. Lazar, C. L. Roland, J. A. Wargo, A. Italiano, C. Sautes-Fridman, H. A. Tawbi, W. H. Fridman, B cells are associated with survival and immunotherapy response in sarcoma. *Nature* **577**, 556–560 (2020).
60. B. A. Helmink, S. M. Reddy, J. Gao, S. Zhang, R. Basar, R. Thakur, K. Yizhak, M. Sade-Feldman, J. Blando, G. Han, V. Gopalakrishnan, Y. Xi, H. Zhao, R. N. Amaria, H. A. Tawbi, A. P. Cogdill, W. Liu, V. S. LeBleu, F. G. Kugerafski, S. Patel, M. A. Davies, P. Hwu, J. E. Lee, J. E. Gershenwald, A. Lucci, R. Arora, S. Woodman, E. Z. Keung, P. O. Gaudreau, A. Reuben, C. N. Spencer, E. M. Burton, L. E. Haydu, A. J. Lazar, R. Zapassodi, C. W. Hudgens, D. A. Ledesma, S. Ong, M. Bailey, S. Warren, D. Rao, O. Krijgsman, E. A. Rozeman, D. Peeper, C. U. Blank, T. N. Schumacher, L. H. Butterfield, M. A. Zelazowska, K. M. McBride, R. Kalluri, J. Allison, F. Petitprez, W. H. Fridman, C. Sautes-Fridman, N. Hacohen, K. Rezvani, P. Sharma, M. T. Tetzlaff, L. Wang, J. A. Wargo, B cells and tertiary lymphoid structures promote immunotherapy response. *Nature* **577**, 549–555 (2020).
61. J. P. Weber, F. Fuhrmann, R. K. Feist, A. Lahmann, M. S. Al Baz, L. J. Gentz, D. V. Van, H. W. Mages, C. Haftmann, R. Riedel, J. R. Grun, W. Schuh, R. A. Krocze, A. Radbruch, M.-F. Mashreghi, A. Hutloff, ICOS maintains the T follicular helper cell phenotype by down-regulating Krüppel-like factor 2. *J. Exp. Med.* **212**, 217–233 (2015).
62. B. A. Heesters, P. Chatterjee, Y. A. Kim, S. F. Gonzalez, M. P. Kuligowski, T. Kirchhausen, M. C. Carroll, Endocytosis and recycling of immune complexes by follicular dendritic cells enhances B cell antigen binding and activation. *Immunity* **38**, 1164–1175 (2013).
63. J. G. Tew, R. P. Phipps, T. E. Mandel, The maintenance and regulation of the humoral immune-response—Persisting antigen and the role of follicular antigen-binding dendritic cells as accessory cells. *Immunol. Rev.* **53**, 175–201 (1980).
64. B. A. Tamburini, M. A. Burchill, R. M. Kedl, Antigen capture and archiving by lymphatic endothelial cells following vaccination or viral infection. *Nat. Commun.* **5**, 3989 (2014).
65. F. E. Mercier, D. B. Sykes, D. T. Scadden, Single targeted exon mutation creates a true congenic mouse for competitive hematopoietic stem cell transplantation: The C57BL/6-CD45.1(STEM) mouse. *Stem Cell Rep.* **6**, 985–992 (2016).
66. J. J. Moon, H. H. Chu, J. Hataye, A. J. Pagan, M. Pepper, J. B. McLachlan, T. Zell, M. K. Jenkins, Tracking epitope-specific T cells. *Nat. Protoc.* **4**, 565–581 (2009).
67. A. Lissina, K. Ladell, A. Skowera, M. Clement, E. Edwards, R. Seggewiss, H. A. van den Berg, E. Gostick, K. Gallagher, E. Jones, J. J. Melenhorst, A. J. Godkin, M. Peakman, D. A. Price, A. K. Sewell, L. Wooldridge, Protein kinase inhibitors substantially improve the physical detection of T-cells with peptide-MHC tetramers. *J. Immunol. Methods* **340**, 11–24 (2009).
68. M. E. Ritchie, B. Phipson, D. Wu, Y. Hu, C. W. Law, W. Shi, G. K. Smyth, limma powers differential expression analyses for RNA-sequencing and microarray studies. *Nucleic Acids Res.* **43**, e47 (2015).
69. L. K. Mackay, M. Minnich, N. A. Kragten, Y. Liao, B. Nota, C. Seillet, A. Zaid, K. Man, S. Preston, D. Freestone, A. Braun, E. Wynne-Jones, F. M. Behr, R. Stark, D. G. Pellicci, D. I. Godfrey, G. T. Belz, M. Pellegrini, T. Gebhardt, M. Busslinger, W. Shi, F. R. Carbone, R. A. van Lier, A. Kallies, K. P. J. M. van Gisbergen, Hobit and Blimp1 instruct a universal transcriptional program of tissue residency in lymphocytes. *Science* **352**, 459–463 (2016).
70. L. K. Mackay, A. Rahimpour, J. Z. Ma, N. Collins, A. T. Stock, M. L. Hafon, J. Vega-Ramos, P. Lauzurica, S. N. Mueller, T. Stefanovic, D. C. Tschärke, W. R. Heath, M. Inouye, F. R. Carbone, T. Gebhardt, The developmental pathway for CD103(+)CD8+ tissue-resident memory T cells of skin. *Nat. Immunol.* **14**, 1294–1301 (2013).
71. J. A. Best, D. A. Blair, J. Knell, E. Yang, V. Mayya, A. Doedens, M. L. Dustin, A. W. Goldrath, P. Monach, S. A. Shinton, R. R. Hardy, R. Jianu, D. Koller, J. Collins, R. Gazit, B. S. Garrison, D. J. Rossi, K. Narayan, K. Sylvia, J. Kang, A. Fletcher, K. Elpek, A. Bellemare-Pelletier, D. Malhotra, S. Turley, J. A. Best, J. Knell, A. W. Goldrath, V. Jovic, D. Koller, T. Shay, A. Regev, N. Cohen, P. Brennan, M. Brenner, T. Kreslavsky, N. A. Bezman, J. C. Sun, C. C. Kim, L. L. Lanier, J. Miller, B. Brown, M. Merad, E. L. Gautier, C. Jakubzik, G. J. Randolph, F. Kim, T. N. Rao, A. Wagers, T. Heng, M. Painter, J. Ericson, S. Davis, A. Ergun, M. Mingueneau, D. Mathis, C. Benoist, The Immunological Genome Project, transcriptional insights into the CD8+ T cell response to infection and memory T cell formation. *Nat. Immunol.* **14**, 404–412 (2013).

Acknowledgments: We thank D. Pinschewer and his laboratory for helpful discussions; J. Roux and F. Geier for expertise and technical advice; R. Tussiwand and her laboratory for feedback and support; and the flow sorting facility and all the animal caretakers at the DBM University of Basel. scRNA-seq was performed at the Genomics Facility Basel, ETH Zurich. Calculations were performed at sciCORE (<http://scicore.unibas.ch/>) scientific computing center and image analysis on the Virtualized Analysis and Data Management Platform at the Biocenter at the University of Basel. **Funding:** The work was supported by research grants to C.G.K. (SNF PP00P3_157520, Freiwillige Akademische Gesellschaft Basel, Forschungsfonds University of Basel, OPO Stiftung and Swiss Life Jubiläumsstiftung) and J.S. (NIH RO1 AI147394 and AI154598). **Author contributions:** C.G.K. conceptualized the project. N.S., D.S., and C.G.K. designed the experiments. N.S., L.C.L., D.K., M.K., Y.M.S., and E.A.M. performed experiments. N.S., D.S., L.C.L., S.I., and C.G.K. analyzed the data. C.G.K. and D.S. wrote the manuscript. D.S., N.S., L.C.L., and C.G.K. visualized the data. C.G.K. acquired funding. J.S. provided resources. C.G.K. supervised the study. **Competing interests:** The authors declare that they have no competing interests. **Data and materials availability:** scRNA-seq data are deposited with the National Center for Biotechnology Information GEO (accession no. GSE146626). All other data needed to evaluate the conclusions in the paper are present in the paper or the Supplementary Materials.

Submitted 11 March 2020
Accepted 11 November 2020
Published 8 January 2021
10.1126/sciimmunol.abb6808

Citation: N. Swarnalekha, D. Schreiner, L. C. Litzler, S. Ifitkhar, D. Kirchmeier, M. Künzli, Y. M. Son, J. Sun, E. A. Moreira, C. G. King, T resident helper cells promote humoral responses in the lung. *Sci. Immunol.* **6**, eabb6808 (2021).

Supplementary Materials for

T resident helper cells promote humoral responses in the lung

Nivedya Swarnalekha, David Schreiner, Ludivine C. Litzler, Saadia Iftikhar, Daniel Kirchmeier, Marco Künzli, Young Min Son, Jie Sun, Etori Aguiar Moreira, Carolyn G. King*

*Corresponding author. Email: carolyn.king@unibas.ch

Published 8 January 2021, *Sci. Immunol.* 6, eabb6808 (2021)
DOI: 10.1126/sciimmunol.abb6808

The PDF file includes:

Fig. S1. Inflammatory T cells at site of infection confound a tissue-residency signature.
Fig. S2. Controlling for T helper function improves tissue-residency signature.
Fig. S3. Protein expression confirms T_H1 and T_{FH} phenotypes in the lung.
Fig. S4. Progressive differentiation of resident CD4⁺ T cell subsets.
Fig. S5. T_{RH} cell generation requires B cells and T cell–intrinsic Bcl6.
Fig. S6. CD4⁺ T_{RH} cells localize in lung B cell clusters.
Fig. S7. Maintenance of T_{RH} cells requires antigen presentation.
Fig. S8. T_{RH} cells are plastic and promote local antibody production during rechallenge.
Reference (71)

Other Supplementary Material for this manuscript includes the following:

(available at immunology.sciencemag.org/cgi/content/full/6/55/eabb6808/DC1)

Table S1 (Microsoft Excel format). Raw data file.
Table S2 (Microsoft Excel format). List of antibodies used for flow cytometry and histology.
Table S3 (Microsoft Excel format). Cluster-defining genes.

Supplementary Figure 1.

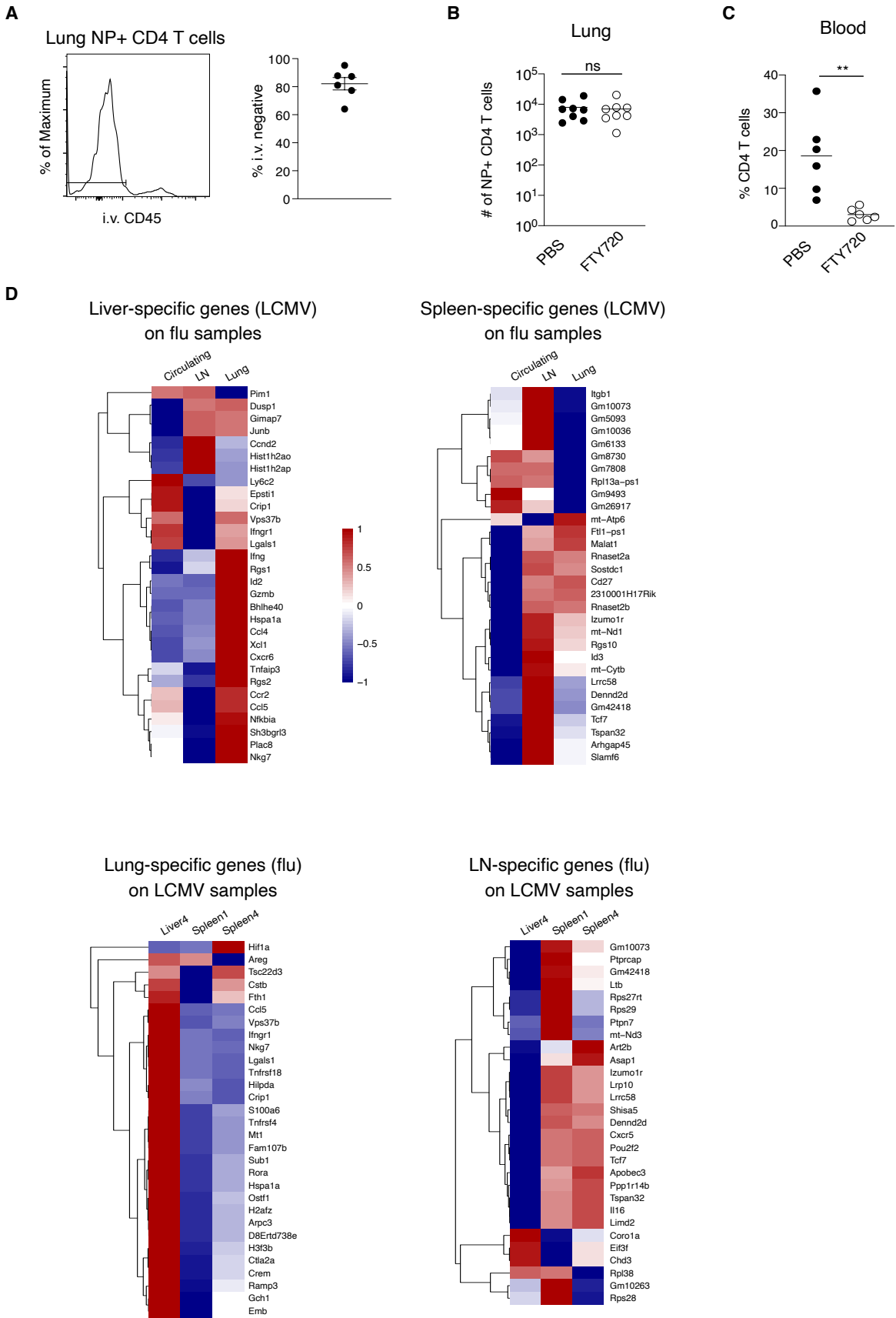


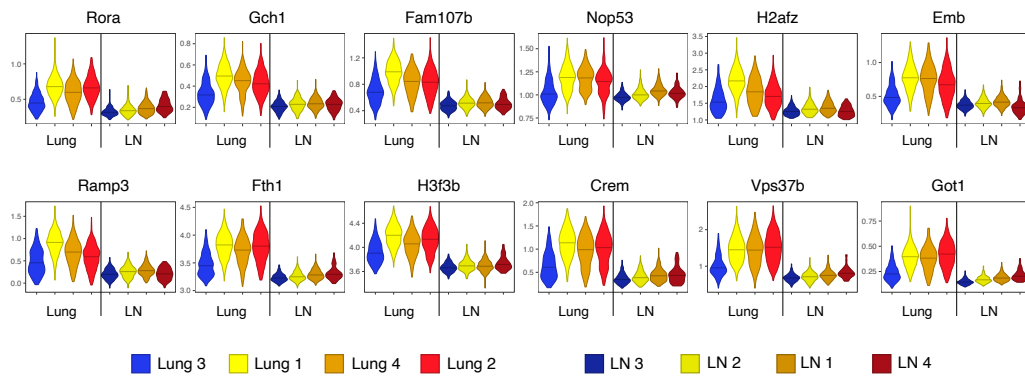
Fig. S1. Inflammatory T cells at site of infection confound a tissue-residency signature

(A) Identification and frequency of NP-specific resident T cells. **(B, C)** Total numbers of NP-specific T cells **(B)** and total CD4⁺ T cell frequencies in blood **(C)** of control and FTY720-treated mice. **(D)** Tissue specific signatures derived from one infection model plotted on data set from the other infection model. Heatmaps show cluster-averaged, scaled centered expression. Thin lines represent mean in B and C. Significance was determined using unpaired Student's t-test. P values are as follows: *P<0.05, **P<0.01, ***P<0.001, ****P<0.0001.

Supplementary Figure 2.

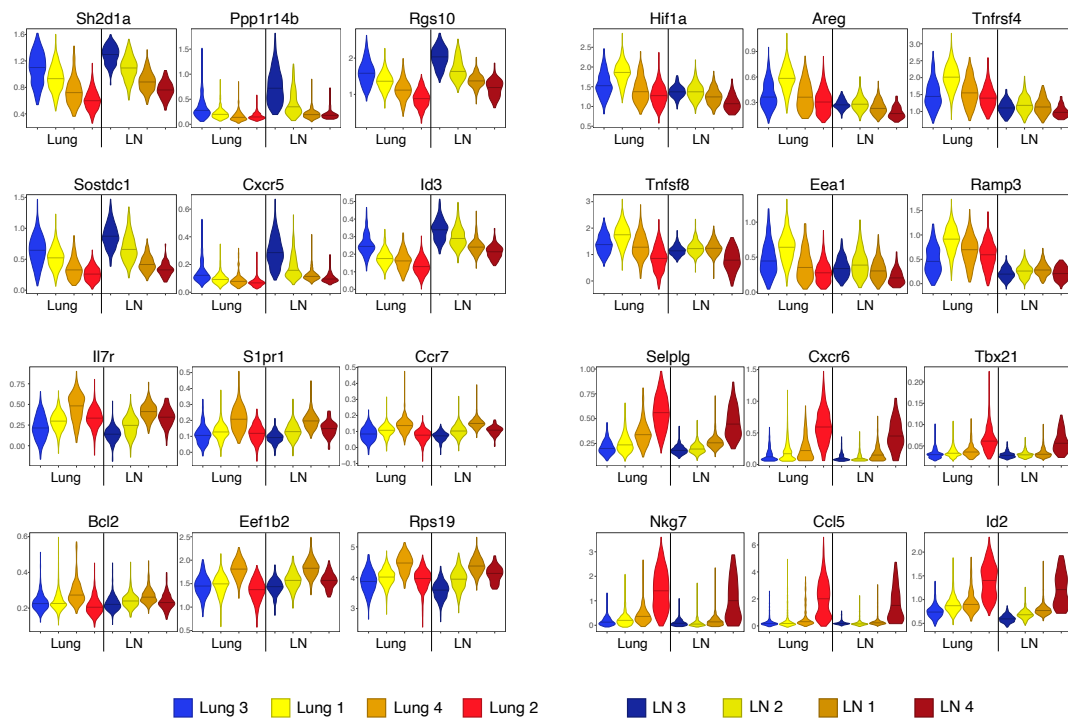
A

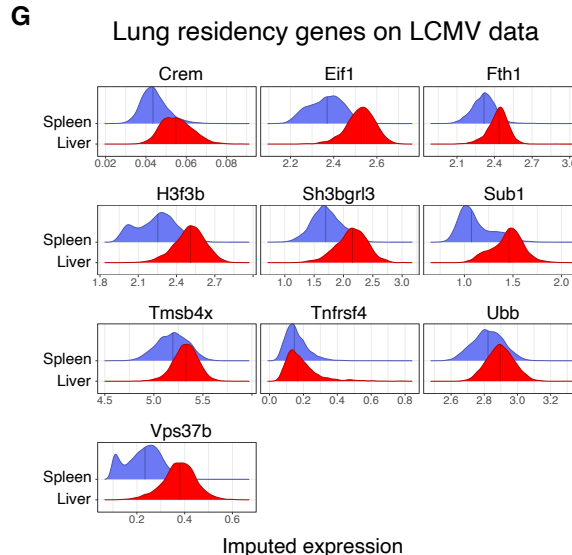
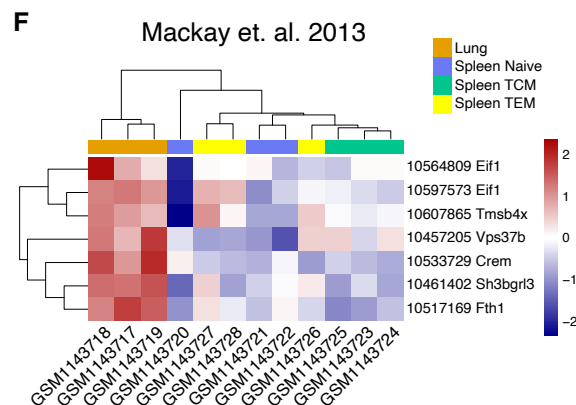
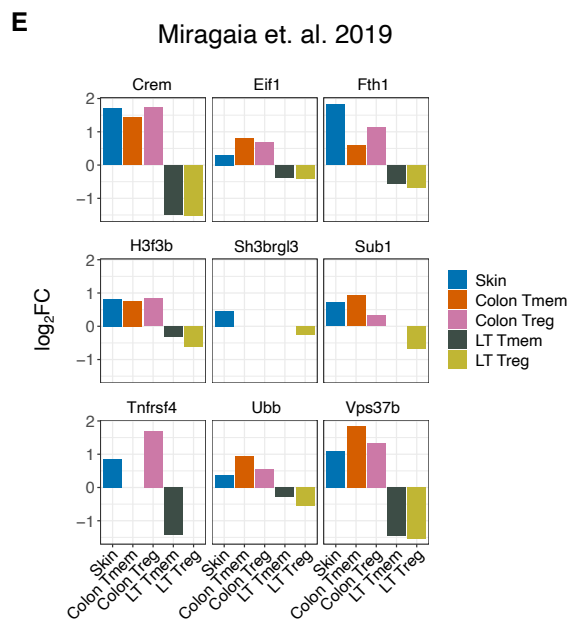
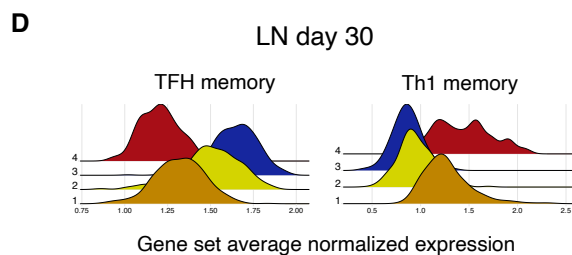
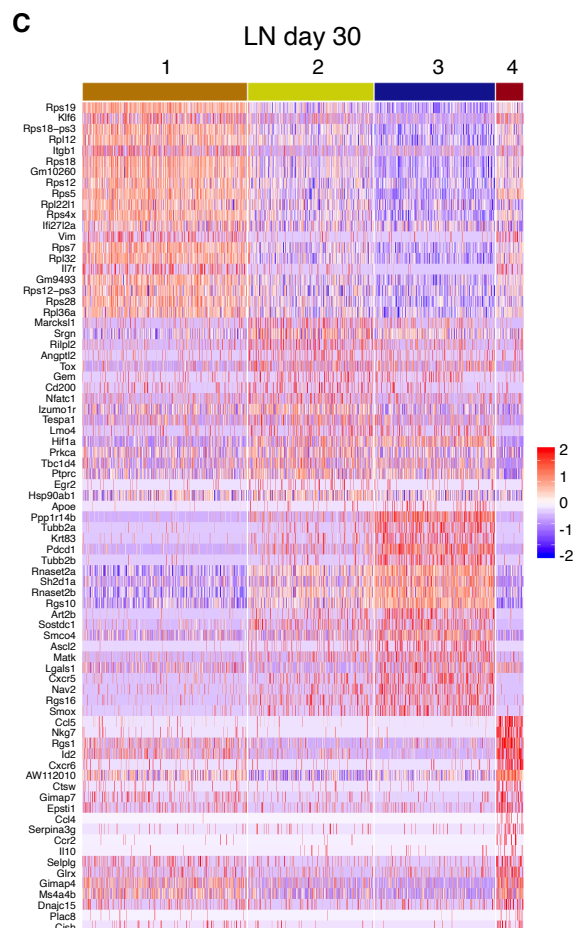
Day 30



B

Day 30





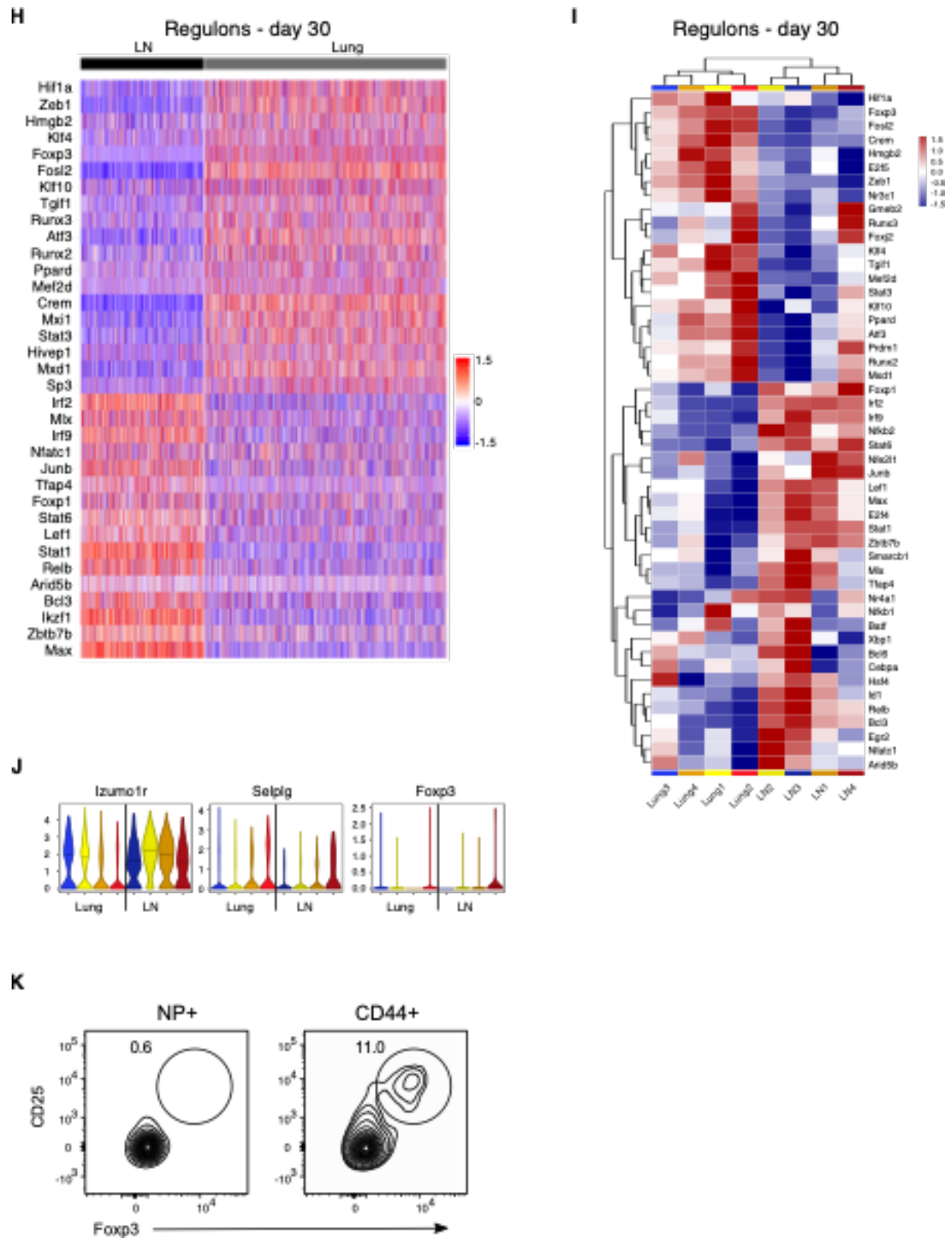


Fig. S2. Controlling for T helper function improves tissue-residency signature

(A) Imputed expression of residency genes. Dropout imputed using

Seurat::AddImputedScore. **(B)** Imputed expression of genes typifying similar clusters in lung and LN: blues = T_{fh} -like, yellows = T_{fh} -like, oranges = TCM-like, red = Th1-like. **(C)** Heatmap showing scaled, centered single cell expression of top 20 genes sorted according to LN cluster average \log_2FC , adjusted P value < 0.05. **(D)** Log-normalized average expression of T_{fh} and Th1 memory signatures(26). **(E)** Conserved tissue residency signature genes on published single cell data set analyzing Treg adaptation to tissue(11). **(F)** Conserved tissue residency signature genes on published data set investigating CD8 TRM(62). **(G)** Imputed expression of conserved tissue residency signature genes on LCMV data. **(H)** Scaled, centered area under curve (AUC) calculated with SCENIC showing top 20 differentially active transcription factors by tissue at day 30. Adjusted P-value < 0.01. **(I)** Scaled, centered, cluster average SCENIC AUC showing top 20 differentially active TFs by tissue and cluster. Adjusted P value < 0.01. **(J)** Log-normalized expression by cluster. **(K)** Foxp3+ cells in the lung. Data in **A** (n=6, representing 3 experiments), **B** (n=8, pooled from 2 experiments) and **C** (n=6, pooled from 2 experiments) were analyzed by unpaired Student's t-test. Thin lines represent mean \pm s.e.m in **A** and mean in **B** and **C**. Data in **I** represents 2 experiments, n=5. P values are as follows: *P<0.05, **P<0.01, ***P<0.001, ****P<0.0001.

Supplementary Figure 3.

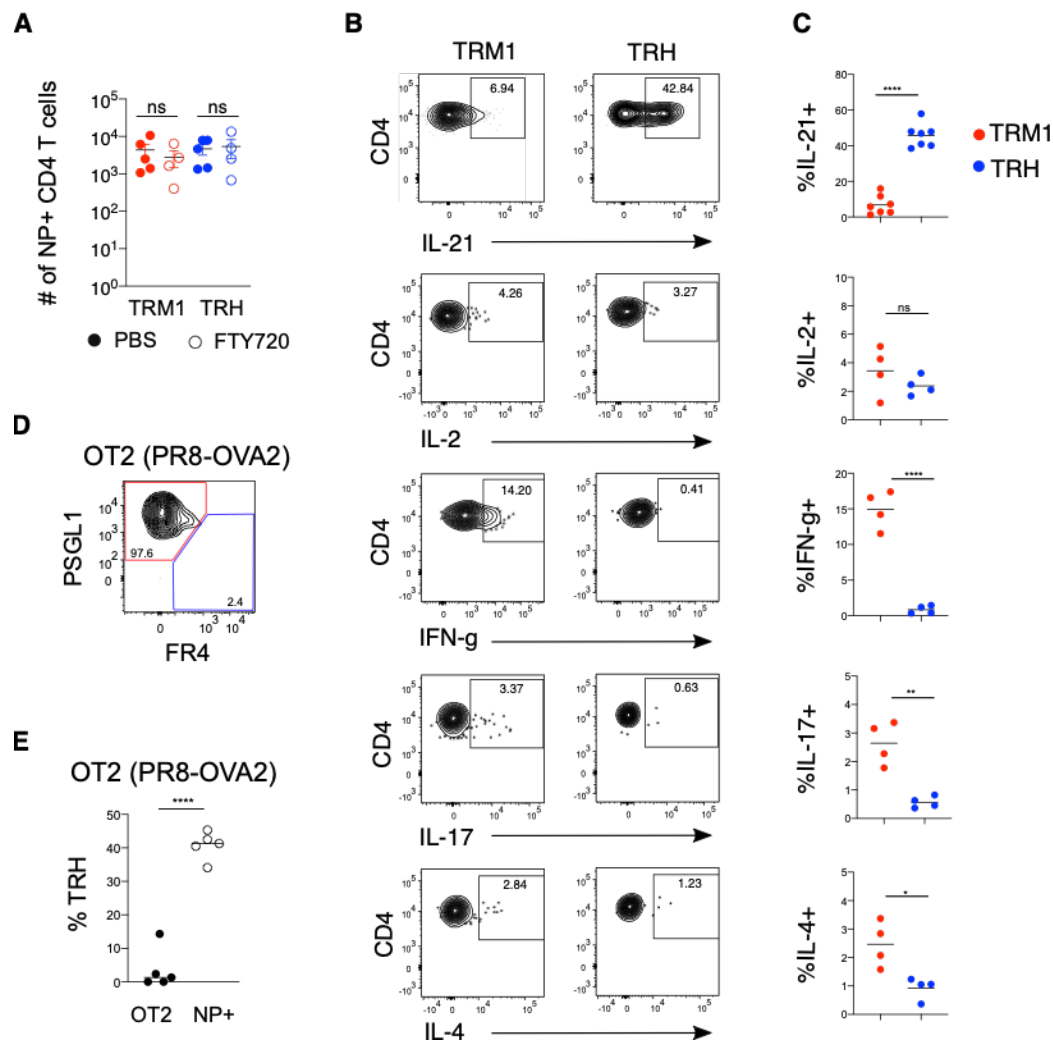


Fig. S3. Protein expression confirms Th1 and T_{fh} phenotypes in the lung

(A) Total numbers of NP-specific non-circulating TRM1 and TRH from PBS and FTY720-treated mice. (B) Representative flow cytometry plot of proportion of cytokine producing NP-specific TRM1 and TRH. (C) Frequencies from B. (D) Representative plot of TRM1 (red) and TRH (blue) among transferred OT2. (E) Frequency of TRH in OT2 and endogenous NP-specific CD4⁺ T cells. Data in A (n=4-5, representing 2 experiments), C (n=7, pooled from 2 experiments for %IL-21 and n=4, representing 2 experiments for others) and E (n=5, representing 2 experiments) were analyzed using unpaired Student's t-test. Thin lines represent

mean \pm s.e.m in **A** and mean in **C and E**. Significance was determined using unpaired Student's t-test. P values are as follows: *P<0.05, **P<0.01, ***P<0.001, ****P<0.0001.

Supplementary Figure 4.

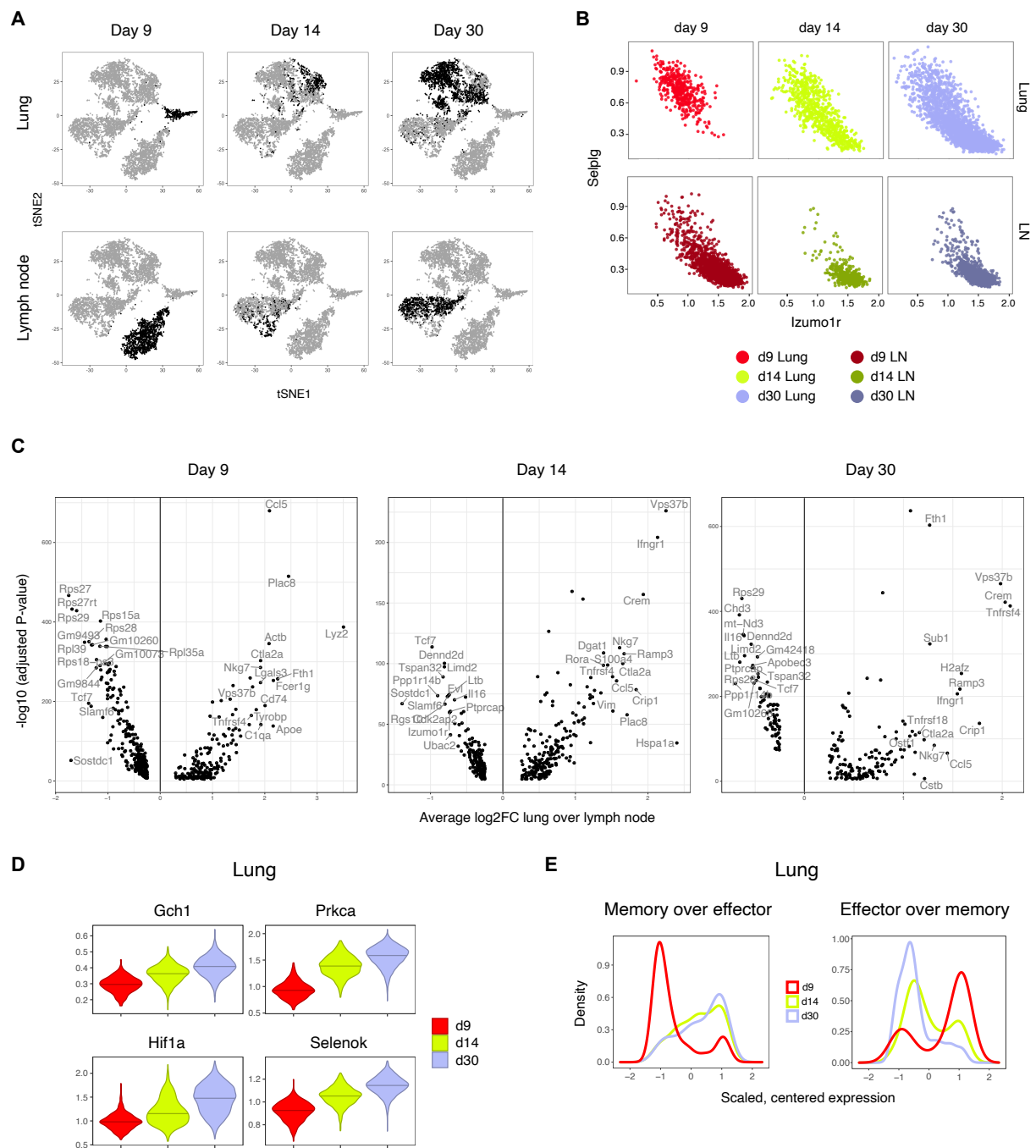


Fig. S4. Progressive differentiation of resident CD4⁺ T cell subsets

(A) tSNE of scRNA-seq data by tissue and time point. (B) Imputed expression of *Izumo1r* and *Selplg* by tissue and time point. (C) Differentially expressed genes discriminating lung (+) from LN (-) across time points. (D) Imputed expression of selected genes in the lung across time points. (E) Scaled centered expression of

gene set average scores across time points. Gene sets derived from differential expression analysis between effector and memory cells in published data⁷⁰, adjusted P Value < 0.05.

Supplementary Figure 5.

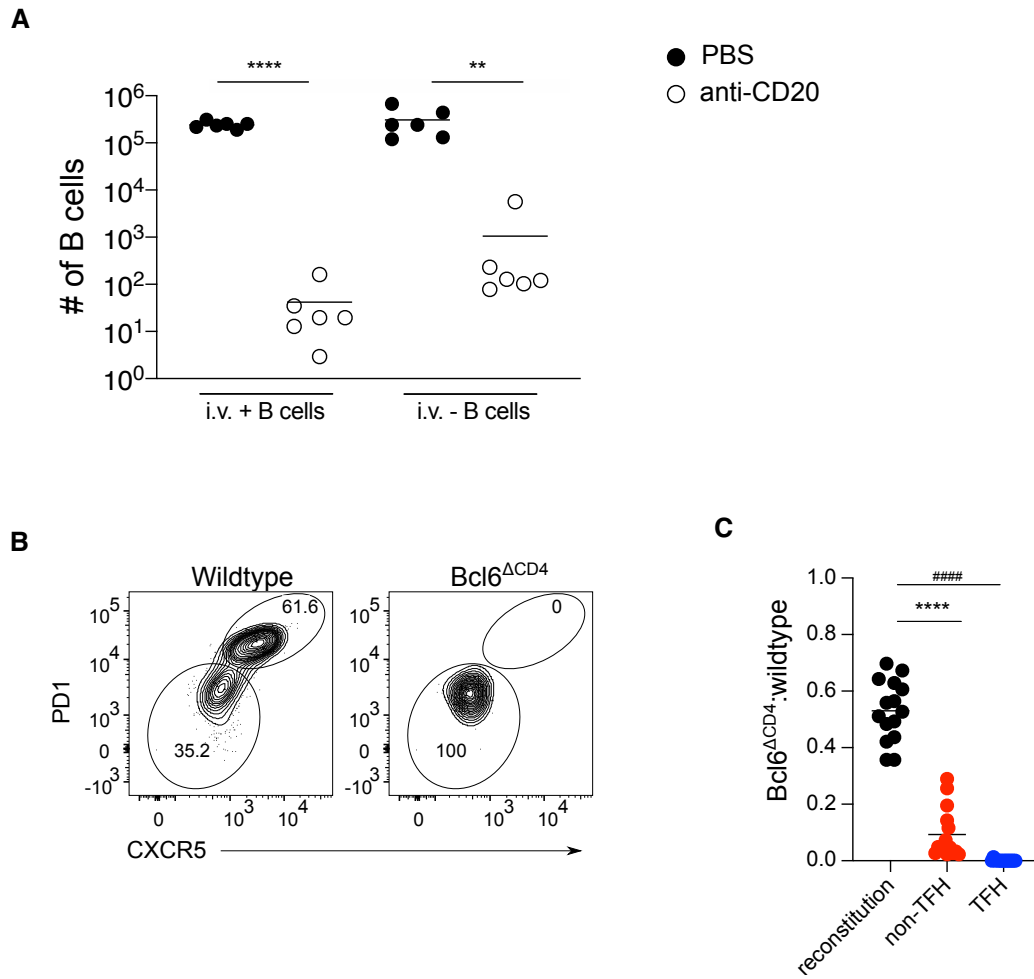


Fig. S5. TRH cell generation requires B cells and T cell intrinsic Bcl6

(A) Total numbers of iv⁺ and iv⁻ B cells in control and B cell depleted mice. **(B)** NP-specific T_{fh} and non-T_{fh} cells of mLN from control and Bcl6-deficient subsets. **(C)** Bcl6^{ΔCD4}:control ratio of CD4⁺ T cells after reconstitution from blood (pre-infection), NP-specific non-T_{fh} and T_{fh}. Thin lines represent mean in **(A)** (n=6, representing 2 experiments) and **(C)** (n=15, pooled from 3 experiments). Significance was determined by unpaired Student's t-test. P values are as follows: *P<0.05, **P<0.01, ***P<0.001, ****P<0.0001.

Supplementary Figure 6.

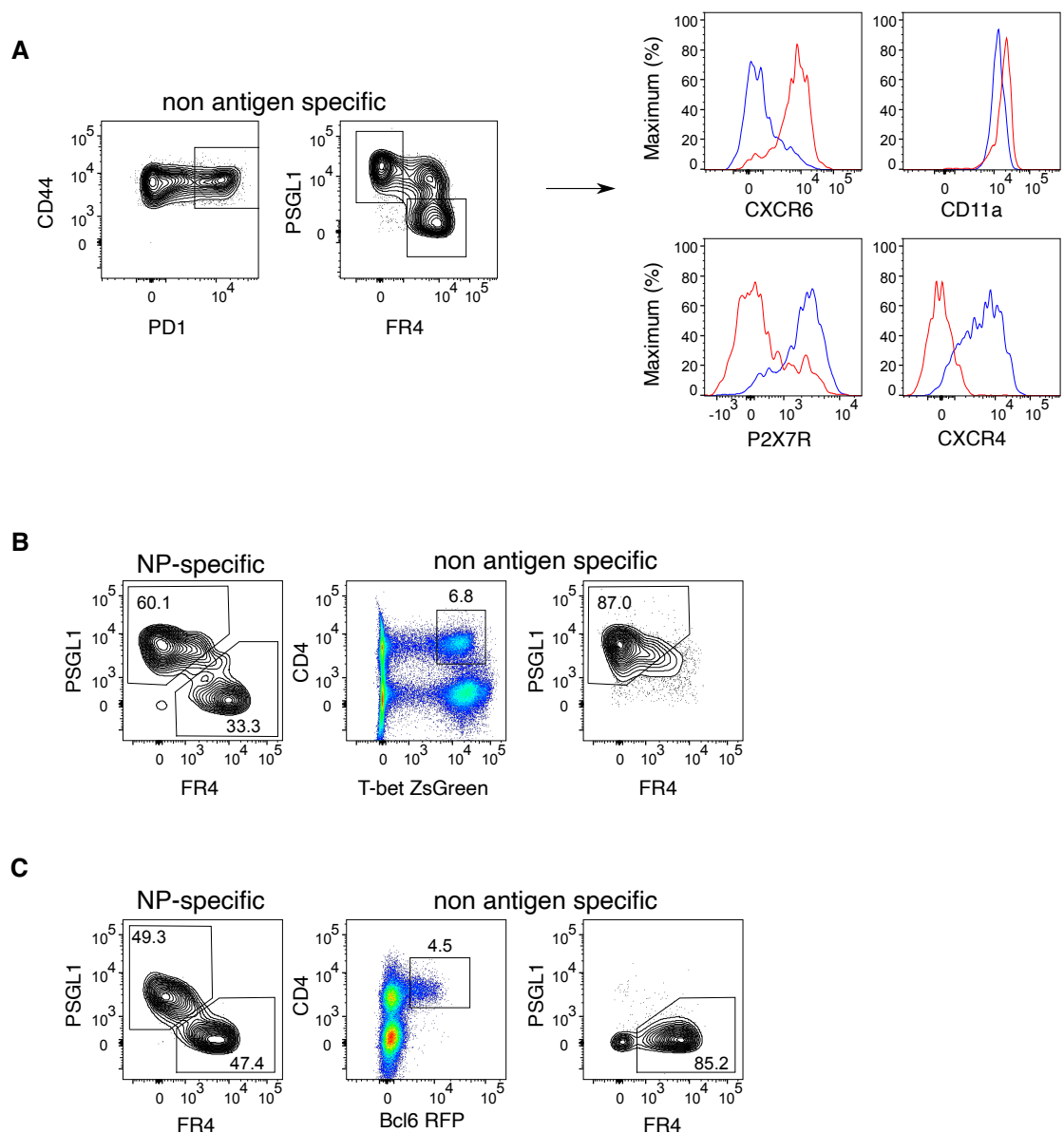


Fig. S6. CD4⁺ TRH cells localize in lung B cell clusters

(A) Representative gating strategy for identification of non-antigen specific resident CD4⁺ T cells (left) and phenotypic marker expression on gated TRM1 and TRH cells (right). **(B, C)** Flow cytometry plot representation of CD4⁺T-bet ZsGreen⁺ cells within TRM1 gate **(B)** and CD4⁺Bcl6 RFP⁺ cells within TRH gate **(C)**. NP-specific TRM1 and TRH are shown on the left for comparison (n=4, representing 2 experiments).

Supplementary Figure 7.

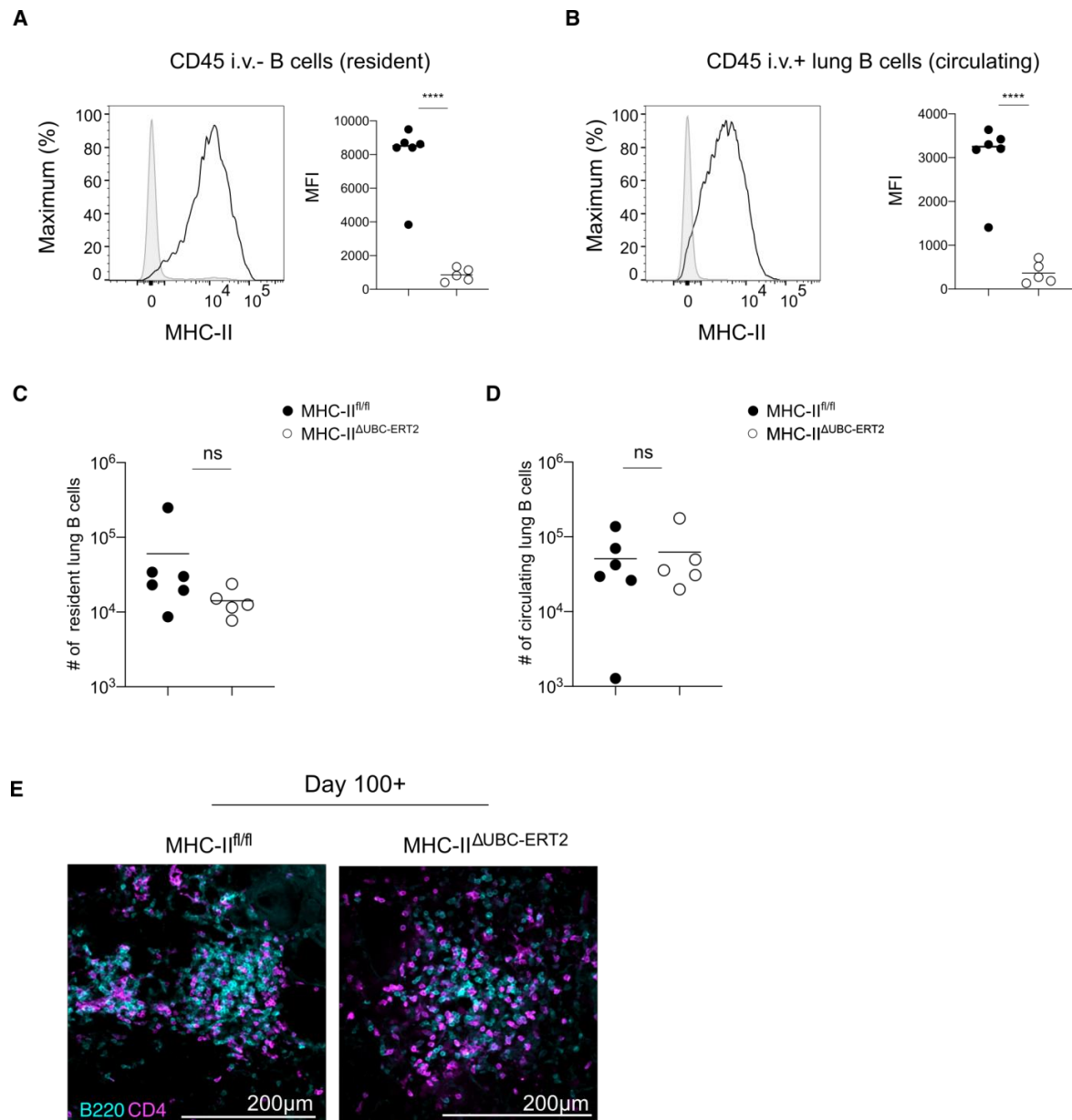


Fig. S7. Maintenance of TRH cells requires antigen presentation

(**A, B**) Histograms (left) and quantification (right) of MHC-II expression on iv⁻ (**A**) and iv⁺ B cells (**B**) upon inducible deletion of MHC-II. (**C, D**) Total numbers of iv⁻ (**C**) and iv⁺ (**D**) lung B cells. (**E**) Representative X40 immunofluorescence confocal images with staining for indicated markers from MHC-II^{fl/fl} and MHC-II^{ΔUBC-ERT2} mice inducibly-deleted 100 days post-infection. Scale bars: 200μm. Thin lines represent

mean in A, B, C and D (n=5-6, representing 2 experiments). Significance was determined using unpaired Student's t-test. P values are as follows: *P<0.05, **P<0.01, ***P<0.001, ****P<0.0001.

Supplementary Figure 8.

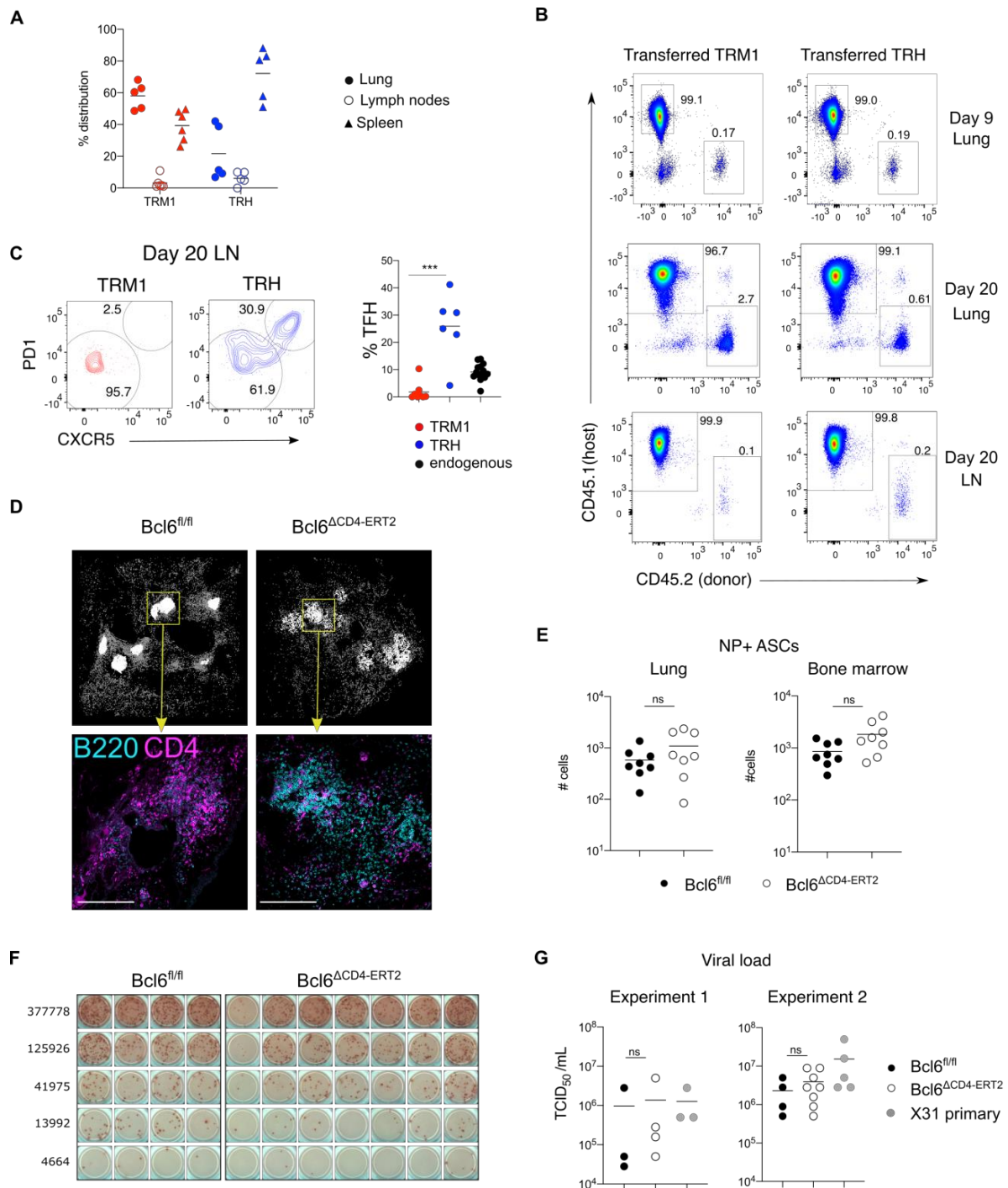


Fig. S8. TRH cells are plastic and promote local antibody production during re-challenge

(A) Percentage distribution of transferred TRM1 and TRH from tissues of TRM1 and TRH recipients at ~16 hours after transfer. **(B)** Flow cytometry plots representing proportion of resident CD4⁺ T cells in donor vs host in TRM1 and TRH recipients at days 9 and 20 post challenge in lung and mLN. **(C)** Representative flow cytometry plot and frequencies of CXCR5⁺ PD1⁺ T_{fh} cells in re-challenged TRM1 and TRH recipients in mLN at day 20. **(D)** Spatial distribution of CD4⁺ cell objects (top) quantified from immunofluorescence confocal images (bottom) from lungs of Bcl6^{fl/fl} and Bcl6^{ΔCD4-ERT2} mice, 30 days post-infection. Each dot represents a CD4⁺ T cell object, located in a B220⁺ area (white), or outside B220⁺ areas (grey). **(E)** Number of NP-specific IgG ASCs from lung and bone marrow of Bcl6^{fl/fl} and Bcl6^{ΔCD4-ERT2} mice, 35 days after primary infection (tamoxifen treatment to delete Bcl6 between day 21-26). **(F,G)** Analysis of lungs of Bcl6^{fl/fl} and Bcl6^{ΔCD4-ERT2} mice 4 days after X31 re-challenge. **(F)** Representative pictures of ELISpot for NP-specific IgG ASCs. **(G)** Viral titers obtained from lungs of Bcl6^{fl/fl} and Bcl6^{ΔCD4-ERT2} mice. X31 primary infected mice are shown as controls. Thin lines represent mean in **A** (n=5-6, pooled from 2 experiments), **C** (n = 6-8, pooled from 2 experiments), **F** (n=8, pooled from 2 experiments) and **G** (n=3-8, 2 experiments). Significance was determined using unpaired Student's t-test. P values are as follows: *P<0.05, **P<0.01, ***P<0.001, ****P<0.0001.

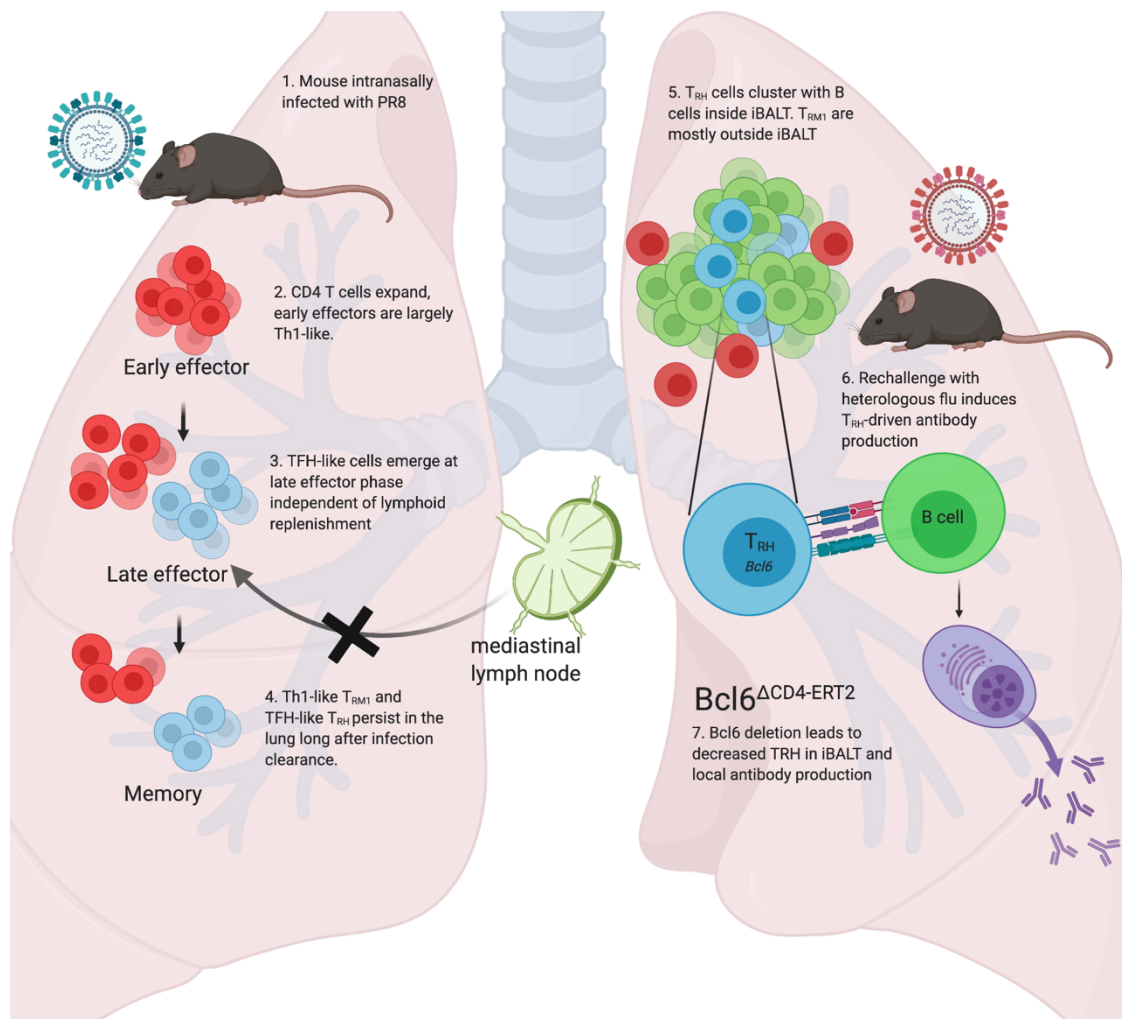


Fig3. Graphical abstract

5. Discussion

5.1 Heterogeneity and tissue-specific genes

Our study utilizes single cell RNA sequencing analysis of tissue resident NP-specific CD4 TRM that overcomes the biases occurring due to bulk sequencing analyses. Considering polyclonal antigen-specific cells over monoclonal TCR transgenic models helps identify cellular heterogeneity in the TRM compartment. We identified circulating T cells, Th1-like TRM1 cells and two types of TFH-like TRH cells in the lung, generated after influenza infection. We were able to find phenotypically similar populations in the draining LN. By comparing Th1-like or TFH-like cells in both organs, we were able to pinpoint genes commonly enriched in tissue that were independent of cell phenotype such as *Fth1*, *Tnfsf4* and *Eif1*. TRH cells exhibit

greater heterogeneity than what could be resolved by flow cytometry. One cluster displayed a classical lymphoid signature with enrichment of *Tcf7*, implicated in T cell plasticity and *Id3*, associated with memory populations²⁶. The other TRH cluster was enriched in *HIF-1α* among other genes.

5.2 *HIF-1α and possible role in TRM regulation*

HIF-1α is a transcription factor that controls cell responses to low oxygen. HIF-1α is commonly stabilized in hypoxic conditions. HIF-1α dimerizes with HIF-1β prior to nuclear translocation where the complex binds to targets that promote cellular adaptation to hypoxia. HIF-1α activation promotes a glycolytic metabolism in T cells, supplying energy essential for expansion, differentiation and function. T cell metabolism changes occurring during cellular processes or pathology can impact HIF stability and activity⁸¹. Extrinsic factors like TCR and co-stimulatory signaling that initiates downstream mTOR activity, pro- and anti-inflammatory cytokines can promote HIF-1α protein stability regardless of oxygen availability⁸². Extended hypoxic signaling can also provide a negative feedback to HIF activity in T cells through microRNAs^{83,84}. Extensive cross-talk between metabolic pathways adds additional complexity to HIF-1α regulation and activity⁸⁵.

HIF-1α regulation of T cell differentiation is multifaceted and depends on the immune context. Contrasting studies on the role of HIF-1α in TFH cells have been reported. One study reports a TFH induction block by HIF-1α over-expression in mice lacking VHL⁸⁶, an enzyme that ubiquitinates HIF for proteasomal degradation⁸⁷. Here HIF-1α stabilization promoted increased glycolysis and GAPDH activation, eventually repressing ICOS expression essential for TFH differentiation and maintenance. Another study reports the decrease in TFH, GC B cells and antibody production with HIF-1α deletion⁸⁸. In addition to confirming the latter observations, one other study also associates HIF-1α deficiency with decreased glycolysis⁸⁹. The caveats of these studies are that they have been performed with full knockout models or

gene deletions prior to T cell activation which fail to provide an insight into the temporal role of HIF-1 α in T cell differentiation and function.

We observe a gradual upregulation of *Hif1a* over time in CD4 antigen-specific NP cells in the lung, compared to the lymphoid NP cells. HIF-1 α upregulation coincides with the emergence of TRH in the tissue and iBALT formation. A HIF-stabilizing hypoxic environment is a feature of immunological niches that support immune activity. At day 30 after infection, the genes regulated by HIF-1 α were enriched in TRM indicating regulatory activity of the protein. The role of HIF-1 α in regulating long-lived TRH maintenance and function in the tissue is an open question. Preliminary experiments with inducible deletion of HIF-1 α in CD4 T cells after infection resolution did not significantly impact TRM numbers, suggesting that the transcription factor is dispensable for survival. With a deletion reporter, we were able to observe a decrease in CD27 among HIF-deleted TRH. CD27 is a TRAF-linked tumor necrosis factor receptor family member implicated in TCR induced expansion, B cell activation, T cell memory maintenance and optimal response kinetics⁹⁰. This leads to the hypothesis that HIF-deficient TRH would sub-optimally support a recall response. The downstream impact on local antibody production upon TRH re-activation would be an interesting follow-up study.

Although single cell RNA sequencing analysis shows that the two TRH clusters are regulated by *Bcl6* and *Hif1a*, the gene expressions in the respective subsets are not mutually exclusive. This opens up another question about the link between BCL6 and HIF-1 α in regulating TRH cells. BCL6 has been shown to repress glycolytic pathway genes controlled by HIF-1 α in CD4 T cells⁹¹. This suggests that a block in *Bcl6* should rescue HIF-1 α and associated target gene expression. In our data, *Bcl6* deletion results in the re-localization of TRH to outside the iBALT. Do cells that lose *Bcl6* expression upregulate *Hif1a* or do these cells also downregulate *Hif1a* as a result of exiting their immunological niche? How does TRH identity change? These questions can be answered by inducible deletion models with a simultaneous fluorescence reporter readout of the proteins being investigated. A deletion reporter in these mouse models

would ensure that the cells that lose protein expression are correctly identified in flow cytometric or histological analysis.

Amphiregulin (AREG), encoded by *Areg*, is among the top cluster-defining genes of the HIF-1 α + TRH subset. AREG is an Epidermal Growth Factor (EGF)-like molecule that promotes host tolerance by sustaining lung tissue integrity and homeostasis following infection-induced tissue damage⁹². Early amphiregulin production by Tregs in influenza infected mice prevented excessive tissue damage⁹³, highlighting a potential role of TRM- derived AREG in tissue repair, possibly regulated by HIF-1 α . In preliminary experiments conducted by us, no change in TRM-derived AREG protein was observed with late phase deletion of HIF-1 α in CD4 T cells, but re-challenge of those mice resulted in decreased AREG expression. In a recall environment, HIF stabilization and downstream activity could be promoted by more TCR signaling and inflammatory environment associated hypoxia. The absence of HIF at this time point could significantly impact the quality of T cell-mediated immune response. More work needs to be done in this direction to assess the exact role of the HIF-1 α + TRH subset in the tissue, particularly during a recall response. Complicating this effort, tissue processing and cell isolation can significantly alter the metabolic state of the cells and falsely report HIF-1 α expression. To reliably assess the role of this protein in vivo, histology and spatial sequencing studies⁹⁴ can be employed that allow tissue environment examination without niche disruption.

5.3 Dynamics of long-term T-B interactions in the tissue

In our study we observed that B cell depletion negatively impacted the generation of TRH cells but the role of resident B cells in the maintenance of TRH is yet to be determined.

T-B signaling constitutes pMHC-II-TCR, ICOS-ICOSL and CD40-CD40L interactions among others⁹⁵. Our data shows that MHC-II deletion at late time points did not impact TRH numbers or iBALT structure. This suggests that non-cognate T-B interactions are sufficient to support maintenance of long-lived TRH. Mozdzanowska et al., showed that transfer of MHC-II

knockout cells into CD8-depleted μ MT recipients followed by influenza infections led to mice surviving the disease but non-clearance of infection that correlated with lower antigen-specific antibody production⁹⁶. This showed that non-cognate T-B interaction can provide some level of immune protection. ICOS-ICOSL interactions were shown to be essential for the maintenance of long-lived TFH and local antibody production²⁶. In another study, iBALT disruption correlated with decrease in local and systemic antibody levels⁶⁷. Taken together, these observations indicate that ICOS-ICOSL interactions between TRM and resident B cells could be crucial for maintenance of iBALT structure and TRH survival.

An interesting question is how long are these iBALT structures maintained? Is the 'quality' of iBALT changing with time and what are the implications on the recall response? Time course analysis of iBALT structures showed a gradual waning of iBALT size by day 100+ after IAV infection⁶⁴. A study looking at lymphoid GC long after LCMV infection clearance observed a 'return' to naïve-like structure with no apparent GC structures present. However, long-lived TFH cells continued to persist and maintain their glycolytic signature²⁶. What is the fate of memory B cells upon iBALT shrinkage? Do these cells persist in other locales in the tissue, egress out or undergo apoptosis? It is important to carry out long term studies to assess iBALT longevity and subsequent impact on resident T and B cell maintenance and recall response.

In our study, CD4 T cell-specific *Bcl6* deletion after infection clearance altered iBALT structures but had no significant impact on the resident B cell numbers. Local antibody production was decreased only upon recall infection. These results suggest that BCL6-deficient TRM may still be able to provide sufficient help to B cells in the tissue for survival but not enough to promote differentiation into plasma cells that produce antibodies. Work by Adachi et al., showed that persistent lung GCs preferentially support cross-reactive resident memory B cell derived antibody production that can protect from heterologous flu strains⁹⁷. The authors also report that B cells with HA cross-reactivity preferentially accumulate in the tissue vs lymphoid organs. Tan et al., observed higher proportions of NP-specific vs HA-

specific GC B cells in the lung⁶⁴. With respect to influenza infections, both long-lived resident B cells with specificity to conserved epitopes and cross-reactive memory B cells possess the potential to protect against heterologous strains. The role of TRH in balancing the response from the two compartments is an interesting avenue for further investigation.

There are contrasting studies on how B cells of varying specificities expand, populate the secondary response and shape long lasting immunity^{98,99,100}. One study describes a cyclical program undergone by switched memory B cells to remodel antibody specificities upon vaccine-boosts⁹⁸. A contrasting study shows that memory B cells rarely undergo secondary GC reactions, and that prime-boost reactions restrict the diversity of antibody-producing cells¹⁰⁰. Pape et al., propose a temporally changing memory B cell scenario with a decline in switched Ig B cells and long-lived GC-inexperienced IgM+ cells⁹⁹. Flavivirus heterologous infections have been shown to select for low avidity cross-reactive memory B cells that bypass secondary GC-mediated affinity maturation resulting in selection of cross-reactive clones¹⁰¹, a mechanism that has proven to be detrimental to rechallenged individuals^{102, 103}. Preliminary data generated in our lab showed a trending increase in cross-reactive HA serum antibody titers upon late CD4-specific Bcl6 deletion. Is this trend also recapitulated in the tissue? Is there a proportional decrease of strain-specific HA-antibodies? Is this phenomenon occurring due to altered help provided by re-localized TRH? These observations warrant a closer look into localization of resident B cells of various specificities and highlight the potential of transcriptionally altering TRH to modulate the immune repertoire.

5.4 Caveats and Outlook

5.4.1 Caveats of TRM study design

Although the TRM field is gaining momentum especially with the current pandemic situation, some caveats are to be considered when interpreting the data. Lymphocyte isolation by tissue digestion and processing can introduce biases in cell subsets and underestimate cell numbers

present in the tissue¹⁰⁴. The technique of perfusion to remove circulating cells from the tissue in order to consider only “resident” cells for analysis does not result in complete elimination of cells present in the vasculature⁴³. The method of intravenous antibody injection to label circulating cells can also positively stain TRM localized close to blood vessels depending on the wait period before organ harvest. Microscopic techniques that are essential for obtaining tissue location information of TRM prove challenging for the identification of antigen-specific cells with tetramers. Tissue removal, processing and re-introduction into circulation can alter the surface phenotype and metabolic state of TRM cells^{33, 32}.

5.4.2 CD8 T cell depletion to study CD4 TRM in influenza models

To individually assess the role of CD4 TRM-mediated protective responses, we depleted CD8 T cells before re-challenge. Re-challenge of CD8 T cell depleted mice interferes with the cooperation between the CD8 T cells, non-neutralizing antibodies and alveolar macrophages that are essential for viral control¹⁰⁵. Better settings to investigate CD4 TRM, especially TFH-like TRH cells are M.tb infection models⁵⁵ and tumors¹⁰⁶. In these models, granulomas¹⁰⁷ and tertiary lymphoid structures^{108, 109, 110} resembling iBALT structures have been defined that correlate with latent infection or positive prognosis respectively. B cells residing in these structures have been used as correlates of protection, possibly helped by TFH-like cells.

5.4.3 Contribution of CD4 TRM to OAS

Original antigenic sin (OAS) or antigenic priming refers to the immune system's ability to preferentially utilize immunological memory based on prior infection when a slightly different secondary infection occurs. One school of thought associated with the generation and preservation of memory to primary infection as a means of protection from future challenge infections is the contribution to OAS¹¹¹. In our setup, the possibility that preservation and recalling of NP-specific memory cells might hinder HA-specific responses to drifted influenza strains cannot be overlooked.

5.4.4 Relevance of TRM study in the fight against pandemics

For vaccine development studies, the age and sex of the individual should be taken into consideration as younger individuals and females contribute to statistically higher recovery cases^{112,113}. Sex hormones have been shown to affect B cell positioning in germinal centers¹¹⁴ and older individuals harbor phenotypically altered splenic TFH¹¹⁵ or fibrosis-associated lung CD8 TRM¹¹⁶. Although there might be an age or sex-specific role for CD4 TRM in modulating localization and phenotype of proximal immune cells, it is beyond the scope of this thesis.

Knowledge of CD4 TRM and their function have highlighted their possible role in protection against the COVID pandemic. CD4 TRM have been shown to be protective in the SARS mouse model³¹. Presence of SARS-CoV2 specific CD4 T cells has been associated with less-severe disease^{117,118}. In severe COVID cases that resulted in death, loss of Bcl6 expressing TFH correlating with diminished GCs was reported¹¹⁹. Lungs from SARS-CoV2 infected macaques show iBALT formation and antigen-specific TFH cells and GC in the mediastinal lymph node supporting antigen-specific IgG responses¹²⁰. These studies further highlight the possible role of TFH-like TRM in supporting iBALT and local GC responses for antibody-mediated protection, increasing the interest in considering TRM as an attractive vaccine candidate.

6. References

1. Iwasaki, A. & Omer, S. B. Why and How Vaccines Work. *Cell* **183**, 290–295 (2020).
2. Riedel, S. Edward Jenner and the History of Smallpox and Vaccination. *Bayl. Univ. Med. Cent. Proc.* **18**, 21–25 (2005).
3. Linterman, M. A. & Hill, D. L. Can follicular helper T cells be targeted to improve vaccine efficacy? *Frontiers in Immunology* **5**, (2016).
4. Koutsakos, M., Nguyen, T. H. O. & Kedzierska, K. With a Little Help from T Follicular Helper Friends: Humoral Immunity to Influenza Vaccination. *J. Immunol.* **202**, 360–367 (2019).
5. Pepper, M. *et al.* Functional SARS-CoV-2-specific immune memory persists after mild COVID-19. *Res. Sq.* (2020) doi:10.21203/rs.3.rs-57112/v1.
6. Herati, R. S. *et al.* Successive annual influenza vaccination induces a recurrent oligoclonotypic memory response in circulating T follicular helper cells. *Sci. Immunol.* **2**, (2017).
7. Zhang, J. *et al.* Circulating CXCR3+ Tfh cells positively correlate with neutralizing antibody responses in HCV-infected patients. *Sci. Rep.* **9**, 10090 (2019).
8. Crotty, S. T Follicular Helper Cell Differentiation, Function, and Roles in Disease. *Immunity* **41**, 529–542 (2014).
9. Dan, J. M. *et al.* Immunological memory to SARS-CoV-2 assessed for greater than six months after infection. <http://biorxiv.org/lookup/doi/10.1101/2020.11.15.383323> (2020) doi:10.1101/2020.11.15.383323.

10. Gasper, D. J., Tejera, M. M. & Suresh, M. CD4 T-cell memory generation and maintenance. *Crit. Rev. Immunol.* **34**, 121–146 (2014).
11. *Hematology: basic principles and practice.* (Elsevier, 2018).
12. De Silva, N. S. & Klein, U. Dynamics of B cells in germinal centres. *Nat. Rev. Immunol.* **15**, 137–148 (2015).
13. Deenick, E. K. & Ma, C. S. The regulation and role of T follicular helper cells in immunity. *Immunology* **134**, 361–367 (2011).
14. Tubo, N. J. *et al.* Single naive CD4⁺ T cells from a diverse repertoire produce different effector cell types during infection. *Cell* **153**, 785–796 (2013).
15. Keck, S. *et al.* Antigen affinity and antigen dose exert distinct influences on CD4 T-cell differentiation. *Proc. Natl. Acad. Sci.* **111**, 14852–14857 (2014).
16. Snook, J. P., Kim, C. & Williams, M. A. TCR signal strength controls the differentiation of CD4⁺ effector and memory T cells. *Sci. Immunol.* **3**, eaas9103 (2018).
17. Ruterbusch, M., Pruner, K. B., Shehata, L. & Pepper, M. In Vivo CD4⁺ T Cell Differentiation and Function: Revisiting the Th1/Th2 Paradigm. *Annu. Rev. Immunol.* **38**, 705–725 (2020).
18. Li, J., Lu, E., Yi, T. & Cyster, J. G. EB12 augments Tfh cell fate by promoting interaction with IL-2-quenching dendritic cells. *Nature* **533**, 110–114 (2016).
19. DiToro, D. *et al.* Differential IL-2 expression defines developmental fates of follicular versus nonfollicular helper T cells. *Science* **361**, eaao2933 (2018).
20. Hong, S. *et al.* B Cells Are the Dominant Antigen-Presenting Cells that Activate Naive CD4⁺ T Cells upon Immunization with a Virus-Derived Nanoparticle Antigen. *Immunity* **49**, 695–708.e4 (2018).
21. Arroyo, E. N. & Pepper, M. B cells are sufficient to prime the dominant CD4⁺ Tfh response to Plasmodium infection. *J. Exp. Med.* **217**, e20190849 (2020).
22. Choi, Y. S. *et al.* ICOS Receptor Instructs T Follicular Helper Cell versus Effector Cell Differentiation via Induction of the Transcriptional Repressor Bcl6. *Immunity* **34**, 932–946 (2011).
23. Pepper, M., Pagán, A. J., Igyártó, B. Z., Taylor, J. J. & Jenkins, M. K. Opposing signals from the Bcl6 transcription factor and the interleukin-2 receptor generate T helper 1 central and effector memory cells. *Immunity* **35**, 583–595 (2011).
24. Nakayama, S. *et al.* Early Th1 Cell Differentiation Is Marked by a Tfh Cell-like Transition. *Immunity* **35**, 919–931 (2011).
25. Sheikh, A. A. & Groom, J. R. Transcription tipping points for T follicular helper cell and T-helper 1 cell fate commitment. *Cell. Mol. Immunol.* (2020) doi:10.1038/s41423-020-00554-y.
26. Künzli, M. *et al.* Long-lived T follicular helper cells retain plasticity and help sustain humoral immunity. *Sci. Immunol.* **5**, eaay5552 (2020).
27. Teijaro, J. R., Verhoeven, D., Page, C. A., Turner, D. & Farber, D. L. Memory CD4 T Cells Direct Protective Responses to Influenza Virus in the Lungs through Helper-Independent Mechanisms. *J. Virol.* **84**, 9217–9226 (2010).
28. Penaloza-MacMaster, P. *et al.* Vaccine-elicited CD4 T cells induce immunopathology after chronic LCMV infection. *Science* **347**, 278–282 (2015).
29. Gensous, N. *et al.* T Follicular Helper Cells in Autoimmune Disorders. *Front. Immunol.* **9**, 1637 (2018).
30. Gowthaman, U. *et al.* Identification of a T follicular helper cell subset that drives anaphylactic IgE. *Science* **365**, eaaw6433 (2019).
31. Zhao, J. *et al.* Airway Memory CD4⁺ T Cells Mediate Protective Immunity against Emerging Respiratory Coronaviruses. *Immunity* **44**, 1379–1391 (2016).
32. Szabo, P. A., Miron, M. & Farber, D. L. Location, location, location: Tissue resident memory T cells in mice and humans. *Sci. Immunol.* **4**, eaas9673 (2019).
33. Schenkel, J. M. & Masopust, D. Tissue-Resident Memory T Cells. *Immunity* **41**, 886–897 (2014).
34. Masopust, D. & Soerens, A. G. Tissue-Resident T Cells and Other Resident Leukocytes. *Annu. Rev. Immunol.* **37**, 521–546 (2019).
35. Masopust, D. Preferential Localization of Effector Memory Cells in Nonlymphoid Tissue. *Science* **291**, 2413–2417 (2001).
36. Hogan, R. J. *et al.* Activated Antigen-Specific CD8⁺ T Cells Persist in the Lungs Following Recovery from Respiratory Virus Infections. *J. Immunol.* **166**, 1813–1822 (2001).
37. Reinhardt, R. L., Khoruts, A., Merica, R., Zell, T. & Jenkins, M. K. Visualizing the generation of memory CD4 T cells in the whole body. *Nature* **410**, 101–105 (2001).
38. Teijaro, J. R. *et al.* Cutting Edge: Tissue-Retentive Lung Memory CD4 T Cells Mediate Optimal Protection to Respiratory Virus Infection. *J. Immunol.* **187**, 5510–5514 (2011).
39. Jiang, X. *et al.* Skin infection generates non-migratory memory CD8⁺ TRM cells providing global skin immunity. *Nature* **483**, 227–231 (2012).
40. Schenkel, J. M., Fraser, K. A. & Masopust, D. Cutting Edge: Resident Memory CD8 T Cells Occupy Frontline Niches in Secondary Lymphoid Organs. *J. Immunol.* **192**, 2961–2964 (2014).
41. Wu, T. *et al.* Lung-resident memory CD8 T cells (T_{RM}) are indispensable for optimal cross-protection against pulmonary virus infection. *J. Leukoc. Biol.* **95**, 215–224 (2014).
42. Beura, L. K. *et al.* Intravital mucosal imaging of CD8⁺ resident memory T cells shows tissue-autonomous recall responses that amplify secondary memory. *Nat. Immunol.* **19**, 173–182 (2018).
43. Anderson, K. G. *et al.* Intravascular staining for discrimination of vascular and tissue leukocytes. *Nat. Protoc.* **9**, 209–222 (2014).
44. Turner, D. L. *et al.* Lung niches for the generation and maintenance of tissue-resident memory T cells. *Mucosal Immunol.* **7**, 501–510 (2014).
45. Schreiner, D. & King, C. G. CD4⁺ Memory T Cells at Home in the Tissue: Mechanisms for Health and Disease. *Front. Immunol.* **9**, 2394 (2018).
46. Snyder, M. E. *et al.* Generation and persistence of human tissue-resident memory T cells in lung transplantation. *Sci. Immunol.* **4**, eaav5581 (2019).
47. Zuber, J. *et al.* Bidirectional intra-graft alloreactivity drives the repopulation of human intestinal allografts and correlates with clinical outcome. *Sci. Immunol.* **1**, eaah3732–eaah3732 (2016).
48. Slütter, B. *et al.* Dynamics of influenza-induced lung-resident memory T cells underlie waning heterosubtypic immunity. *Sci. Immunol.* **2**, eaag2031 (2017).
49. Hayward, S. L. *et al.* Environmental cues regulate epigenetic reprogramming of airway-resident memory CD8⁺ T cells. *Nat. Immunol.* **21**, 309–320 (2020).
50. Stolley, J. M. *et al.* Retrograde migration supplies resident memory T cells to lung-draining LN after influenza infection. *J. Exp. Med.* **217**, (2020).
51. Mackay, L. K. *et al.* Hobit and Blimp1 instruct a universal transcriptional program of tissue residency in lymphocytes. *Science* **352**, 459–463 (2016).

52. Kumar, B. V. *et al.* Human Tissue-Resident Memory T Cells Are Defined by Core Transcriptional and Functional Signatures in Lymphoid and Mucosal Sites. *Cell Rep.* **20**, 2921–2934 (2017).
53. Grassi, F. The P2X7 Receptor as Regulator of T Cell Development and Function. *Front. Immunol.* **11**, 1179 (2020).
54. Devarajan, P. *et al.* CD4 Effectors Need to Recognize Antigen Locally to Become Cytotoxic CD4 and Follicular Helper T Cells. <http://biorxiv.org/lookup/doi/10.1101/2020.09.03.281998> (2020) doi:10.1101/2020.09.03.281998.
55. Moguche, A. O. *et al.* ICOS and Bcl6-dependent pathways maintain a CD4 T cell population with memory-like properties during tuberculosis. *J. Exp. Med.* **212**, 715–728 (2015).
56. Hondowicz, B. D., Kim, K. S., Ruterbusch, M. J., Keitany, G. J. & Pepper, M. IL-2 is required for the generation of viral-specific CD4⁺ Th1 tissue-resident memory cells and B cells are essential for maintenance in the lung. *Eur. J. Immunol.* **48**, 80–86 (2018).
57. Hondowicz, B. D. *et al.* Interleukin-2-Dependent Allergen-Specific Tissue-Resident Memory Cells Drive Asthma. *Immunity* **44**, 155–166 (2016).
58. McKinstry, K. K. *et al.* Effector CD4 T-cell transition to memory requires late cognate interactions that induce autocrine IL-2. *Nat. Commun.* **5**, 5377 (2014).
59. Strutt, T. M., McKinstry, K. K., Kuang, Y., Bradley, L. M. & Swain, S. L. Memory CD4⁺ T-cell-mediated protection depends on secondary effectors that are distinct from and superior to primary effectors. *Proc. Natl. Acad. Sci.* **109**, E2551–E2560 (2012).
60. Ren, H. M. *et al.* IL-21 from high-affinity CD4 T cells drives differentiation of brain-resident CD8 T cells during persistent viral infection. *Sci. Immunol.* **5**, eabb5590 (2020).
61. Zundler, S. *et al.* Hobit- and Blimp-1-driven CD4⁺ tissue-resident memory T cells control chronic intestinal inflammation. *Nat. Immunol.* **20**, 288–300 (2019).
62. Li, C. *et al.* The Transcription Factor Bhlhe40 Programs Mitochondrial Regulation of Resident CD8⁺ T Cell Fitness and Functionality. *Immunity* **51**, 491–507.e7 (2019).
63. Son, Y. M. *et al.* Tissue-resident CD4⁺ T helper cells assist protective respiratory mucosal B and CD8⁺ T cell memory responses. <http://biorxiv.org/lookup/doi/10.1101/2020.02.28.970400> (2020) doi:10.1101/2020.02.28.970400.
64. Tan, H.-X. *et al.* Inducible Bronchus-Associated Lymphoid Tissues (iBALT) Serve as Sites of B Cell Selection and Maturation Following Influenza Infection in Mice. *Front. Immunol.* **10**, 611 (2019).
65. Moyron-Quiroz, J. E. *et al.* Role of inducible bronchus associated lymphoid tissue (iBALT) in respiratory immunity. *Nat. Med.* **10**, 927–934 (2004).
66. Hwang, J. Y. *et al.* Inducible Bronchus-Associated Lymphoid Tissue (iBALT) Attenuates Pulmonary Pathology in a Mouse Model of Allergic Airway Disease. *Front. Immunol.* **11**, 570661 (2020).
67. GeurtsvanKessel, C. H. *et al.* Dendritic cells are crucial for maintenance of tertiary lymphoid structures in the lung of influenza virus-infected mice. *J. Exp. Med.* **206**, 2339–2349 (2009).
68. Low, J. S. *et al.* Tissue-resident memory T cell reactivation by diverse antigen-presenting cells imparts distinct functional responses. *J. Exp. Med.* **217**, e20192291 (2020).
69. Xu, N. *et al.* Vaccine-induced gastric CD4⁺ tissue-resident memory T cells proliferate in situ to amplify immune response against *Helicobacter pylori* insult. *Helicobacter* **24**, (2019).
70. Beura, L. K. *et al.* CD4⁺ resident memory T cells dominate immunosurveillance and orchestrate local recall responses. *J. Exp. Med.* **216**, 1214–1229 (2019).
71. Turner, D. L. & Farber, D. L. Mucosal Resident Memory CD4 T Cells in Protection and Immunopathology. *Front. Immunol.* **5**, (2014).
72. Gong, F., Zheng, T. & Zhou, P. T Follicular Helper Cell Subsets and the Associated Cytokine IL-21 in the Pathogenesis and Therapy of Asthma. *Front. Immunol.* **10**, 2918 (2019).
73. Cheuk, S. *et al.* Epidermal Th22 and Tc17 Cells Form a Localized Disease Memory in Clinically Healed Psoriasis. *J. Immunol.* **192**, 3111–3120 (2014).
74. Sasaki, K. *et al.* Relapsing–Remitting Central Nervous System Autoimmunity Mediated by GFAP-Specific CD8 T Cells. *J. Immunol.* **192**, 3029–3042 (2014).
75. Noble, A. *et al.* Deficient Resident Memory T Cell and CD8 T Cell Response to Commensals in Inflammatory Bowel Disease. *J. Crohns Colitis* **14**, 525–537 (2020).
76. Vemula, S. V., Sayedahmed, E. E., Sambhara, S. & Mittal, S. K. Vaccine approaches conferring cross-protection against influenza viruses. *Expert Rev. Vaccines* **16**, 1141–1154 (2017).
77. Herold, S., Becker, C., Ridge, K. M. & Budinger, G. R. S. Influenza virus-induced lung injury: pathogenesis and implications for treatment. *Eur. Respir. J.* **45**, 1463–1478 (2015).
78. Iuliano, A. D. *et al.* Estimates of global seasonal influenza-associated respiratory mortality: a modelling study. *The Lancet* **391**, 1285–1300 (2018).
79. Sant, A. J., DiPiazza, A. T., Nayak, J. L., Rattan, A. & Richards, K. A. CD4 T cells in protection from influenza virus: Viral antigen specificity and functional potential. *Immunol. Rev.* **284**, 91–105 (2018).
80. Chapman, T. J. & Topham, D. J. Identification of a Unique Population of Tissue-Memory CD4⁺ T Cells in the Airways after Influenza Infection That Is Dependent on the Integrin VLA-1. *J. Immunol.* **184**, 3841–3849 (2010).
81. Taylor, C. T. & Colgan, S. P. Regulation of immunity and inflammation by hypoxia in immunological niches. *Nat. Rev. Immunol.* **17**, 774–785 (2017).
82. Dang, E. V. *et al.* Control of TH17/Treg Balance by Hypoxia-Inducible Factor 1. *Cell* **146**, 772–784 (2011).
83. Bruning, U. *et al.* MicroRNA-155 Promotes Resolution of Hypoxia-Inducible Factor 1 Activity during Prolonged Hypoxia. *Mol. Cell. Biol.* **31**, 4087–4096 (2011).
84. Wang, H. *et al.* Negative regulation of Hif1a expression and TH17 differentiation by the hypoxia-regulated microRNA miR-210. *Nat. Immunol.* **15**, 393–401 (2014).
85. Pollizzi, K. N. & Powell, J. D. Integrating canonical and metabolic signalling programmes in the regulation of T cell responses. *Nat. Rev. Immunol.* **14**, 435–446 (2014).
86. McGettrick, A. F. & O'Neill, L. A. J. The Role of HIF in Immunity and Inflammation. *Cell Metab.* **32**, 524–536 (2020).
87. Lee, J. H., Elly, C., Park, Y. & Liu, Y.-C. E3 Ubiquitin Ligase VHL Regulates Hypoxia-Inducible Factor-1 α to Maintain Regulatory T Cell Stability and Suppressive Capacity. *Immunity* **42**, 1062–1074 (2015).

88. Cho, S. H. *et al.* Hypoxia-inducible factors in CD4⁺ T cells promote metabolism, switch cytokine secretion, and T cell help in humoral immunity. *Proc. Natl. Acad. Sci.* **116**, 8975–8984 (2019).
89. Dong *et al.* HIF1 α -Dependent Metabolic Signals Control the Differentiation of Follicular Helper T Cells. *Cells* **8**, 1450 (2019).
90. Hendriks, J. *et al.* CD27 is required for generation and long-term maintenance of T cell immunity. *Nat. Immunol.* **1**, 433–440 (2000).
91. Oestreich, K. J. *et al.* Bcl-6 directly represses the gene program of the glycolysis pathway. *Nat. Immunol.* **15**, 957–964 (2014).
92. Zaiss, D. M. W., Gause, W. C., Osborne, L. C. & Artis, D. Emerging Functions of Amphiregulin in Orchestrating Immunity, Inflammation, and Tissue Repair. *Immunity* **42**, 216–226 (2015).
93. Arpaia, N. *et al.* A Distinct Function of Regulatory T Cells in Tissue Protection. *Cell* **162**, 1078–1089 (2015).
94. Ståhl, P. L. *et al.* Visualization and analysis of gene expression in tissue sections by spatial transcriptomics. *Science* **353**, 78–82 (2016).
95. Crotty, S. T Follicular Helper Cell Biology: A Decade of Discovery and Diseases. *Immunity* **50**, 1132–1148 (2019).
96. Mozdzanowska, K., Furchner, M., Zharikova, D., Feng, J. & Gerhard, W. Roles of CD4⁺ T-Cell-Independent and -Dependent Antibody Responses in the Control of Influenza Virus Infection: Evidence for Noncognate CD4⁺ T-Cell Activities That Enhance the Therapeutic Activity of Antiviral Antibodies. *J. Virol.* **79**, 5943–5951 (2005).
97. Adachi, Y. *et al.* Distinct germinal center selection at local sites shapes memory B cell response to viral escape. *J. Exp. Med.* **212**, 1709–1723 (2015).
98. McHeyzer-Williams, L. J., Milpied, P. J., Okitsu, S. L. & McHeyzer-Williams, M. G. Class-switched memory B cells remodel BCRs within secondary germinal centers. *Nat. Immunol.* **16**, 296–305 (2015).
99. Pape, K. A., Taylor, J. J., Maul, R. W., Gearhart, P. J. & Jenkins, M. K. Different B Cell Populations Mediate Early and Late Memory During an Endogenous Immune Response. *Science* **331**, 1203–1207 (2011).
100. Mesin, L. *et al.* Restricted Clonality and Limited Germinal Center Reentry Characterize Memory B Cell Reactivation by Boosting. *Cell* **180**, 92–106.e11 (2020).
101. Wong, R. *et al.* Affinity-Restricted Memory B Cells Dominate Recall Responses to Heterologous Flaviviruses. *Immunity* **53**, 1078–1094.e7 (2020).
102. Sangkawibha, N., Halstead, S. B. & Rojanasuphot, S. Original Antigenic Sin in Dengue. *Am. J. Trop. Med. Hyg.* **32**, 154–156 (1983).
103. Sangkawibha, N. *et al.* RISK FACTORS IN DENGUE SHOCK SYNDROME: A PROSPECTIVE EPIDEMIOLOGIC STUDY IN RAYONG, THAILAND. *Am. J. Epidemiol.* **120**, 653–669 (1984).
104. Steinert, E. M. *et al.* Quantifying Memory CD8 T Cells Reveals Regionalization of Immunosurveillance. *Cell* **161**, 737–749 (2015).
105. Laidlaw, B. J. *et al.* Cooperativity Between CD8⁺ T Cells, Non-Neutralizing Antibodies, and Alveolar Macrophages Is Important for Heterosubtypic Influenza Virus Immunity. *PLoS Pathog.* **9**, e1003207 (2013).
106. Singh, D. *et al.* CD4⁺ follicular helper-like T cells are key players in anti-tumor immunity. <http://biorxiv.org/lookup/doi/10.1101/2020.01.08.898346> (2020) doi:10.1101/2020.01.08.898346.
107. Dutta, N. K. & Karakousis, P. C. Latent Tuberculosis Infection: Myths, Models, and Molecular Mechanisms. *Microbiol. Mol. Biol. Rev.* **78**, 343–371 (2014).
108. Helmink, B. A. *et al.* B cells and tertiary lymphoid structures promote immunotherapy response. *Nature* **577**, 549–555 (2020).
109. Petitprez, F. *et al.* B cells are associated with survival and immunotherapy response in sarcoma. *Nature* **577**, 556–560 (2020).
110. Cabrita, R. *et al.* Tertiary lymphoid structures improve immunotherapy and survival in melanoma. *Nature* **577**, 561–565 (2020).
111. Davis, C. W. *et al.* Influenza vaccine-induced human bone marrow plasma cells decline within a year after vaccination. *Science* **370**, 237–241 (2020).
112. Bunders, M. J. & Altfeld, M. Implications of Sex Differences in Immunity for SARS-CoV-2 Pathogenesis and Design of Therapeutic Interventions. *Immunity* **53**, 487–495 (2020).
113. Dhochak, N., Singhal, T., Kabra, S. K. & Lodha, R. Pathophysiology of COVID-19: Why Children Fare Better than Adults? *Indian J. Pediatr.* **87**, 537–546 (2020).
114. Zhao, R. *et al.* A GPR174–CCL21 module imparts sexual dimorphism to humoral immunity. *Nature* **577**, 416–420 (2020).
115. Lefebvre, J. S., Masters, A. R., Hopkins, J. W. & Haynes, L. Age-related impairment of humoral response to influenza is associated with changes in antigen specific T follicular helper cell responses. *Sci. Rep.* **6**, 25051 (2016).
116. Goplen, N. P. *et al.* Tissue-resident CD8⁺ T cells drive age-associated chronic lung sequelae after viral pneumonia. *Sci. Immunol.* **5**, eabc4557 (2020).
117. Rodda, L. B. *et al.* Functional SARS-CoV-2-Specific Immune Memory Persists after Mild COVID-19. *Cell* S0092867420315658 (2020) doi:10.1016/j.cell.2020.11.029.
118. Szabo, P. A. *et al.* Analysis of respiratory and systemic immune responses in COVID-19 reveals mechanisms of disease pathogenesis. <http://medrxiv.org/lookup/doi/10.1101/2020.10.15.20208041> (2020) doi:10.1101/2020.10.15.20208041.
119. Kaneko, N. *et al.* Loss of Bcl-6-Expressing T Follicular Helper Cells and Germinal Centers in COVID-19. *Cell* **183**, 143–157.e13 (2020).
120. Elizaldi, S. R. *et al.* SARS-CoV-2 infection induces germinal center responses with robust stimulation of CD4 T follicular helper cells in rhesus macaques. <http://biorxiv.org/lookup/doi/10.1101/2020.07.07.191007> (2020) doi:10.1101/2020.07.07.191007.

7. Appendix

NIVEDYA SWARNALEKHA

Email: nivedya.swarnalekha@unibas.ch, nivedyas@gmail.com
Address: Hegenheimerstrasse 173, 4055 Basel, Switzerland
Mobile: +41 78 619 03 83
Linkedin: <https://www.linkedin.com/in/nivedya-swarnalekha-45a21a40/>
Nationality: Indian
Date of Birth: July 11th 1990



Research/Work Experience

02/2016 – 03/2021 Doctor of Philosophy in Immunology (Advisor: Prof. Dr. Carolyn King)
University Hospital of Basel, Department of Biomedicine (Switzerland)

10/2014 – 01/2016 Science Content Writer
Sciencehopper Education Private Limited, Bangalore, India.

10/2012 – 09/2013 Volunteer Teacher
Make A Difference, Trivandrum, India

12/2011 - 06/2012 Project Intern at Biocon Research Limited, Bangalore, India
B.Tech Thesis: "Process Optimization for Enhancing Antibody
Production through Fed-Batch Culture Systems in Engineered CHO
cells"

Education

02//2016 – 11/03/2021 Doctor of Philosophy in Immunology (Advisor Prof. Dr. Carolyn King)
University Hospital of Basel, University of Basel, Department of Biomedicine
(Switzerland)

09/2013 – 11/2014 Master of Science in Biotechnology (with Distinction)
The University of Edinburgh (Scotland, UK)

06/2014 – 08/2014 Master's thesis: "Investigation of the Role of Retinoic Acid in the Generation
of Regulatory T-cells" (Mark: 84%)
The Queens Medical Research Institute, The University of Edinburgh

05/2008 – 05/2012 Bachelor of Technology in Industrial Biotechnology (GPA:8.22/10)
(SASTRA University, India)

Publications

T resident helper cells promote humoral responses in the lung

Nivedya Swarnalekha, David Schreiner, Ludivine C. Litzler, Saadia Iftikhar, Daniel Kirchmeier, Marco Künzli, Young Min Son, Jie Sun, Etori Aguiar Moreira, Carolyn G. King, Science Immunology

Science Immunology, 2021 January 8. doi: 10.1126/sciimmunol.abb6808
Link: <https://immunology.sciencemag.org/content/6/55/eabb6808>

Long-lived T follicular helper cells retain plasticity and help sustain humoral immunity

Marco Künzli, David Schreiner, Tamara C. Pereboom, **Nivedya Swarnalekha**, Ludivine C. Litzler, Jonas Lötscher, Yusuf I. Ertuna, Julien Roux, Florian Geier, Roman P. Jakob, Timm Maier, Christoph Hess, Justin T. Taylor and Carolyn G. King

Science Immunology, 2020 March 6. doi: 10.1126/sciimmunol.aay5552

Link: <https://immunology.sciencemag.org/content/5/45/eaay5552>

Presentations

10/2019	Poster presentation 3rd Annual Meeting of Upper Rhine Immunology (URI) Group Basel, Switzerland
09/2019	Poster presentation Swiss Society for Allergology and Immunology (SSAI) Congress Lugano, Switzerland
02/2018	Oral presentation Wolfsberg Meeting 2018, Thun, Switzerland
04/2017	Poster presentation University of Basel Immunology Community (UBICO) Retreat Engelberg, Switzerland
10/2016	Poster presentation University of Basel Immunology Community (UBICO) Retreat Engelberg, Switzerland

Supervision of students/junior researchers

09/2018	Lara Kroczeck, Intern
07/2019	Elif Karabatak, Master's Student
11/2020-present	Tagore Sanketh Bandaru, PhD Student Jean de Lima, PhD Student Mara Esposito, Masters' student

Personal skills

Languages	English (native language), German (basic)
IT skills	GraphPad Prism (Statistics) FlowJo (Flow cytometry data analysis) Inkscape
Hobbies/Interests	Writing, Travelling